Coronary Physiology and Quantitative Myocardial Perfusion

6

K. Lance Gould, Tung T. Nguyen, Richard Kirkeeide, and Nils P. Johnson

Why Coronary Physiology and Quantitative Perfusion?

Clinical orientation of our positron emission tomography (PET) images and quantitative data for our integrated *Cardiac Positron Imaging and Consultation Report* comprises the core of evidenced-based, optimal, highly personalized clinical care as essential to cardiology as angiograms, stents, bypass surgery, and vigorous medical management. It illustrates the power of quantitative regional myocardial perfusion as optimal gatekeeper or guidance for complex coronary artery disease (CAD) as requested by the revascularization team and referring physicians. Though our integrated technical and clinical approach may be unique, it demonstrates the principles and a standard of clinical coronary physiology for personalized patient management.

Our guiding philosophy is uncompromising, self-critical analysis of every case and every protocol, driven by hard data, which takes precedence over preconceived bias or silo thinking that may degrade our science and patient care. Continuous ongoing critical clinical and technical data review evolves our technology and protocols toward coronary physiologic truth for every patient, uncontaminated by suboptimal physiologic data, ego, financial interests, or competitive academic bias.

K. L. Gould (✉)
Weatherhead PET Center for Preventing and Reversing Atherosclerosis, University of Texas Medical School at Houston, Houston, TX, USA
e-mail: k.lance.gould@uth.tmc.edu

T. T. Nguyen · N. P. Johnson
Division of Cardiology, University of Texas Medical School at Houston, Houston, TX, USA

R. Kirkeeide
Department of Internal Medicine, McGovern Medical School, University of Texas Health Sciences Center at Houston, Houston, TX, USA

V. Dilsizian, J. Narula (eds.), *Atlas of Nuclear Cardiology*, https://doi.org/10.1007/978-3-030-49885-6_6

PET data are displayed as if looking at a patient who is transparent or as viewed by a cardiologist on fluoroscopy or a surgeon opening the chest (Fig. 6.1). The views are as if walking around the patient, seeing through to the right or septal side of the left ventricle (LV), then anterior, lateral, and inferior views, corresponding to the distributions of the three major coronary arteries. The pixel-based quantitative images define the actual perfusion size and severity of individual arteries down to tertiary branches, without assumed or standardized coronary artery distributions, which often differ from the actual regional perfusion of each coronary artery for a specific individual.

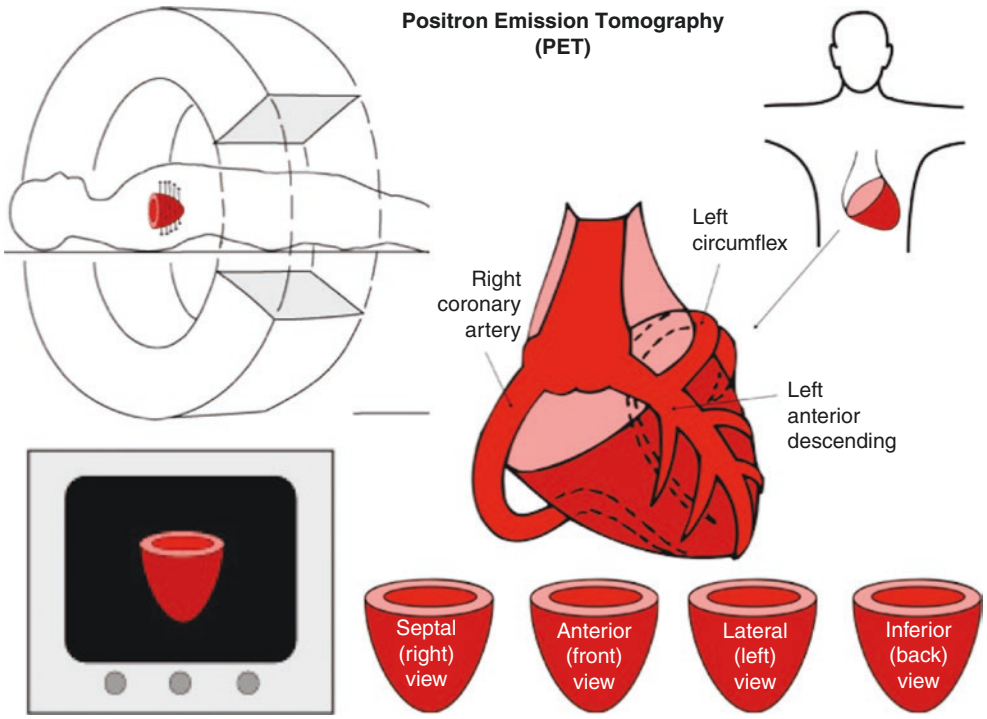

Fig. 6.1 Clinical orientation of positron emission tomography (PET) images

Our *Cardiac Positron Imaging and Consultation Report* includes a complete cardiovascular history, review of all prior tests (including angiogram, if done), physical exam, summary of conclusions, and recommendations, whether for medical treatment only, for angiography or revascularization, or for either option depending on clinical judgment, individual circumstances, and informed patient preference. Every regional and global abnormality for focal and diffuse CAD is reported, including objectively measured regional size and severity for each coronary artery (down to tertiary branches) on relative and quantitative images. The report also addresses symptoms or issues needing explanation, and includes recommendations for or against invasive procedures.

Over 40 years of our experience with quantitative coronary angiography and cardiac PET indicate that cardiologists and cardiac surgeons will not use or depend on any data or images that they cannot easily, quickly, and comprehensively understand directly related to their fluoroscopic or surgical views of the heart. These same physiologic-anatomic views, combined with comprehensive clinical integration by an experienced clinical cardiologist/physiologist consultant generates an evolving bidirectional trust within the cardiac team, in which quantitative coronary physiology drives optimal patient outcomes documented by hard outcomes in peer-reviewed publications.

The case in Fig. 6.2 illustrates the use of coronary physiology and quantitative perfusion. The *Cardiac Positron Imaging and Consultation Report* shown in Table 6.1 integrates the individual physiology, technical details, and clinical data for the same patient, as acquired routinely every day for every patient. For this case, PET shows severe stress defects (blue) in arterial distributions of the first septal perforator (basal septum) and a large first diagonal branch (anterior) with adequate only mildly reduced coronary flow capacity (CFC) (yellow) in the distribution of the left anterior descending (LAD), characteristic of LAD occlusion at their trifurcation proximal to a patent bypass graft. Myocardial steal in the septal and diagonal regions are typical for occlusion or severe stenosis with collaterals to viable myocardium.

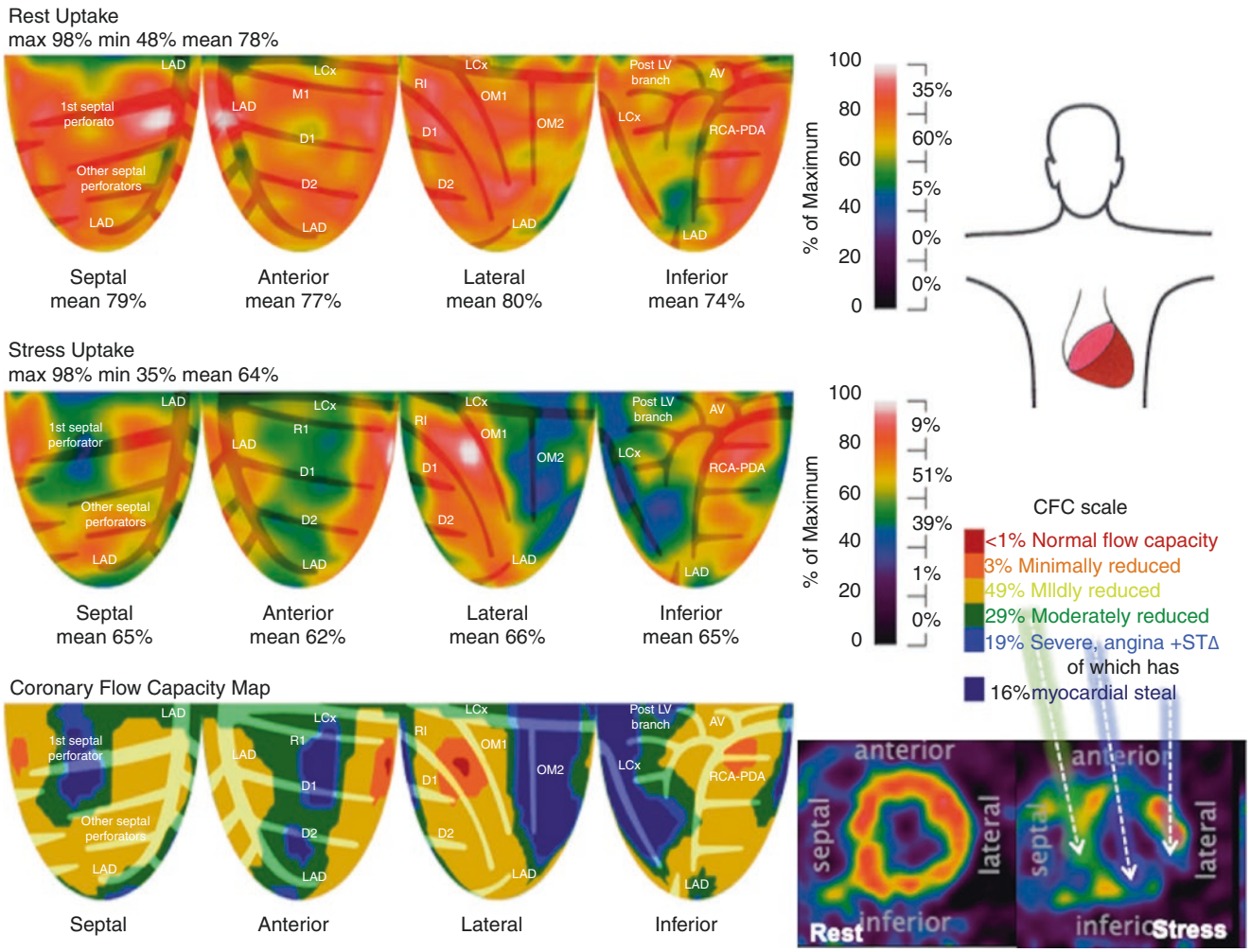

Fig. 6.2 A case study of coronary physiology and quantitative perfusion. The patient is a 66-year-old man referred for preoperative risk stratification prior to hip replacement. Cardiac history includes CAD after coronary artery bypass graft surgery (CABG) in 2009 and percutaneous coronary intervention (PCI) with a stent to the left anterior descending artery (LAD) in 2014. Residual risk factors include hypertension, hyperlipidemia, prior tobacco use, family history of CAD, atrial fibrillation, and exertion angina with dyspnea. The CFC map color codes each pixel for severity of combined stress perfusion in ml/m/g and coronary flow reserve (CFR), with the size and severity of every arterial distribution as the percentage of LV in the color-coded bar legend

1. The relative PET images show the following:
(i) A small, moderate, inferoapical, resting non-transmural scar involving 4% of the LV in the distribution of the distal LAD coronary artery, wrapping around the apex
(ii) A large, severe, lateral and inferolateral stress-induced defect involving 20% of the LV in the distribution of the mid left circumflex (LCx) coronary artery distal to the first obtuse marginal branch (OM1)
(iii) A large, moderate to severe, anterior, stress-induced defect involving 20% of the LV in the distribution of the diagonal branches off the LAD coronary artery, with a mild apical defect consistent with diffuse narrowing of a patent LAD
(iv) A small, moderate to severe, inferoseptal stress-induced defect involving 8% of the LV in the distribution of the proximal right coronary artery supplying the basal inferior septum with adequate distal perfusion suggesting adequate distal RCA perfusion due to excellent collaterals or a patent mid-RCA bypass graft
2. Coronary flow reserve (CFR) in the most severe stress-induced perfusion defect is 0.61, indicating myocardial steal in the anterior, inferoseptal, lateral, and inferolateral areas, reflecting collaterals to viable myocardium. Outside these severe defects (*blue*), absolute myocardial perfusion capacity is moderately reduced in border zones (*green*) and mildly reduced (*yellow*) diffusely throughout the heart but above thresholds for ischemia. Native arteries or bypass grafts to the LAD, RCA, and OM1 are likely patent
3. CT scan shows dense coronary calcification in all the coronary arteries
4. PET perfusion images show abnormal left ventricular contraction with anterior, lateral, and inferolateral hypokinesis and ejection fraction of 41% with stress
5. Depending on clinical judgment and circumstances, the PET findings suggest that coronary angiogram with a potential revascularization procedure may be appropriate due to the following:
(i) Angina and shortness of breath with activity and dipyridamole stress
(ii) 2.5 mm ST depression with dipyridamole stress
(iii) Large, severe, stress-induced defects involving 48% of viable myocardium
(iv) Decreased stress ejection fraction with subendocardial and transmural ischemia
(v) PET findings suggest severe stenosis or chronic Total occlusion (CTO) of a collateralized dominant LCx, whereas the pattern and distribution of the anterior defect suggest moderate stenosis of several smaller diagonals off a diffusely narrowed LAD

Excluded for simplicity, the patient identifiers, date of test, indication, brief history, the rest of the report includes 2 pages with brief history, details on the protocol, patient's blood pressure, ECG recordings, and symptomatic responses during stress, the full quantitative data and color-coded maps as shown in Fig. 6.2 for absolute flow and subendocardial perfusion, if appropriate

Table 6.1 Cardiac positron imaging and consultation report

There is a large severe defect in the mid left circumflex (LCx) distribution (blue) also with myocardial steal suggesting occlusion with collaterals. The native right coronary artery (RCA) and the first obtuse marginal (OM1) or their bypass grafts are patent (yellow to orange) with mildly reduced CFC due to diffuse CAD. The tomograms show subendocardial ischemia ranging from mild to severe to transmural ischemia.

For this high-risk case, the PET prior to angiogram focuses potential intervention on the physiologically largest, most severe and accessible target for stenting the total or subtotal occlusion of the mid LCx artery supplying a large, viable region not readily evaluable by a nonopacified artery beyond the occlusion. This pattern of severe disease proximal to patent bypass grafts is common as demonstrated later in this chapter for a different patient.

Clinical Coronary Physiology

Phasic and mean coronary blood flow measured in cc/min by an electromagnetic flow meter in experimental coronary stenosis illustrates a concept fundamental to clinical coronary physiology [1–11]. From Fig. 6.3, in the absence of stenosis (*upper tracing*), coronary flow increases to four times resting baseline flow during pharmacologic vasodilation stress. The ratio of stress to resting blood flow is called Coronary Flow Reserve (CFR), normally at least 4.0 in all mammalian species, including humans. With moderate stenosis imposed on the artery, resting perfusion remains normal but the phasic variation is damped. During vasodilation stress, however, flow increases to only two times baseline, for a reduced CFR of 2.0. The ratio of maximum stress flow with stenosis to maximum flow without stenosis is called the relative Coronary Flow Reserve (relCFR). The abnormal relCFR is expressed as a fraction of the normal CFR, seen in Fig. 6.3 as 2.0/4.0 for a relCFR of 0.5.

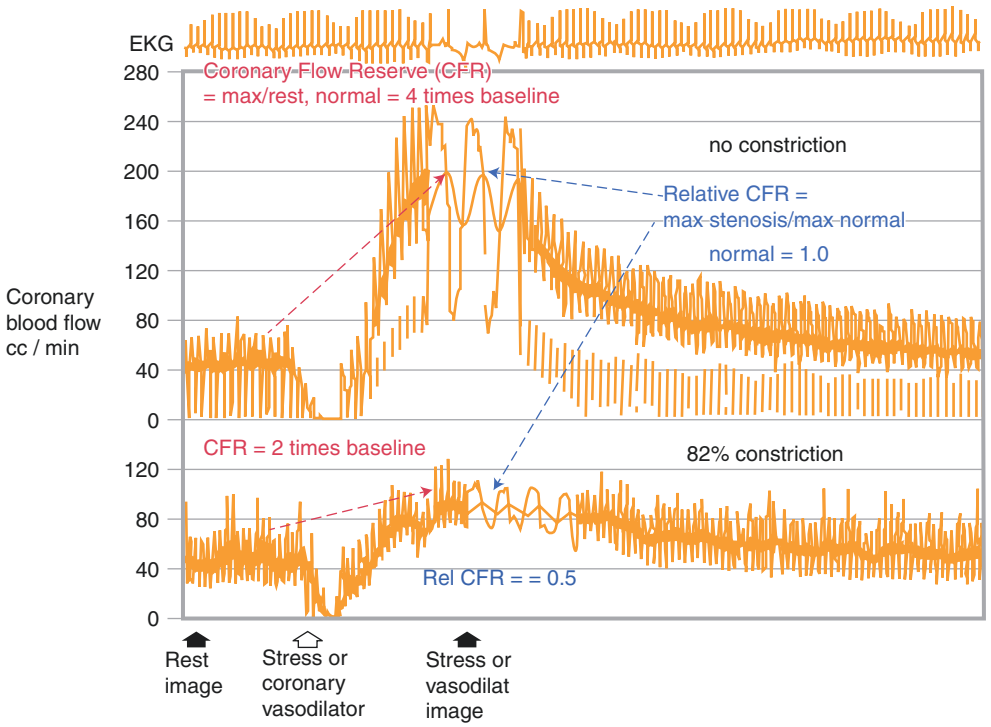

Fig. 6.3 Coronary flow reserve (CFR), rest and stress coronary blood flow. (*From* Gould et al. [1]; with permission from Elsevier)

Coronary flow in cc/min increases with the diameter of the artery and distal myocardial mass or the size of distal microvascular bed. For comparison among different-sized arteries and distal myocardial mass, the quantitative metric is cc/min/g of myocardium, called *myocardial perfusion*. Because the units of cc/min/g cancel for the ratio of stress perfusion to rest perfusion, the stress/rest perfusion ratio is still called CFR (Fig. 6.4) to reference the original concept and the terms most widely used, although some literature refers to myocardial perfusion reserve (MPR).

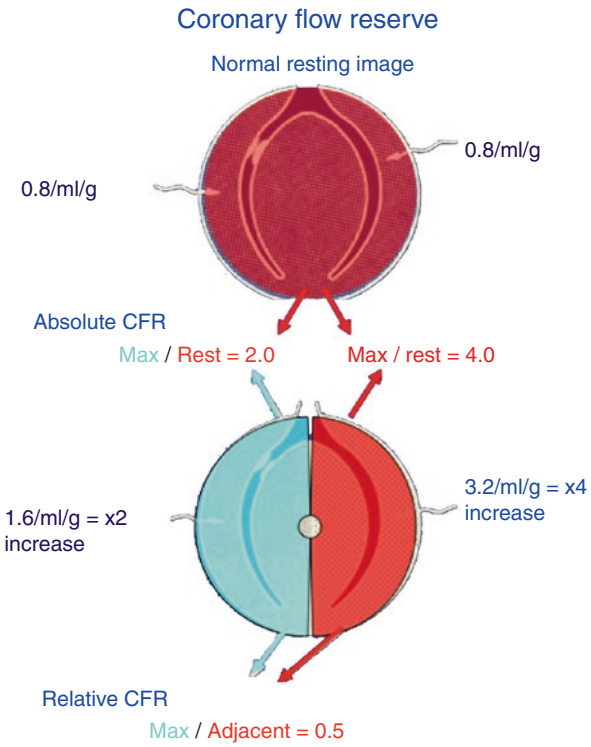

Fig. 6.4 Relative CFR and perfusion imaging

On stress perfusion images of activity alone, regional abnormalities are identified by less activity than other, higher-activity regions, or presumed normal areas, and hence are called relative defects. Therefore, non-quantitative relative stress perfusion images may have a regional defect at very high or very low absolute stress perfusion in cc/min/g. Relative stress perfusion defects are widely read out as ischemia despite having adequate or even high absolute stress flow, well above the low perfusion necessary to cause ischemia defined as angina, significant ST depression >1 mm on ECG, or regional contractile dysfunction. Most relative perfusion defects indicate differential distribution of stress perfusion without low quantitative perfusion causing ischemia defined by these criteria.

As an evolutionary survival mechanism, the mammalian coronary arterial system has the capacity to increase coronary blood flow over four times resting baseline flow in order to meet extreme conditions or activity. Because high coronary blood flow is not needed between such extraordinary demands, at resting conditions the coronary arterioles are vasoconstricted as a high-resistance microvascular bed. Therefore, coronary stenosis will not alter resting blood flow until the resistance of the stenosis is as high or higher than the resistance of the vasoconstricted coronary arterioles. Consequently, resting coronary blood flow may remain normal for severe stenosis up to 80% diameter narrowing, though mild to moderate stenosis of 50–80% diameter narrowing reduces the capacity to increase flow and CFR (Fig. 6.5).

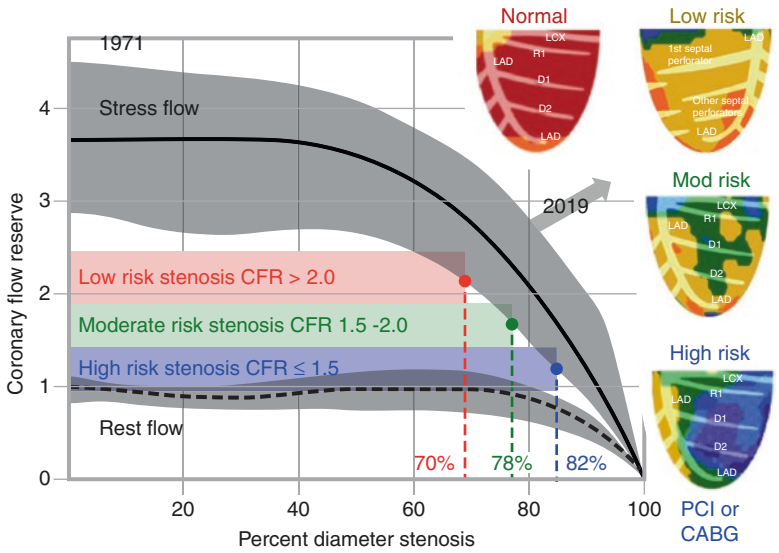

Fig. 6.5 CFR related to percent diameter narrowing of a single focal experimental stenosis. The single anterior views of PET images are color-coded for normal subjects (*red*), for mild to moderate stenosis (*yellow and green*) and for severe stenosis (*blue*), reflecting the risk of adverse coronary events superimposed on the graph of CFR versus % diameter stenosis

In patients, CAD is commonly viewed as focal stenosis but is nearly always associated with diffuse atherosclerosis or multiple stenosis causing heterogeneous, diffuse, irregular narrowing throughout the vessel [12–14] (Fig. 6.6). The pathologic anatomy and corresponding true pressure flow pathophysiology are a complex integration of multiple interactive stress flows, CFRs, and intracoronary pressures for each branching segment within each single coronary artery and its branches.

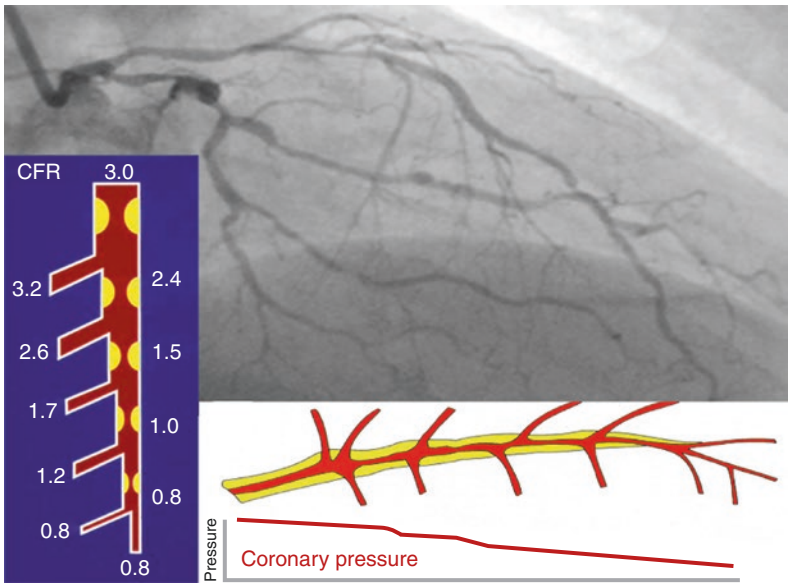

Fig. 6.6 Stenosis and diffuse CAD in patients. Each artery has a family of multiple flows, CFRs, and pressures along its length and branches

The fluid dynamic mechanisms of interspersed focal or diffuse narrowing between arterial branches is documented as "coronary branch steal." Branch steal during stress flow is caused by flow shunted away from more distal arterial segments as pressure progressively falls along the vessel length owing to cumulative viscous pressure loss from diffuse narrowing and disordered flow or vortex shedding at focal narrowing between branches [2, 12–15] (Fig. 6.7).

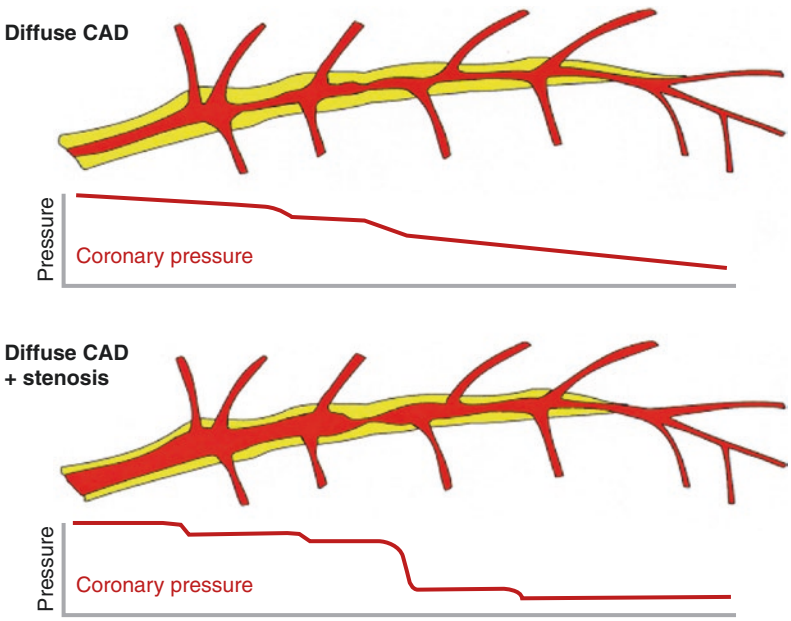

Fig. 6.7 Patterns of pressure loss along arterial length during stress flow for focal and diffuse CAD

Intracoronary pressure pull-back recordings during vasodilation stress identify sudden pressure jumps (or drops) at focal stenosis separate from or in addition to the graded gradual pressure change due to diffuse narrowing.

We developed an integrated fluid dynamic model of the entire coronary arterial tree, relating arterial diameters to summed branch lengths distal to each arterial segment and hence to myocardial mass validated experimentally. The model predicts normal arterial diameters for each vessel segment compared with the measured diameters, thereby predicting the extent of atherosclerotic narrowing in each arterial segment, shown in Fig. 6.8 as yellow thickening superimposed on the clinical angiogram [16].

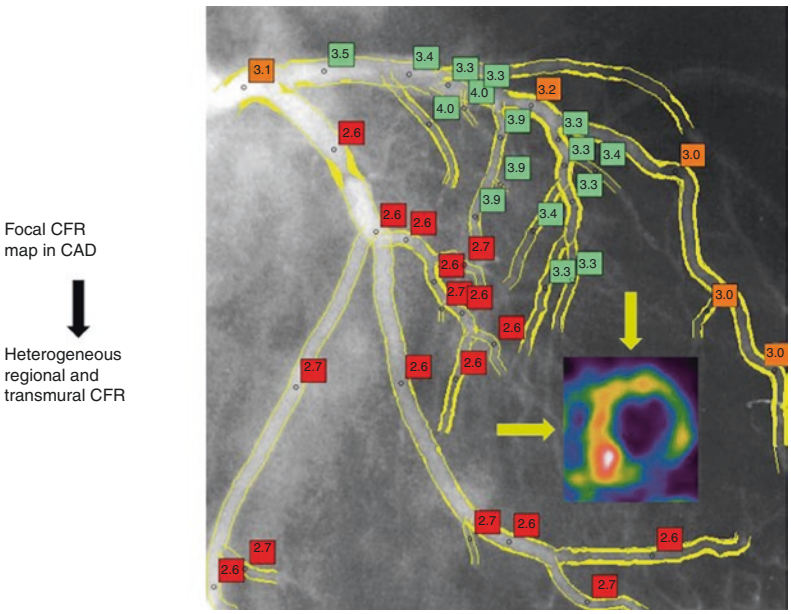

Fig. 6.8 CFR values for the entire left coronary artery tree on a clinical coronary angiogram. The extent of atherosclerotic narrowing in each arterial segment is shown as yellow thickening superimposed on the clinical angiogram. This coronary tree is then analyzed by validated fluid dynamic equations integrated for all dimensions of diameter in millimeters, relative narrowing, length of each narrowing, normal expected diameters, and branch steal for each arterial segment. The results show a wide range of CFRs for each arterial segment, labeled in *red* for the LAD, *green* for the LCx, and *orange* for a large obtuse marginal branch

This coronary tree is then analyzed by validated fluid dynamic equations integrating for all dimensions of diameter in millimeters, relative narrowing, length of each narrowing, normal expected diameters, and branch steal for each arterial segment. The results show a wide range of CFRs for each arterial segment, with no single value characterizing each artery. Therefore, there is no single CFR characterizing a single coronary artery, but rather a wide range of different CFRs along its length and among its branches.

Figure 6.9 illustrates an experimental study in which coronary blood flow was measured by electromagnetic flow meter, aortic pressure was measured by a small catheter inserted into the aorta, and intracoronary pressure was measured by a small coronary catheter implanted in the left circumflex coronary artery distal to an inflatable variable cuff stenosis [17–19]. Without a coronary stenosis, coronary blood flow increases four times during vasodilatory stress for a CFR of 4.0, with no mean aortic to coronary pressure gradient. With stenosis, CFR is reduced to 2.0 with a large pressure gradient across the stenosis. Experimentally [20] and in humans [21], myocardial ischemia does not develop until distal coronary pressure is approximately 35 mm Hg.

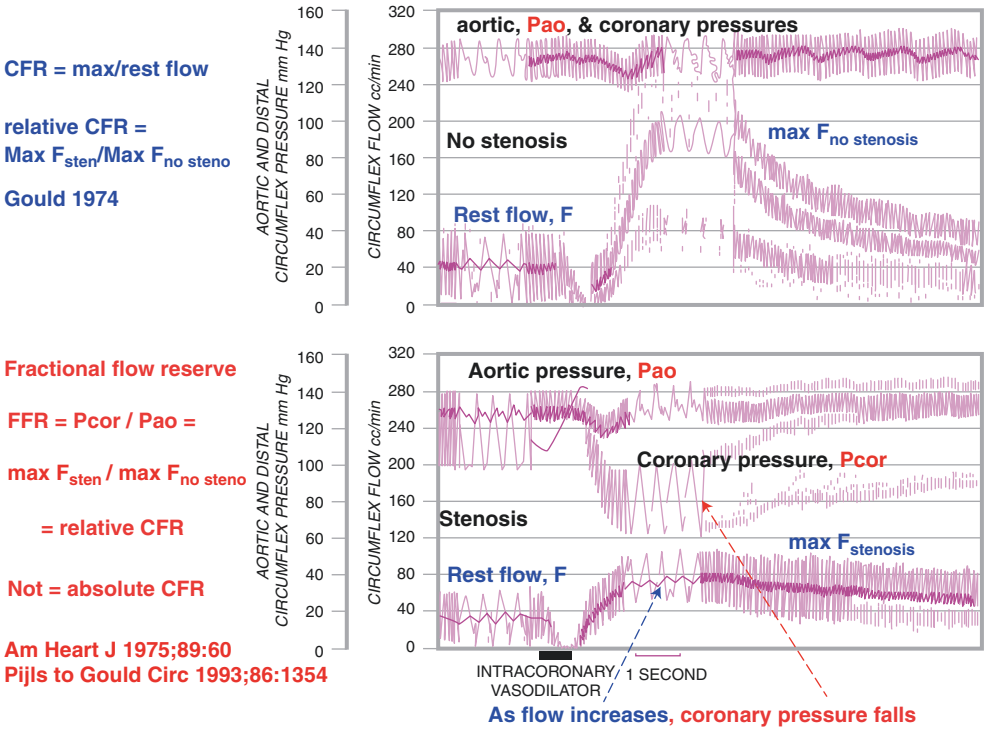

Fig. 6.9 Coronary blood flow, coronary pressure, and fractional flow reserve (FFR) in an experimental study [17–19]. In the *upper panel*, without a coronary stenosis, coronary blood flow increases four times during vasodilatory stress for a CFR of 4.0 with no mean aortic to coronary pressure gradient. In the *lower panel*, CFR is reduced to 2.0 with a peak 50 mm Hg pressure gradient across the stenosis (aorta 130 mm Hg minus coronary 80 mm Hg). (*From* Gould et al. [2]; with permission from Mosby)

For a single focal stenosis, the fractional ratio of the lowest coronary pressure during vasodilation stress to aortic pressure is called fractional flow reserve (FFR). FFR is proportional to the ratio of peak stress flow with stenosis to peak flow without stenosis (that is, relative CFR). Relative CFR and FFR therefore reflect the physiologic severity of the stenosis relative to presumed normal values.

Note that relative CFR and FFR do not indicate absolute stress flow or absolute CFR derived in cc/min/g. Relative CFR and FFR of 0.5 might be due to mild stenosis at very high values of non-ischemic absolute flow, or it might be associated with low absolute flow and CFR, causing ischemia. Relative CFR and FFR therefore do not indicate ischemia defined as angina, ST depression (STΔ), or regional contractile dysfunction; they only indicate relative regional differences in blood flow or perfusion.

Figure 6.10 shows the diastolic fluid dynamic equations for the pressure gradient–flow relation for individual heart beats during increasing flow after vasodilator stress [22, 23]. The increasingly steep pressure flow curve for each diastole indicates dynamically increasing stenosis severity due to flow-induced vasodilation around a fixed cuff stenosis that increases percent stenosis and progressive pressure loss related to flow squared. For each single heart cycle, the diastolic pressure gradient–flow curves fit a quadratic fluid dynamic equation: $\Delta P = AQ + BQ^2$ for volumetric flow; or, in terms of average cross-sectional flow velocity, $\Delta P = CV + DV^2$, where the first term quantifies pressure loss due to viscous friction and the second term quantifies pressure loss due to disordered flow or vortex shedding at the stenosis exit. The terms A, B, C, and D include constants and arterial lumen dimension raised to the fourth power.

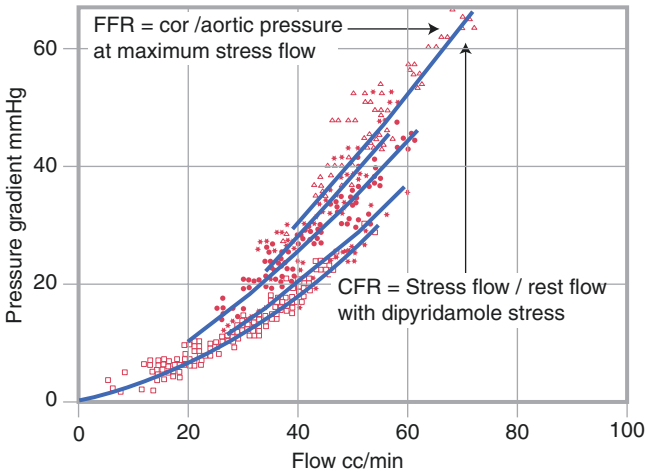

Fig. 6.10 Diastolic pressure–flow curves across a single focal stenosis related to CFR and FFR. On these composite pressure gradient–flow plots, the peak pressure gradient expressed as a ratio to aortic pressure is FFR, and the peak flow expressed as ratio to rest flow is CFR. As derived from this quadratic equation and ignoring collateral flow for simplicity (as used clinically), the relative CFR is related to FFR by the following equation:

$$FFR = P_{cor}/P_{ao} = \max Q_{sten}/\max Q_{nosten}$$

where P is aortic and coronary pressure during maximum stress flow and Q is maximum stress flow with and without stenosis. These ratios reflect relative flow reserve, not absolute perfusion of CFR based on mL/min/g, an important difference between relative and quantitative perfusion imaging abnormalities. (*From* Gould et al. [22]; with permission from Wolters Kluwer.)

The same fluid dynamic model of the coronary artery tree described for Fig. 6.8 predicts a range of coronary pressures and FFR values along each arterial branch, expressed in Fig. 6.11 as pressures relative to aortic pressure of 100 or percent rather than fractions. The coronary artery is characterized by a wide range of pressures at maximum hyperemia, with no single pressure or FFR value to summarize adequately the coronary arteries.

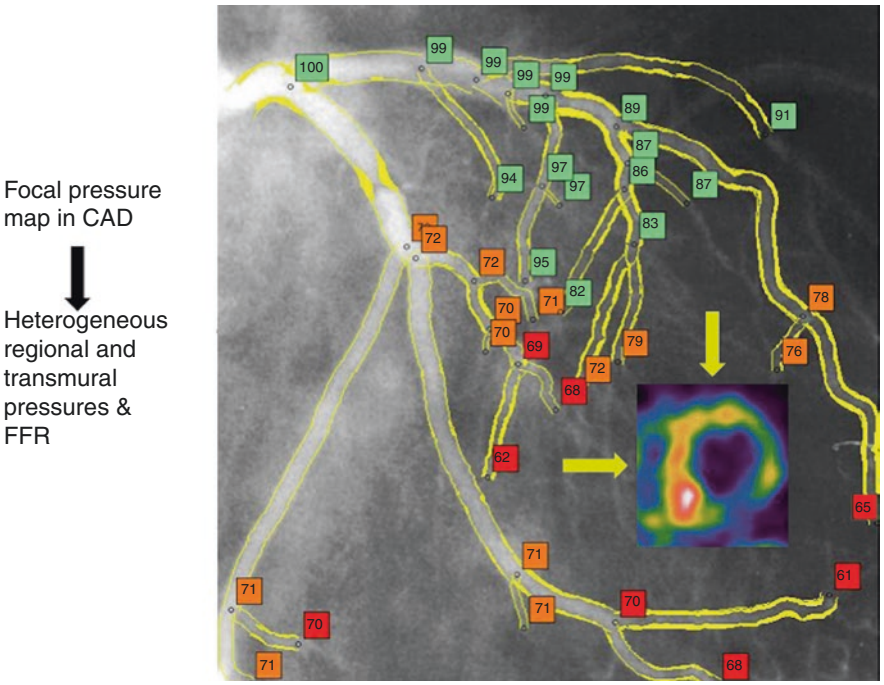

Fig. 6.11 Pressure or FFR values for the entire left coronary artery on a clinical coronary angiogram, expressed as the percentage of aortic pressure. The inset relative tomogram also shows the regional and average global subendocardial/subepicardial perfusion ratio

Though it is an essential step beyond angiographic percent diameter stenosis, a single CFR or FFR value as now determined clinically fails to capture the true pathophysiology of the coronary artery tree in CAD, as illustrated in Figs. 6.2, 6.6, 6.8, and 6.11. In contrast, as developed subsequently in this chapter, quantitative perfusion in cc/min/g on a per-pixel basis by PET maps every artery and branch of the coronary tree for rest and stress perfusion in cc/min/g, per-pixel CFR, and their combination as per-pixel CFC to account for global or regional perfusion heterogeneity.

The pixel data also provide relative stress perfusion or FFR of quantitative stress PET images (FFRpet) derived as the relative map of absolute stress perfusion in cc/min/g, as opposed to relative uptake, or the relative tomogram showing the regional and average global subendocardial/subepicardial perfusion ratio. These basic physiologic and fluid dynamic concepts are essential for understanding and using clinical coronary physiology for optimal patient management based on PET or any other technology for quantifying myocardial perfusion and physiologic severity of coronary artery disease.

Experimentally, transmural perfusion measured by radiolabeled microspheres is normally slightly lower in the subepicardium than in the subendocardium, which is subject to greater wall stress, oxygen demands, and capillary recruitment [2, 7, 20–26]. With coronary perfusion pressure falling to below 35–40 mm Hg, subendocardial perfusion falls as subepicardial perfusion is maintained (Fig. 6.12). During vasodilation stress, a low FFR due to focal or diffuse epicardial narrowing causes reduced subendocardial perfusion. Consequently, reduced subendocardial perfusion metrics are due to falling coronary pressure and FFR during vasodilator stress.

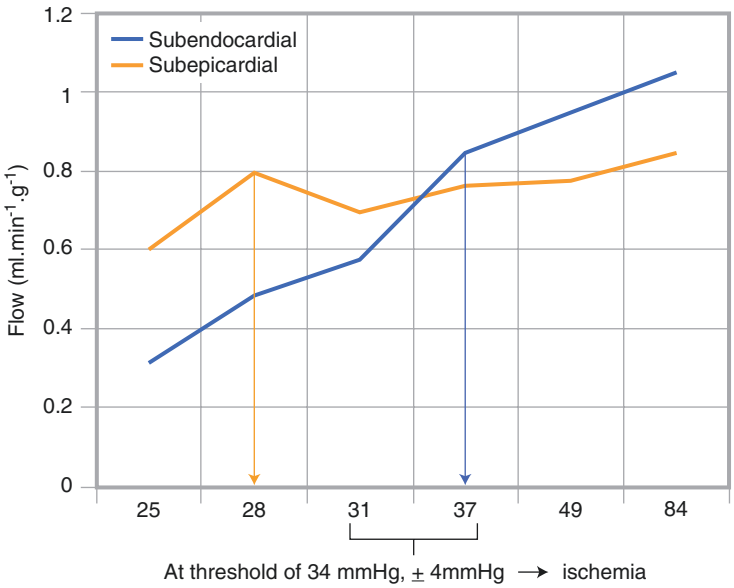

Fig. 6.12 Coronary pressure and subendocardial perfusion. (*From* Hoffman and Buckberg [24]; with permission from the Journal of the American Heart Association)

However, FFR reflects relative pressure drop as a fraction of aortic pressure that rarely reaches this low absolute distal pressure causing ischemia, thereby explaining why angina seldom occurs when clinically measuring FFR ≥0.6. Similarly, a relative subendo/epicardial perfusion ratio may indicate low absolute subendocardial perfusion but not sufficient to cause ischemia. Moreover, mild to severely reduced relative subendocardial perfusion metrics may be associated with angina and ST depression in some individuals but not in others. Like FFR, relative subendocardial perfusion metrics reflect fluid dynamic pressure-flow severity of upstream focal or diffuse narrowing, which may or may not cause ischemia, depending on reduced absolute perfusion in cc/min/g and CFR. Figure 6.13 illustrates reduced subendocardial perfusion due to mild or moderate stenosis during vasodilation stress first reported on experimental stress perfusion tomograms [7, 25].

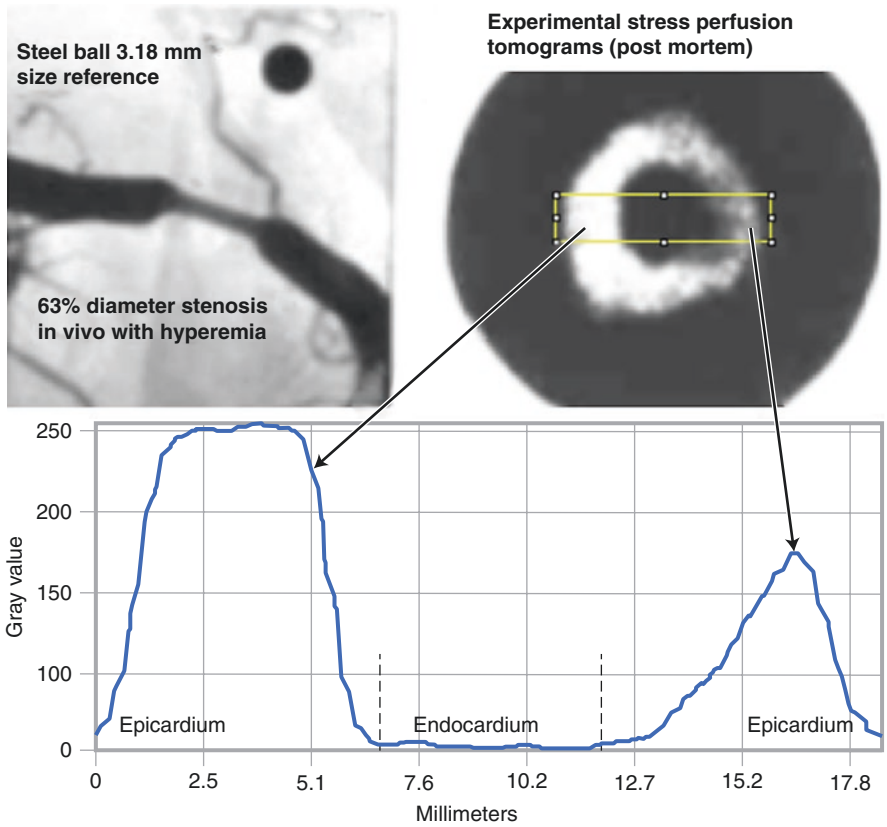

Fig. 6.13 Ex vivo cross-sectional images of in vivo relative transmural perfusion during coronary hyperemia. Intravenous thallium-201 injected in vivo during vasodilation stress and post mortem imaging of LV slices show reduced subendocardial perfusion with a mild coronary artery stenosis. The gray-scale relative activity profiles show severely reduced subendocardial perfusion extending to the subepicardium, thereby reducing transmural perfusion somewhat and hence regional relative and absolute CFR. (*From* Gould and Johnson [25]; with permission from Elsevier)

Large coronary arteries supplying greater distal myocardial mass have higher absolute flow than smaller arteries that supply smaller myocardial mass. For standardized comparison of blow flow in different arteries, flow is therefore expressed as cc/min/g, called *myocardial perfusion* as measured by quantitative PET (Fig. 6.14). The stress/rest ratio is also called *myocardial perfusion reserve*, here considered to be synonymous with coronary flow reserve (CFR), in deference to the extensive physiologic literature on the topic.

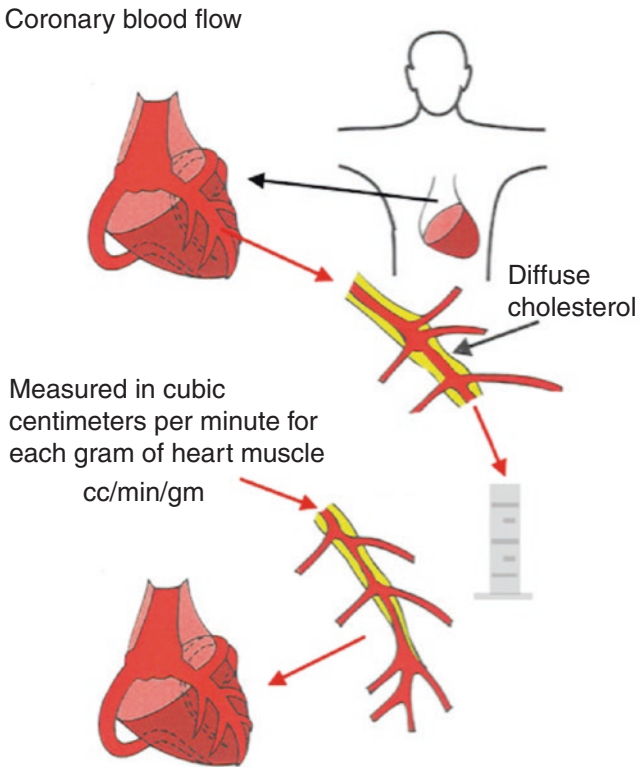

Fig. 6.14 Conceptual schematic of myocardial perfusion as blood flow per gram of myocardium distal to the point of flow measurement

The Literature: Conflicts, Explanations, Resolutions

Figure 6.15 summarizes the literature on quantitative myocardial perfusion by PET [27]. The quantitative perfusion measurements are within similar ranges on average, but several issues impede their use in individual patient management. First, variability in the literature is sufficient to generate mistrust in the values without careful testing and documentation within each PET site. Second, global perfusion measurements are not very useful for assessing the range of heterogeneous focal and diffuse narrowing to guide focal intervention. Third, most PET sites do not understand how to use the quantitative data clinically or report it visually or in text in order to generate trust or reliance by referring or invasive cardiologists for guiding management. Fourth, great variability among PET sites with different protocols and clinical relationships precludes generalized guidelines or consensus on how to make quantitative perfusion measurements, what the different metrics and values indicate, how to report them, what interventions should be done, or on systematic clinical outcomes. This chapter systematically resolves these limitations on the basis of over 8000 cases with follow-up over 10 years.

Population	N	Rest flow (cc/min/gm)	Stress flow (cc/min/gm)	CFR
Normal controls	3,484	0.82 ± 0.06	2.86 ± 1.29	3.55 ± 1.36
Risk factors only	3,592	0.85 ± 0.08	2.25 ± 1.07	2.80 ± 1.39
Established CAD	1,650	0.83 ± 0.10	1.71 ± 0.71	2.02 ± 0.70
Mixed (risk factors and/or known CAD)	4,765	0.97 ± 0.10	1.86 ± 0.58	1.93 ± 0.48
Cardiomyopathy	594	0.73 ± 0.07	1.47 ± 0.56	2.02 ± 0.67
Hypertrophic cardiomyopthy	345	0.90 ± 0.10	1.57 ± 0.33	1.84 ± 0.36
Syndrome X	348	1.06 ± 0.11	2.65 ± 1.31	2.54 ± 1.31
After cardiac transplant	184	1.14 ± 0.18	2.44 ± 1.34	2.29 ± 0.86
	N = 14,962 (from 252 unique publications)			
N-13 ammonica	5,541			
O-15 water	3,167			
Rb-82	6,175			

Fig. 6.15 Quantitative myocardial perfusion by PET in the literature [27]

The data on "ischemic" threshold of stress perfusion in cc/min/g and CFR are even more indeterminate, for several additional reasons. Only two of the reports in the table shown as Fig. 6.16 (Sambuceti and Johnson) measured perfusion during dipyridamole-induced angina or ST depression (STΔ) greater than 1 mm. In all the other reports, the criteria for "ischemia" was defined as FFR ≤0.8 or angiographic severity of ≥50% or ≥70% diameter stenosis on angiogram as a presumed indication of ischemia, rather than actual documented ischemia by angina, significant STΔ or contractile dysfunction [27]. In fact, FFR ≤0.8 during adenosine stress is rarely associated with true angina (distinct from vasodilator side effects) or significant ECG STΔ. Moreover, revascularization based on FFR is not significantly associated with reduced death or MI; hence FFR is a marker of differential relative perfusion, not ischemia. Similarly, an extensive literature documents that angiogram severity does not correlate sufficiently with individual symptoms, physiologic severity, CFR, or outcomes after revascularization to guide these procedures. Therefore, angiogram severity also does not equal ischemia defined as angina, STΔ, or stress wall motion abnormalities in individual patients.

Author	Citation	N	Isotope	Reference Standard	CFR (no units)		Stress flow (cc/min/gm)	
					Cutoff	AUC	Cutoff	AUC
Sambuceti	AJC 1993;72:990	33	N-13	Dipyridamole STΔ	1.75	0.59	1.15	0.6
Muzik	JACC 1998;31:534	51	N-13	Clinically normal group and cath data	2.74	0.91		
Nesterov	Eur J Nucl Med Mol Imaging 2009;36:1594	48	O-15	Catch %Ds>50 (plus FFR in half of cohort)			2.5	
Hajjiri	JACC Cardiovasc Imaging 2009;2:751	27	N-13	Cath %DS≥70	2.0	0.86	1.85	0.90
Kajander	Circulation 2010;122:603	107	O-15	Cath %DS≥50 or FFR≤0.8			2.5	0.95
Johnson	JACC Cardiovasc Imaging 2011;4:990	1,674	Rb-82	Dipyridamole PET Defect, angina/STΔ	1.74	0.91	0.91	0.98
Morton	JACC 2012;60:1546	41	N-13	Cath %DS≥70	1.44	0.83	1.48	0.69
Fiechter	JNM 2012;53:1230	73	N-13	Cath %DS≥50	2.0	0.92		
Danad	JNM 2013;54:55	120	O-15	Cath %DS≥50 (plus FFR in 1/3 of cohort)	2.30	0.81	1.86	0.86

Fig. 6.16 Thresholds of stress perfusion and CFR for "ischemia" [27]. AUC = area under the receiver operating characteristic curve, %DS = percent diameter stenosis, FFR = fractional flow reserve, ST = ST-segment

On the other hand, the threshold in the Johnson report in Fig. 6.16 measured stress perfusion and CFR during dipyridamole-induced angina and STΔ >1 mm. The ischemic threshold was then determined by ROC analysis for that stress perfusion and CFR that best separated patients with angina/STΔ from those without STΔ during dipyridamole stress. Interestingly, the only other report using STΔ as the definition of ischemia during dipyridamole stress reported a threshold close to that of Johnson, unlike the other, much higher perfusion thresholds for "ischemia" defined by FFR or angiographic severity as substitutes for angina, STΔ, or contractile dysfunction.

Conflicts: Which Is Best, CFR or Stress Perfusion?

Figure 6.17 is taken from a report by Gupta et al. [28] in which global stress perfusion was divided by global rest perfusion to get global CFR. Mortality risk for this calculation of global CFR ≤2.0 predicted high mortality risk over follow-up years, as expected, but it purports to claim that global stress perfusion added no predictive value to global CFR for predicting CV mortality, thereby implying no added predictive value of CFC. This conclusion conflicts with other more clinically oriented excellent cardiac PET centers measuring regional perfusion in assumed generalized arterial distributions with the opposite conclusion, namely, that stress perfusion is better than CFR for predicting significant stenosis [29, 30], as in Fig. 6.18.

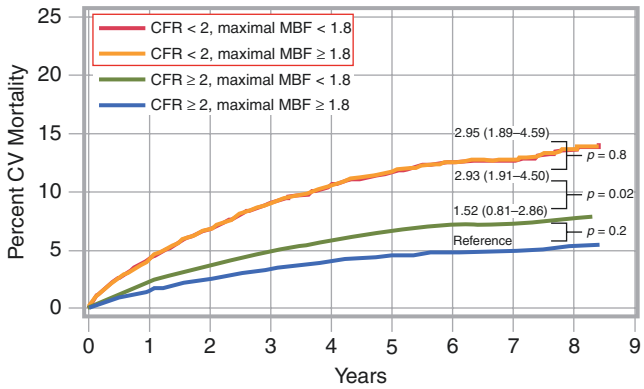

Fig. 6.17 Probability of cardiovascular mortality over time on the basis of CFR impairment and maximal myocardial blood flow (MBF). Mortality risk for this calculation of global CFR ≤2.0 predicted high mortality risk over follow-up years (*red line*) as expected. The plot purports to claim that global stress perfusion (*yellow line*) added no predictive value to global CFR for predicting CV mortality, thereby implying no added predictive value of CFC. (*From* Gupta et al. [28]; with permission from Wolters Kluwer)

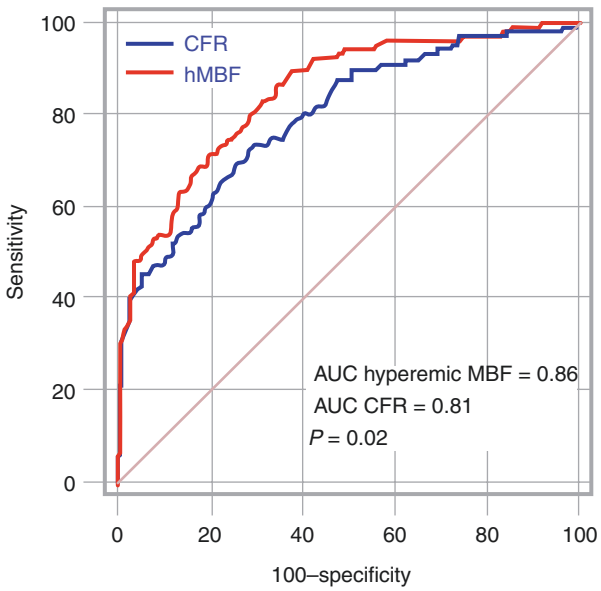

Fig. 6.18 Hyperemic MBF versus CFR for the detection of CAD. (*From* Danad et al. [29]; with permission from the Society of Nuclear Medicine and Molecular Imaging). Hyperemic MBF vs. CFR for detection of CAD. ROC curves for PET parameters tested for all coronary vessels are shown. CFR coronary flow reserve, hMBF hyperemic myocardial blood flow

The data in Fig. 6.17 are profoundly flawed by the use of global stress and CFR [2, 25]. *Global* rest-stress perfusion and *global* CFR averages out all regional rest-stress defects and all regional abnormal CFR defects, as shown in later figures. CFC is by definition the per-pixel distribution of stress perfusion and CFR specifically designed to quantify the common heterogeneous differences and concordances of these two metrics, providing essential physiologic insights for guiding management of CAD and its outcomes. Moreover, the arbitrary stress flow threshold of 1.8 cc/min/g is much higher than the stress perfusion threshold of ≤0.8 associated with documented ischemia as a regional stress PET defect, with angina and STΔ >1 mm in the largest threshold study in the literature [2, 25, 27].

In Fig. 6.18, regional stress perfusion and CFR both correlated with FFR ≤0.8 as the standard of stenosis severity, with the area under the curve (AUC) of receiver operating curves (ROC) for stress perfusion in cc/min/g slightly but significantly better than CFR. The authors concluded that regional stress perfusion provided the better diagnostic performance than regional CFR, the opposite of the prior figure [29]. Although far superior to global perfusion, the data of this figure are also flawed by failing to account for resting perfusion heterogeneity due to endothelial dysfunction that may cause sufficient corresponding heterogeneity of CFR as to falsely indicate or mimic flow-limiting stenosis, thereby decreasing its diagnostic accuracy. This flaw is corrected by mapping pixel values of both stress perfusion and CFR as CFC, accounting for this heterogeneity for the optimal quantification of physiologic severity of diffuse and focal CAD [30].

Conflicts: Which Is Best for Diagnosis of Significant Stenosis, FFR_{CT} or Quantitative PET Perfusion?

A simulated FFR predicted by CT angiography analysis (FFR_{CT}) estimates FFR, a relative CFR, based on angiographic analysis using computational fluid dynamics [31–38]. Figure 6.19 shows AUC of ROC curves for various imaging modalities showing that simulated FFR_{CT} is superior to PET for predicting invasive pressure–derived FFR (Fig. 6.19a) only after excluding the 17% of FFRct failures to produce useable data. When all cases were analyzed for intention to treat, as done for routine clinical purposes, PET is clearly superior for both per patient and per artery analysis (Fig. 6.19b) as noted by the highest AUC of the ROC highlighted in yellow.

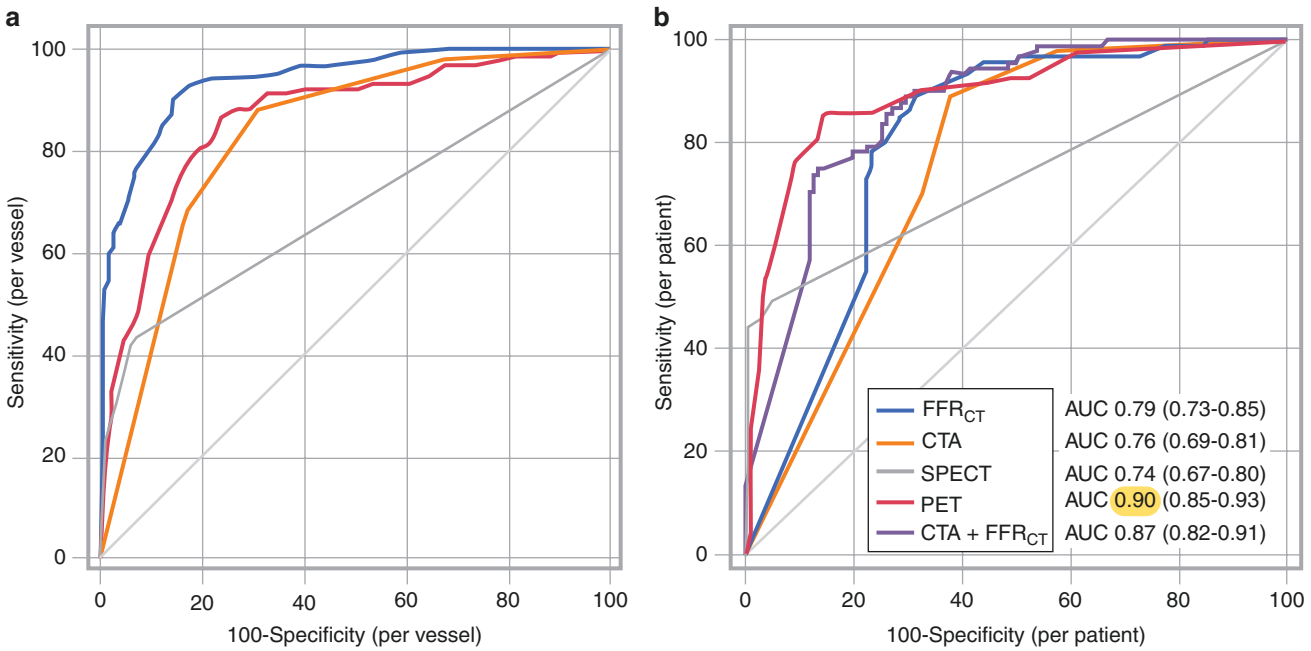

Diagnostic Performance for the Detection of CAD on an Intention-to-Diagnose Basis							
	FFR_{CT}	Coronary CTA	p Value*	SPECT	p Value*	PET	p Value*
Per vessel (n = 612)							
Sensitivity	92 (86-96)	70 (62-77)	<0.001	40 (32-48)	<0.001	80 (73-86)	0.004
Specificity	70 (65-75)	78 (74-82)	0.005	96 (94-98)	<0.001	76 (69-81)	0.013
PPV	52 (45-60)	52 (45-60)	0.727	81 (71-88)	<0.001	61 (53-68)	0.134
NPV	96 (92-98)	86 (82-90)	<0.001	80 (75-84)	<0.001	91 (87-94)	0.015
Diagnostic accuracy	77 (73-80)	76 (73-80)	1.000	81 (78-84)	0.238	80 (77-83)	0.355
AUC	0.83 (0.79-0.86)	0.80 (0.77-0.84)	0.261	0.68 (0.64-0.72)	<0.001	0.86 (0.83-0.89)	0.157

Fig. 6.19 Simulated FFR predicted by CTA analysis (FFR_{CT}) versus quantitative PET perfusion for diagnosis of significant stenosis. (**a**) ROC curves for the various imaging modalities listed. Driessen et al. [31] claim that FFR_{CT} is superior to PET for predicting invasive pressure–derived FFR, but this plot excludes the 17% of cases for which CT data were inadequate. (**b**) Analyzing all cases for intention to treat, as done for routine clinical purposes, PET is clearly superior, with the highest AUC (0.9). (*From* Driessen et al. [31]; with permission from Elsevier)

Conflicts: Which Is Best for Diagnosis of Significant Stenosis, CT Angiography (CTA) or Quantitative PET Perfusion?

In Fig. 6.20, the same PET center reported a previous paper with even stronger conclusions favoring PET. Based on the ROC curves favoring PET for predicting true pressure derived FFR ≤0.8 in this figure, Danad et al. [32] stated a strong conclusion as follows: "This controlled clinical head-to-head comparative study revealed PET to exhibit the highest accuracy for diagnosis of myocardial ischemia. Furthermore, a combined anatomical and functional assessment does not add incremental diagnostic value but guides clinical decision-making in an unsalutary fashion." Later figures explain why CTA and simulated FFR_{CT} fail to reflect the true measured physiologic severity of diffuse and focal CAD.

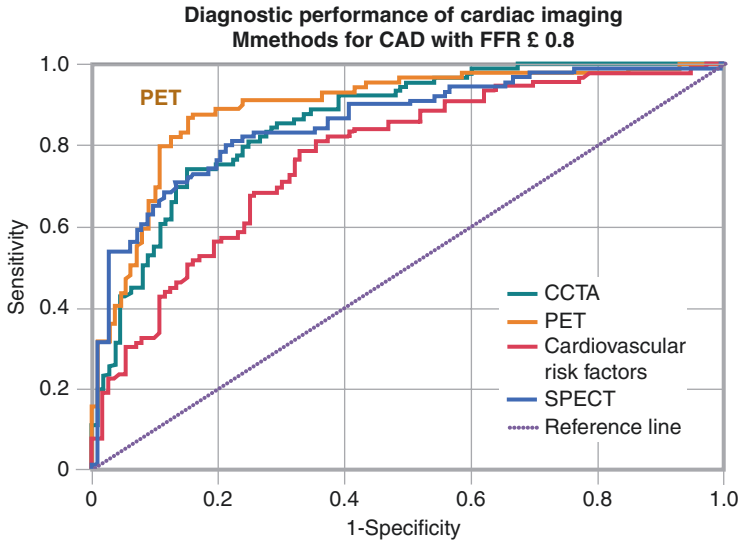

Fig. 6.20 Diagnostic performance of cardiac imaging methods for CAD defined as invasive pressure-derived FFR ≤0.8. CCTA coronary CT angiography. (*From* Danad et al. [32]; with permission from the American Medical Association)

PET superiority over CTA has been reported by other centers doing both [31–36], as summarized in the table shown in Fig. 6.21 (highlighted by the red box). The limited resolution of CTA incurs substantial uncertainty of angiographic arterial border recognition, with test-retest variability of simulated FFRct of 0.2 FFR units on the left Bland Altman scatter plot [35]. Given this variability, for the pressure-derived FFR threshold of 0.8, the simulated FFR_{CT} can be 0.6 or 1.0, an uncertainty that precludes its use for quantifying physiologic severity of CAD to guide revascularization. The right Bland Altman scatter plot is for simulated FFR based on the invasive coronary angiogram that has better resolution than CT angiogram [36]. The variability of simulated FFRangiogram called QFR is smaller than the simulated FFRct but remains unacceptably too high for reliable personalized guidance of interventions in individual patients.

The performace of different tests for anatomically and functionally significant coronary artery disease

Anatomically significant CAD					Functionally significant CAD				
Test	Sensitivity (%), (95% CI)	Specificity (%), (95% CI)	+LR (95% CI)	–LR (95% CI)	Test	Test	Sensitivity (%), (95% CI)	Specificity (%), (95% CI)	+LR (95% CI)	–LR (95% CI)
					ICA		68 (60–75)	73 (55–86)	2.49 (1.47–4.21)	0.44 (0.36–0.54)
Stress ECG	58 (46–49)	62 (54–69)	1.53 (1.21–1.94)	0.68 (0.49–0.93)						
Stress echo	85 (80–89)	82 (72–89)	4.67 (2.95–7.41)	0.18 (0.13–0.25)						
CCTA	97 (93–99)	78 (67–86)	4.44 (2.64–7.45)	0.04 (0.01–0.09)	CCTA		93 (89–96)	53 (37–68)	1.97 (1.28–3.03)	0.13 (0.06–0.25)
SPECT	87 (83–90)	70 (63–76)	2.88 (2.33–3.56)	0.19 (0.15–0.24)	SPECT		73 (62–82)	83 (71–90)	4.21 (2.62–6.76)	0.33 (0.24–0.46)
PET	90 (78–96)	85 (78–90)	5.87 (3.40–10.15)	0.12 (0.05–0.29)	PET		89 (82–93)	85 (81–88)	6.04 (4.29–8.51)	0.13 (0.08–0.21)
Stress CMR	90 (83–94)	80 (69–88)	4.54 (2.37–8.72)	0.13 (0.07–0.24)	Stress CMR		89 (85–92)	87 (83–91)	7.10 (5.07–9.95)	0.13 (0.09–018)

Note: ICA itself was used as a reference standard for the ananomically significant CAD estimates but was included as a technique when FFR was used as the reference. Not every test had enough data using FFR as reference.
CCTA coronary computed tomography angiography; CI, confidence internal; CMR stress cardiac magnetic resonance ECG electrocardiogram ICA invasive coronary angiography; LR likelihood ratio; PET, positron emission tomography; SPECT, single photon emission computed tomography (exercise stress SPECT with or without dipyridamole or adenosine); Stress echo, exercise stress echocardiography.

The performace of non-invasive test to rule-in and rule-out significant coronary artery stenosis in patients with stable angina: a meta-analysis focused on post-test disease probability

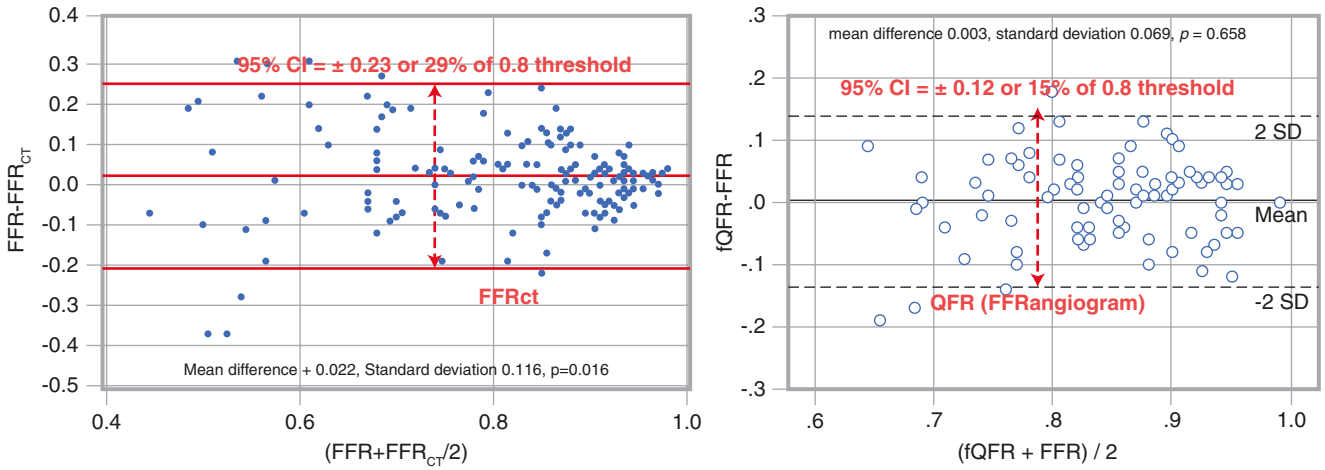

Fig. 6.21 The performance of different tests for anatomically and functionally significant CAD [34]. (*Left*, *From* Koo et al. [35], with permission from Elsevier; *Right*, Tu et al. [36], with permission from Oxford University Press)

Conflicts: What Is the Prevalence of Microvascular Disease?

Figure 6.22a reports reduced global CFR ascribed to microvascular dysfunction in 54% of cases [37], whereas Fig. 6.22b shows 1% prevalence of low CFR in the absence of regional PET perfusion abnormalities confirmed by CTA with no CAD, and 9% prevalence for non-obstructive CAD [38]. The flaw in the high reported prevalence of in Fig. 6.22a is the result of using global CFR, which fails to account for regional perfusion defects due to focal flow-limiting stenosis, which is the most common clinical manifestation of CAD, in addition to diffuse coronary atherosclerosis.

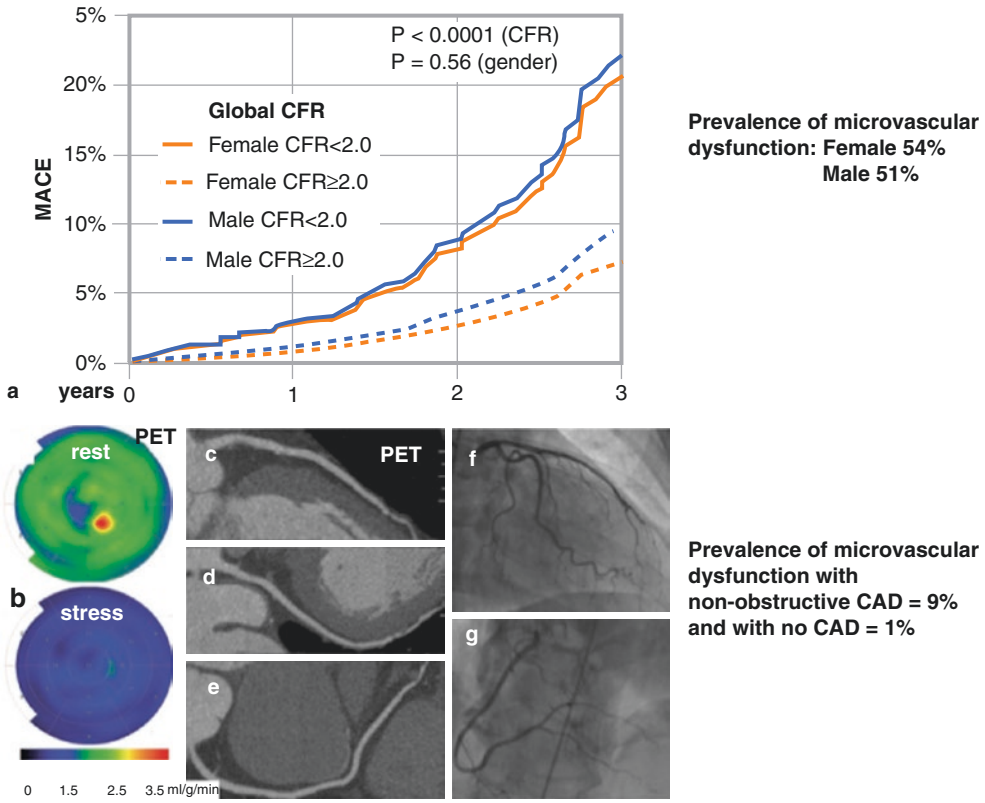

Fig. 6.22 Prevalence of microvascular dysfunction: conflicting conclusions. (**a**) Reduced global CFR is ascribed to microvascular dysfunction in 54% of cases [37]. (**b**) Prevalence of low CFR is 1% in the absence of regional PET perfusion abnormalities confirmed by CTA with no CAD, and 9% for non-obstructive CAD [38]. MACE major adverse cardiac events. (**a** *from* Murthy et al. [37], with permission from the American Heart Association; **b** *from* Stenström et al. [38]; with permission from Oxford University Press)

The table in Fig. 6.23 shows the prevalence of strictly defined microvascular angina in 5900 sequential diagnostic PETs meeting the following criteria: angina, no known CAD, global CFR ≤2.2, and no stress-induced relative defects (defined as no rest-to-stress change >5% of LV with ≤60% of maximum activity). Such strictly defined cases are uncommon, found in only 21 cases (0.4%), with females comprising 62% of the 21 cases, all with risk factors including coronary calcification and with abnormal quantitative PET perfusion images. For this analysis, the CFR threshold of 2.2 was chosen as a compromise between reported thresholds of 2.32 by Doppler wire and 2.0 by PET for microvascular impairment, compared with CFR of 4.2 ± 0.8 for 125 healthy, young volunteers [25].

Mixed Pathophysiologies of microvascular angina and function 5900 PETs

Criteria for microvas angina*	CFR ≤ 2.2*	CFR ≤ 2.2†	CFR > 2.0**	HIGH CFC°
Number of cases from 5900	21 (0.4%)	83 (1.4%)	167 (2.8%)	174 (3%)
Average maximum pixel CFR	2.27 ± 0.5	2.48 ± 0.5	3.91 ± 1.1	3.74 ± 1.2
Microvascular function	impaired	impaired	good	good
FFRpet < 0.7 for >10% LV††	9/21 (43%)	45/84 (54%)	53/167 (32%)	43/174 (25%)
Female	62%	39%	35%	48%
Risk factors or coronary Ca+	yes	yes	yes	yes
MI or death over 9 years***	2/21 (9.5%)	8/83(9.6%)	9/167 (5.4%)	6/174 (3.5%)
Approximate MI or death/yr	1%/yr	0.8%/yr	0.6%/yr	0.4%/yr

Fig. 6.23 Prevalence of strictly defined microvascular angina, subclinical coronary atherosclerosis and mortality risk in 5900 diagnostic rest stress quantitative PETs [25]. *Angina, *No known CAD*, global CFR ≤ 2.2 and no stress induced relative defects defined as rest to stress change of >5% of LV with ≤60% of maximum activity. †Angina, *Known CAD* by angiogram, procedures or events but no stress induced relative defects as defined above. ††Fractional Flow Reserve as relative absolute stress perfusion PET reflecting low subendocardial perfusion. **Angina, global CFR >2.2, no stress induced relative defects as defined above, includes *No Known CAD* and *Known CAD* by angiogram, procedures or events but no stress induced relative defects as defined above. °Angina, High Coronary Flow Capacity (>70% of the LV normal (red) or minimally reduced (orange) CFC (CFR >2.4 and stres > 1.8 cc/min/g)). +MESA risk score >7%

If the above criteria are expanded to include established CAD by angiography, procedures, or clinical events but still with no relative stress defects as defined above, prevalence of angina without obstructive CAD is somewhat greater, 83 of 5900 (1.4%), with 39% female. Approximately half had relative stress perfusion or fractional flow reserve of quantitative stress PET images <0.7 (FFRpet) for >10% of LV. This reduced FFRpet associated with reduced relative subendocardial perfusion is consistent with a fall in coronary pressure due to sufficient microvascular function to increase perfusion through mild, diffuse, epicardial coronary atherosclerosis, with a corresponding fall in coronary pressure causing low subendocardial perfusion.

During follow-up of up to 9 years, there were 8 MIs or deaths among the 83 cases of angina with diffuse but no obstructive CAD (9.6%, or approximately 1.0% per year), consistent with treated risk factors. These observations from our large cohort expand prior limited reports on strictly defined microvascular syndromes with a similar low prevalence and relatively low risk [25]. In comparison, severely reduced CFC is associated with a 30% prevalence of MI, death, or stroke during a comparable period [39].

A core relevant clinical insight is that the same strictly defined microvascular dysfunction but without angina is common (ie, global CFR ≤2.2, and no stress-induced relative defects as previously defined). Asymptomatic microvascular dysfunction as defined above was measured in 734 of 5900 patients (12.4%), with females comprising 39%; 96% had risk factors or coronary calcium. Over 9 years of follow-up, there were 20 MIs or deaths among the 734 patients (2.7%, approximately 0.3% per year), consistent with treated risk factors [25].

Thus, microvascular dysfunction defined above is common *without angina*. It is comparably prevalent in men and women and is nearly always associated with risk factors, coronary calcium, or subclinical CAD. It is associated with a relatively low risk of MI or death for treated risk factors.

In addition to the essential distinction between global and regional CFR, as shown above, global CFR may also reflect inadequate methodology that precludes reliable regional perfusion measurements. Prior literature indicating failed quantitative flow data in 12% of cardiac PETs [22] is not suitable for clinical purposes. By contrast, in our reported 5900 sequential clinical PETs with routinely quantified myocardial perfusion, only 0.7% of all studies had suboptimal flow data, due primarily to scanner failure or venous abnormalities precluding arterial input [25].

Making Physiologic Displays That Are Clinically Useful

Even though cardiologists and cardiac surgeons continuously use terms like *low coronary blood flow*, *ischemia*, and *revascularization to improve coronary blood flow*, most of them have never performed measurements or understood them quantitatively, including the threshold for ischemia or mortality risk, its relation to diffuse or multi-stenosis or to coronary pressure or FFR measurement or to subendocardial perfusion or its multiple control mechanisms. Because of the large, conflicting literature, they also may poorly understand the changes after revascularization—that is, clinical quantitative coronary physiology and the PET technology that best quantifies it.

A confusing jumble of distorted perfusion anatomy and quantitative data (as in Fig. 6.24) characterizes most displays of quantitative PET perfusion. These displays fail to inform, clarify, or improve clinical application of quantitative coronary physiology for patient management. Cardiologists will not use or depend on any data or images that they cannot easily, quickly, comprehensively, and correctly understand, interpret, and relate directly to their deeply embedded fluoroscopic, angiographic, or surgical views of the heart. Such displays also reveal a fundamental misunderstanding of the complex interdependency of coronary-specific imaging physics and dynamic coronary physiology. At the boundaries of epicardium and endocardium, activity is the lowest and most variable, thereby making the borders drawn in this figure highly uncertain. A calculated average perfusion within these boundaries is therefore also so highly variable as to preclude clinical reliability.

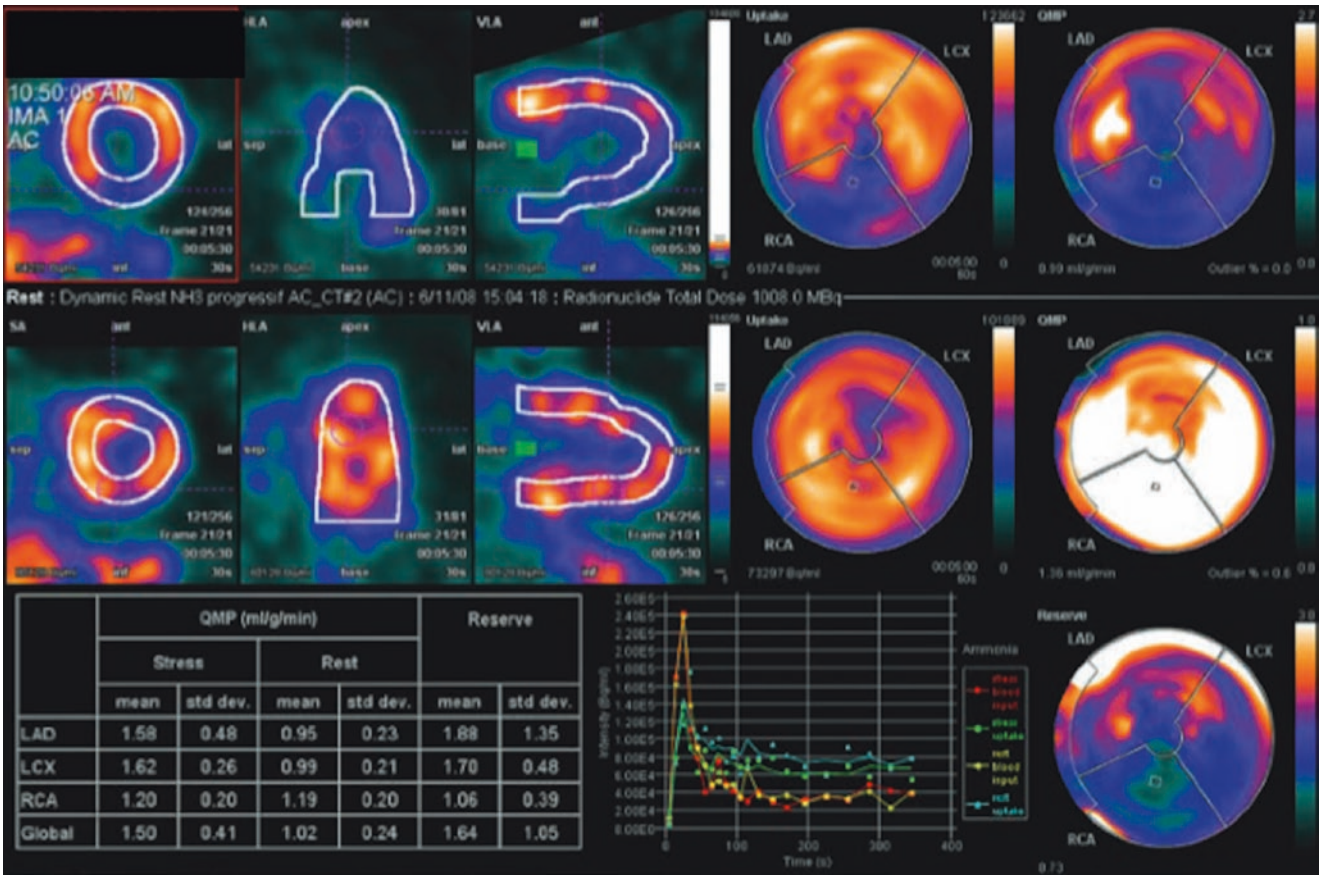

	QMP (ml/g/min)				Reserve	
	Stress		Rest			
	mean	std dev.	mean	std dev.	mean	std dev.
LAD	1.58	0.48	0.95	0.23	1.88	1.35
LCX	1.62	0.26	0.99	0.21	1.70	0.48
RCA	1.20	0.20	1.19	0.20	1.06	0.39
Global	1.50	0.41	1.02	0.24	1.64	1.05

Fig. 6.24 A confusing jumble of distorted perfusion anatomy and quantitative data, characteristic of most displays of quantitative PET perfusion that are not commonly readily understood by interventionalists

Clinically relevant and anatomically correct physiologic views (as appear later in this chapter), with comprehensive clinical integration by an experienced, self-critical, clinical cardiologist-physiologist consultant, generate an evolving bidirectional trust within the cardiac team, in which quantitative coronary physiology drives optimal patient outcomes that are documented by hard outcomes in peer-reviewed publications.

The display in Fig. 6.25 concerns a patient who had risk factors, dense coronary calcium, an equivocal or positive SPECT scan and rest stress PET at another institution. However, the referring cardiologist was not able to understand or make a clinical decision about an invasive or medical approach from this quantitative display or its report. Therefore, he sent the patient to Houston for a definitive, clinically oriented rest-stress PET recommendation, including our *Cardiac Positron Imaging and Consultation Report* with the images in Fig. 6.26.

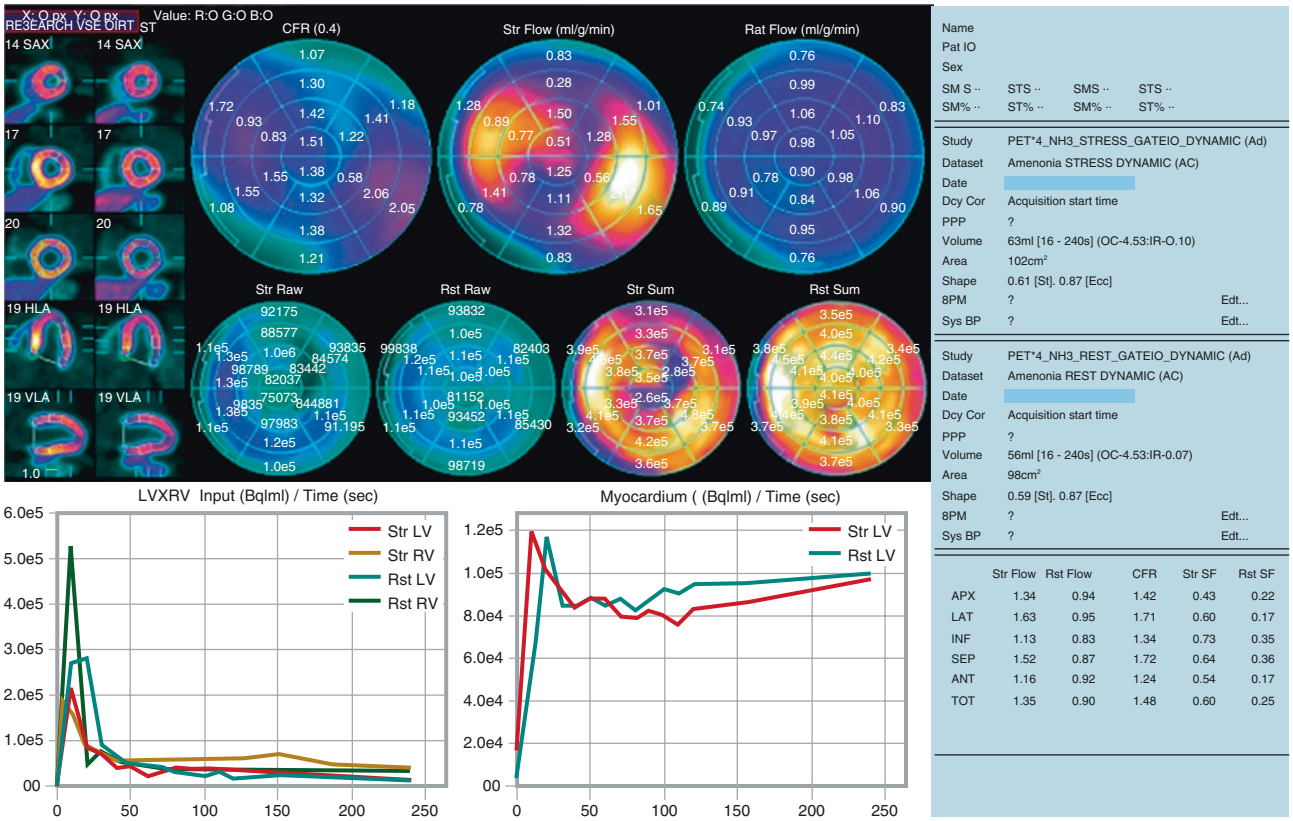

Fig. 6.25 Case example of a confusing physiologic display and report that was not readily understood by the referring cardiologist

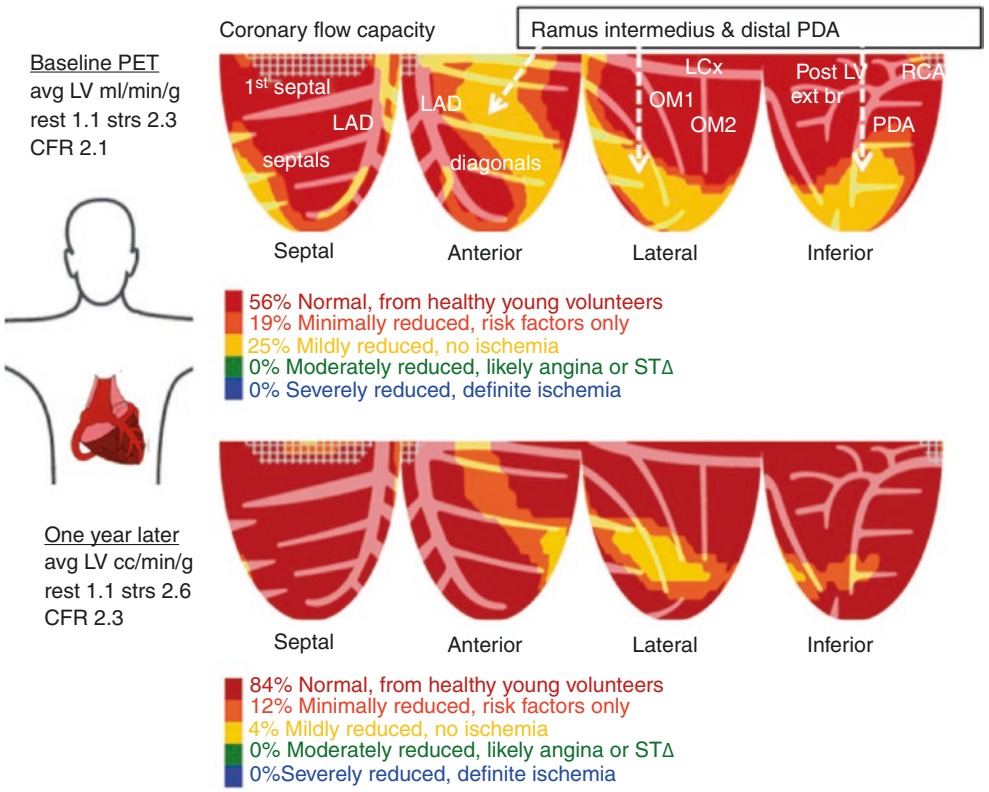

Fig. 6.26 The same case as in Fig. 6.25, definitively resolved by a CFC map. The CFC map for this patient showed mildly reduced CFC in 25% of the LV, well above ischemic levels. The distribution is characteristic of a large ramus intermedius distribution, typically extending to the lateral apex. The mildly reduced CFC in the distal and inferior apex is typical of diffuse RCA or wrap-around LAD disease. The patient had no angina or STΔ, and CFC is good to excellent throughout the remaining 75% of the LV

The referring cardiologist and patient immediately understood the images of Fig. 6.26 showing mildly reduced CFC in the distribution of Ramus Intermedius branch associated with very low risk over 10 years that would not be benefited by PCI; the risk may be increased by such a procedure since the risk of the procedure is higher than the 10-year risk of adverse events for this mildly reduced CFC [39]. The PET data and report therefore indicated intense medical management without an invasive angiogram. Both the patient and cardiologist were satisfied by the recommendation for appropriate vigorous risk factor management without an invasive procedure [2, 25, 27, 39–49].

To confirm this management decision, repeat PET 1 year later showed substantially improved CFC, which is mildly reduced in only 4% of the LV, with good to excellent CFC in the remaining 96% of LV, compared with mildly reduced CFC in 25% of the LV on the prior PET. Careful study of the prior common PET display in Fig. 6.25 indicates an abnormality corresponding to the baseline PET in Houston, but the 17-segment bulls-eye display spatially distorts the anatomic perfusion distribution and makes quantitative numbers difficult to see or interpret. The 17-segment method often mis-assigns coronary perfusion territories and cannot account for inherent morphological and regional artery-specific variability in different patients [14, 50–56].

True full-quadrant views of the LV and its coronary artery tree are visually distorted on the bulls-eye view, as illustrated by the example in Fig. 6.27, which shows a severe inferolateral and inferior apical defect. In order to fit the true full quadrant views into the pie display, basal segments must be enlarged and apical segments must be reduced in size [14]. Consequently, a stress defect comprising 19% of the LV appears visually on the bulls-eye display to comprise only 7% of the bulls-eye, primarily inferior because the lateral component is largely distorted out of the bulls-eye image. Although the calculated size of the defect as a percentage of all LV pixels is the same for both displays, the appearance is sufficiently distorted on the bullseye display to mislead visually driven decisions typical of cardiology or to breed distrust of numbers that fail to match the visual impression of size.

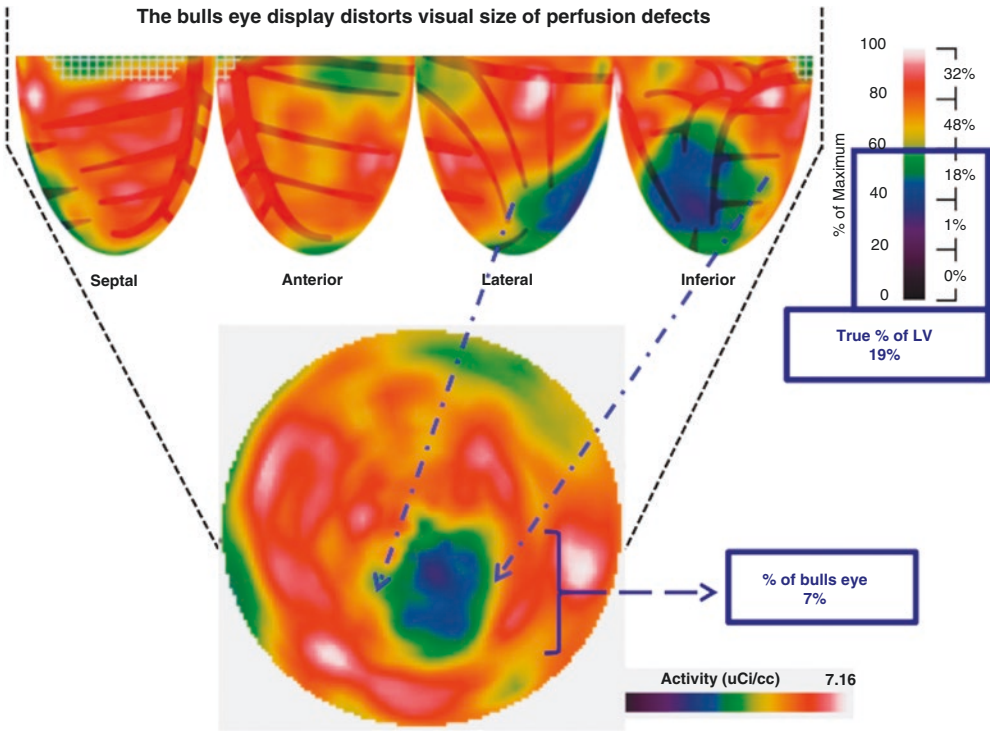

Fig. 6.27 Distortion of spatial perfusion anatomy by the bulls-eye display. To fit the full quadrant views of this example into the pie, basal segments must be enlarged and apical segments must be reduced in size. Consequently, a stress defect comprising 19% of the LV appears visually on the bulls-eye display to comprise only 7% of the bulls-eye, primarily inferior because the lateral component is largely distorted out of the bulls-eye image

Accordingly, we developed the four-quadrant topographic display to make the visual perfusion distribution match the quantitative size and severity of quantitative perfusion in coronary artery anatomic arterial distributions, as if actually looking at a transparent patient. This map of personalized perfusion anatomy for each artery and all its branches avoids the assumed generic 17-segment arterial distribution imposed on perfusion data, which forces flow values into arbitrary compartments that are commonly different from actual arterial and perfusion anatomy in any individual patient. A significant literature documents the errors and disadvantages of 17-segment bulls-eye displays [14, 50–56].

Interacting Clinical Physiology and Imaging Physics

Figure 6.28 illustrates the principles of measuring myocardial perfusion experimentally and by PET [14, 49, 57]. The interacting principles of imaging physics and quantifying myocardial perfusion derive from myocardial perfusion measured experimentally by radiolabeled microspheres. When radiolabeled microspheres are injected into the left atrium for adequate LV mixing, rapid arterial blood samples are drawn over precise time intervals to produce an arterial time-activity curve input distributed to the coronary arteries with 100% trapping of the microspheres in myocardium.

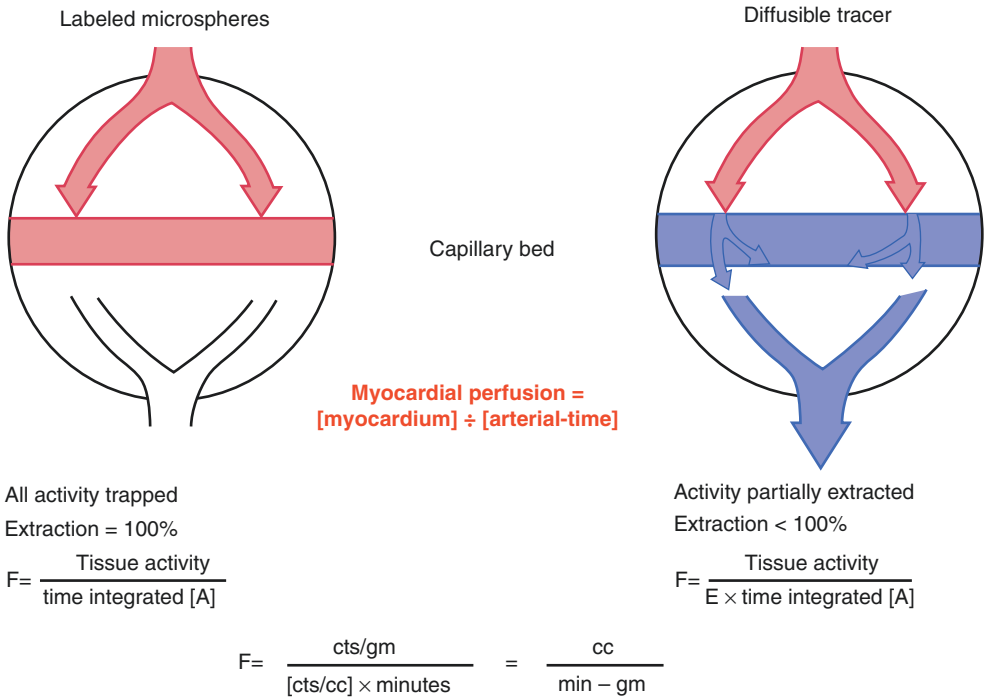

Fig. 6.28 Principles of measuring myocardial perfusion by PET [14, 49, 57]. (*From* Gould et al. [49]; with permission from McGraw-Hill Education)

Post mortem, the LV is diced into small pieces in a detailed map of each tissue sample for its location in the LV. Each myocardial sample is weighed and counted in a well counter. The measured activity in each myocardial sample divided by the arterial time-activity curve gives perfusion in cc/min/g of each small myocardial sample, which is mapped back to its position in the LV, thereby providing an LV map of perfusion in cc/min/g displayed in numbers, iso-contour lines, and gray or color scale schema.

PET perfusion imaging employs the same principle, using intravenous radionuclides that distribute as a time-activity arterial curve to the coronary arteries, best measured in the left atrium by PET imaging (for reasons shown later). Most of the radionuclides commonly used clinically are not 100% trapped by myocardium, but are only partially extracted. This extraction fraction ranges from 60% to 90%, depending on the radionuclide and on myocardial perfusion, decreasing as perfusion increases. Each pixel of quantified myocardial activity by PET divided by the arterial time-activity curve in the left atrium, corrected for partial extraction, gives cc/min/g in the LV location of that pixel.

As flow increases, myocardial trapping or extraction falls for the radionuclides most commonly used in clinical PET (Fig. 6.29). The mathematical perfusion model for each radionuclide accounts for this flow-dependent extraction to acquire the flow-independent myocardial retention for each pixel divided by the time-activity arterial input, thereby giving perfusion in cc/min/g analogous to the microsphere method. The claim that a radionuclide with high extraction measures perfusion better than a radionuclide with lower extraction is not true, as the correct perfusion model for each radionuclide has been proven experimentally to measure perfusion accurately when compared with the standard of radiolabeled microspheres.

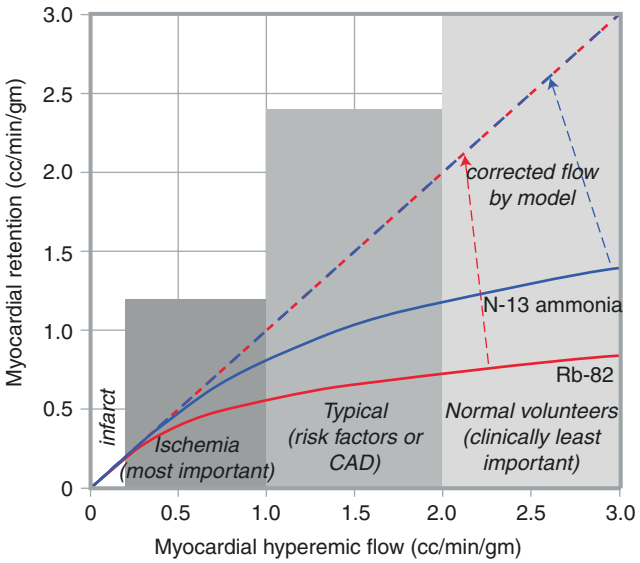

Fig. 6.29 Flow-dependent myocardial extraction of radionuclides

Figure 6.30 shows protocols for quantitative perfusion imaging using Rb-82 and dipyridamole, regadenoson, or adenosine vasodilator stress [2, 25, 27, 39–43, 49, 57–59]. Each stress has a different timing sequence to produce maximal stress perfusion, as systematically tested and reported by this clinical laboratory and now used worldwide.

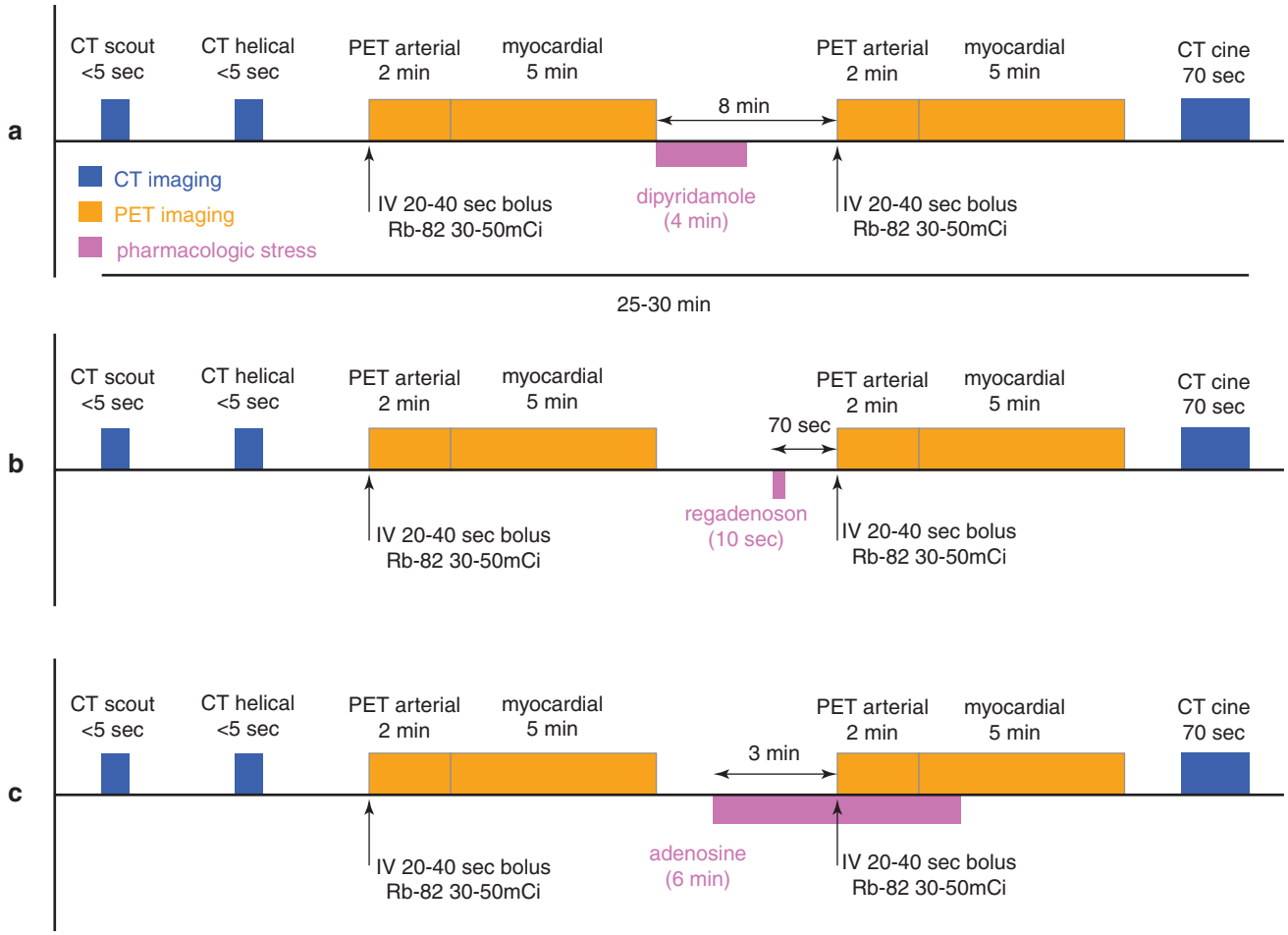

Fig. 6.30 Protocols for quantitative perfusion imaging using Rb-82 and dipyridamole (**a**), regadenoson (**b**), or adenosine (**c**) vasodilator stress. Each stress has a different timing sequence to produce maximal stress perfusion

Figure 6.31 shows normal rest and stress images of myocardial activity for one of four quadrant views, with a color bar scale of activity in μCi/cc [49]. The CT attenuation scan shows anatomy of the various vascular structures. The early arterial activity images acquired over the first 2 minutes after starting Rb-82 infusion show the left atrium and ascending aorta as sites for region of interest (ROI) placement to acquire the time-activity arterial input to the flow-model equations for each myocardial pixel. ROI placement is guided by the PET image activity, not the CT scan that is not reliable for obtaining correct arterial activity.

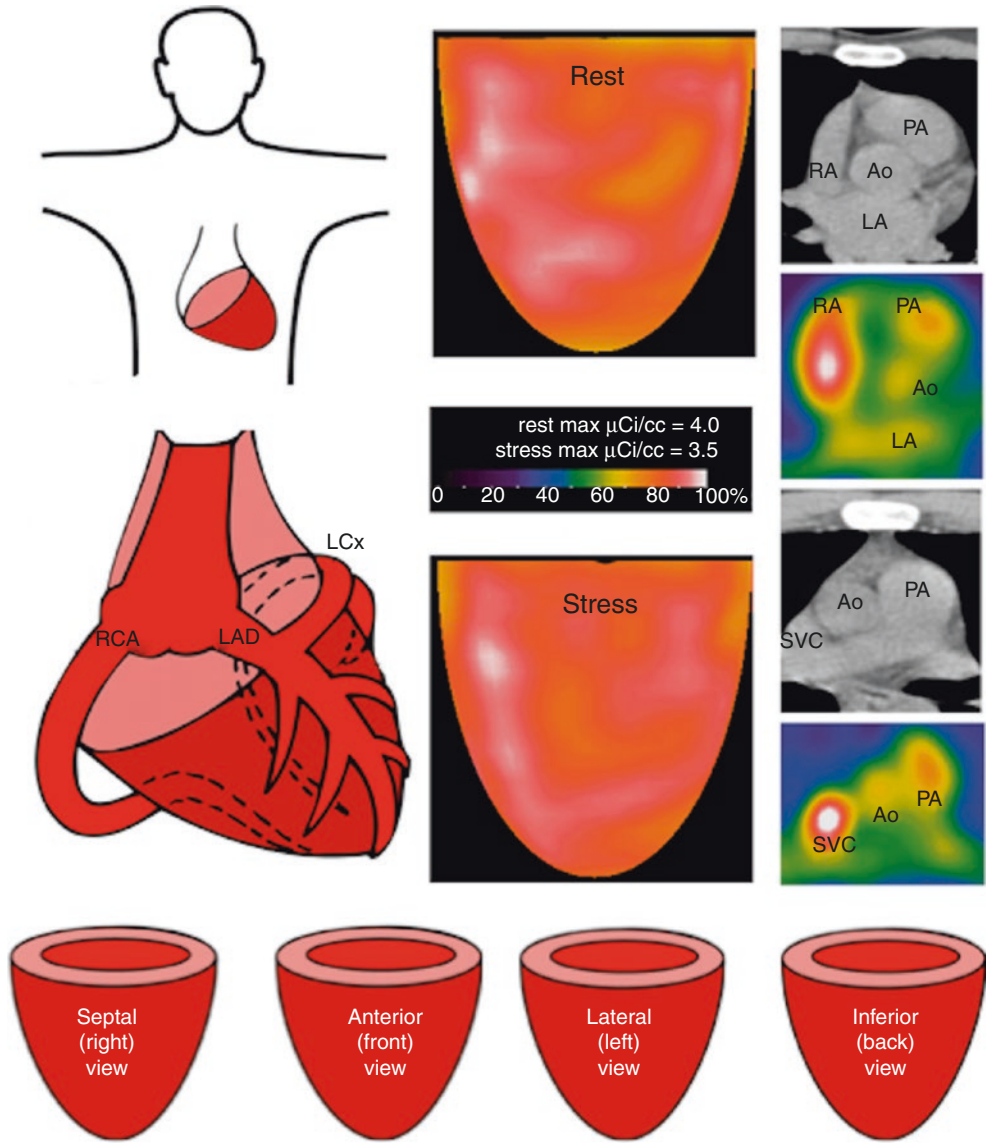

Fig. 6.31 Schematic orientation of cardiac PET images [49]. The CT anatomy is shown only to familiarize the reader with the arterial phase activity structures (LA and aorta). (*From* Gould et al. [49]; with permission from McGraw-Hill Education)

The rest and stress time-activity plots seen in Fig. 6.32 are fit to the mathematical flow model to solve for the unknowns, one of which is myocardial perfusion in cc/min/g for each pixel of the image. This method, called *compartmental modeling*, requires short serial images of 10–15 seconds each, in order to construct the time-activity curves [14, 49, 57]. However, such short images are very "noisy," with such great statistical variability of activity as to degrade calculated perfusion so much that perfusion on a pixel basis is not reliable, thereby requiring large, arbitrary segments of the LV to average out statistical uncertainty.

Compartmental modeling - four unknowns & two measured

$$M(t)=V_F C_a(t)*bte^{-at} + F[1- e^{-(0.45+0.16F)/F}] \int_0^t C_a(x)*bxe^{-ax}dx$$ Where
M(t), Ca(t) are measured. F, V_F, a, b are found by curve fitting the model.

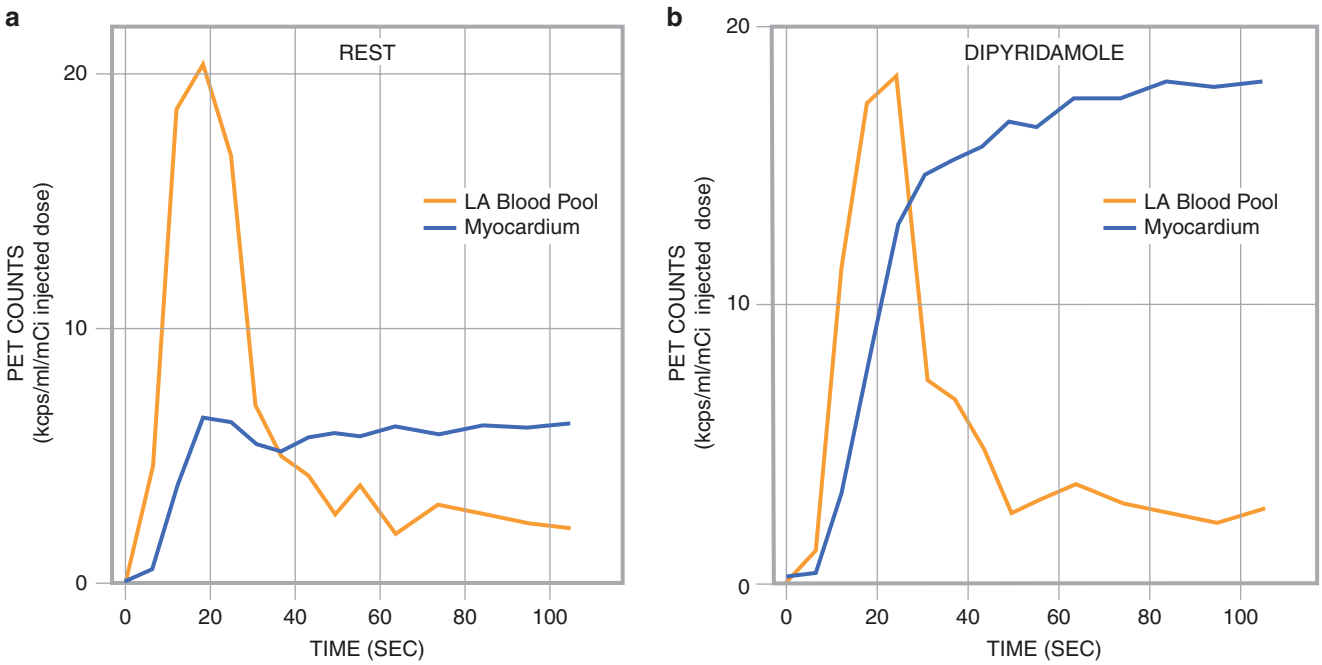

Fig. 6.32 Experimental arterial and myocardial time-activity curves. The rest and stress time-activity plots are fit to the mathematical flow model to solve for the unknowns (*red terms*), one of which is myocardial perfusion in mL/min/g for each pixel of the image. (*Reproduced with permission from* Yoshida et al. [57])

These short images are also of such poor quality as to preclude repeatable, accurate location of an ROI directly on the central left atrium or aorta for arterial activity in a dynamically moving heart. With each systole, the heart translates inferior and medially by 1–2 cm, and another 2 cm or more during the respiratory cycle [14, 49, 58]. To overcome this degradation of data, other PET sites estimate the left atrial site for ROI by back projection from later myocardial images, which may not be optimally located in the left atrium of the moving, translating heart.

To overcome such image degradation, for 2D imaging we developed a "simplified" acquisition protocol and model (Fig. 6.33), which has the least variability (±10%) reported in the literature [14, 49, 58]. Our "simple" 2D imaging model acquires a 2-minute image and a 5-minute image beginning with intravenous infusion of Rb-82 (with a half life of 75 seconds) from a commercially available Rb-82/strontium-82 generator. The single early 2-minute image provides good images for optimally placing an ROI in the central left atrium and aorta of several tomographic slices to find the optimal integrated arterial time-activity value within the range of cardiac motion, while avoiding spillover activity from venous structures, particularly the pulmonary arteries immediately adjacent to both the aorta and left atrium.

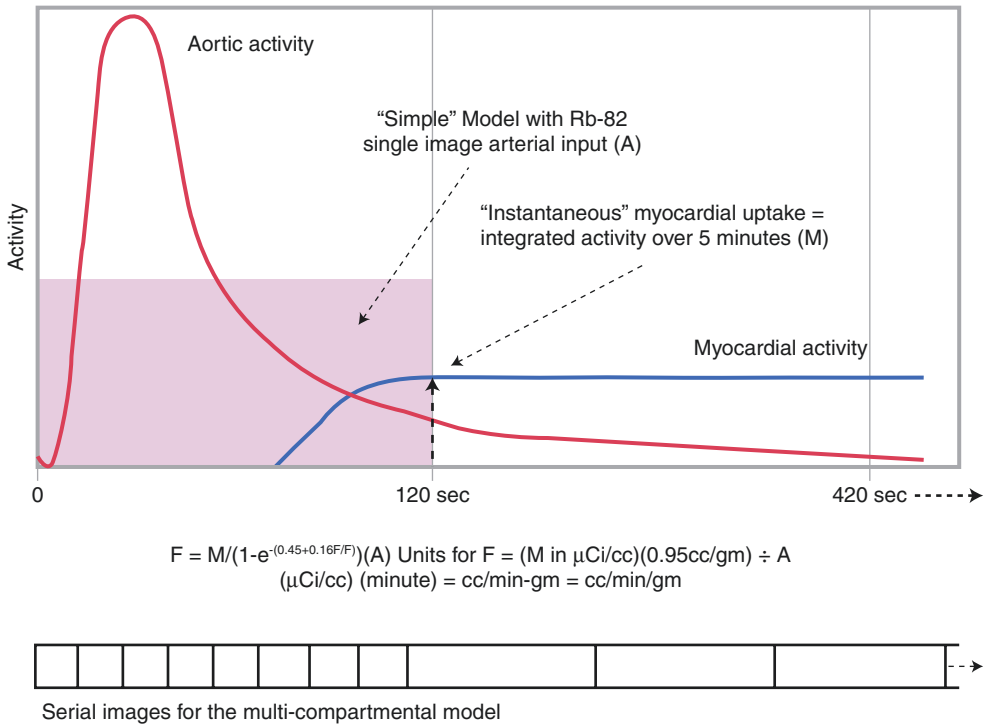

Fig. 6.33 Solution to limitations of short serial statistically poor images used in compartmental modeling. The protocols for serial short images for compartmental modeling to determine perfusion are shown schematically at the bottom of this figure. (*From* Gould et al. [49]; with permission from McGraw-Hill Education)

The good 2-minute arterial image quality also minimizes statistical noise and corresponding variability in perfusion measurements for each pixel mapped back to the LV. This approach avoids assuming arbitrary large regions for perfusion measurements needed to reduce statistical noise of short serial images in compartmental analysis. Because Rb-82 extracted into myocardium is trapped and does not "leak out" within its imaged half-life, decay-corrected myocardial activity remains constant, thereby providing high-quality myocardial images for regional per-pixel distribution of perfusion.

Figure 6.34 illustrates the proximity of venous structures, right atrium (RA), and pulmonary arteries (PA) as sources of potential activity spillover that erroneously increases arterial input and erroneously lowers perfusion values. Alternatively, heart translation and motion may move the left atrium or aorta in and out of an arbitrary, estimated left atrium (LA) or aortic (Ao) location—"smearing the activity" and thereby recording lower than true activity with consequent erroneously high perfusion values. Our high-quality 2-minute and 5-minute images avoid these issues inherent in compartmental modeling of multiple serial short, statistically poor images.

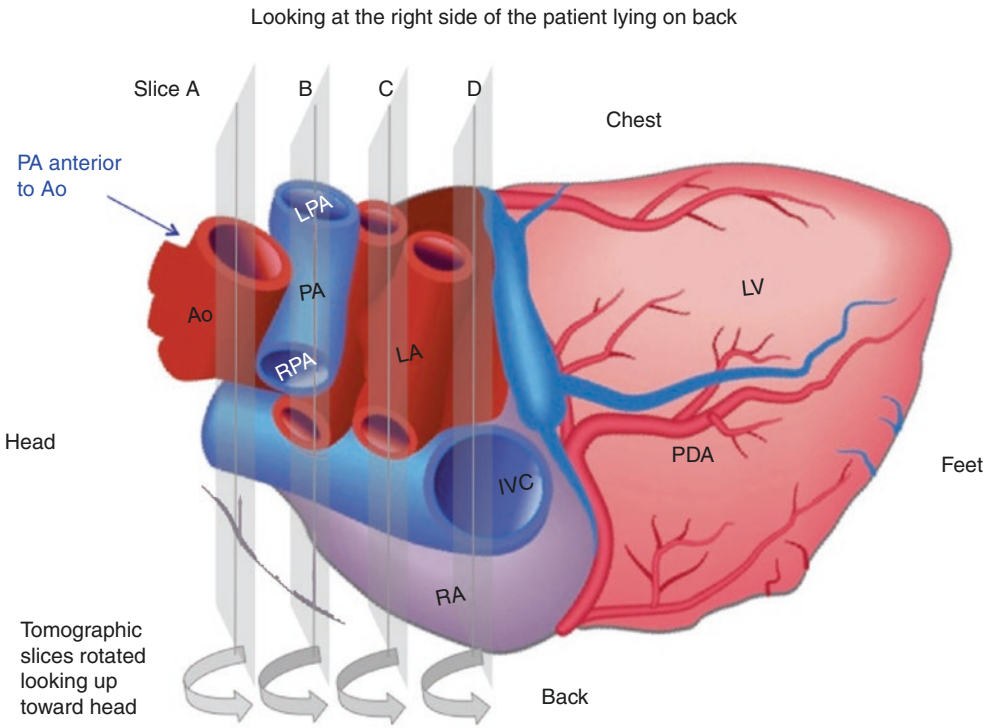

Fig. 6.34 Vascular anatomy and cross-sectional slices. IVC inferior vena cava, PDA posterior descending artery. (*From* Gould et al. [49]; with permission from McGraw-Hill Education)

Figure 6.35 presents PET and CT views of arterial activity and anatomy [49, 58–60]. The early 2-minute image during intravenous infusion of Rb-82 shows characteristic three round structures of activity that is highest in the superior vena cava (SVC), next highest in pulmonary artery (PA) and lowest in left atrium (LA) and ascending aorta because of cardiac output diluting the intravenous activity. Arterial activity is measured in the small ROIs placed optimally in the central LA and ascending aorta.

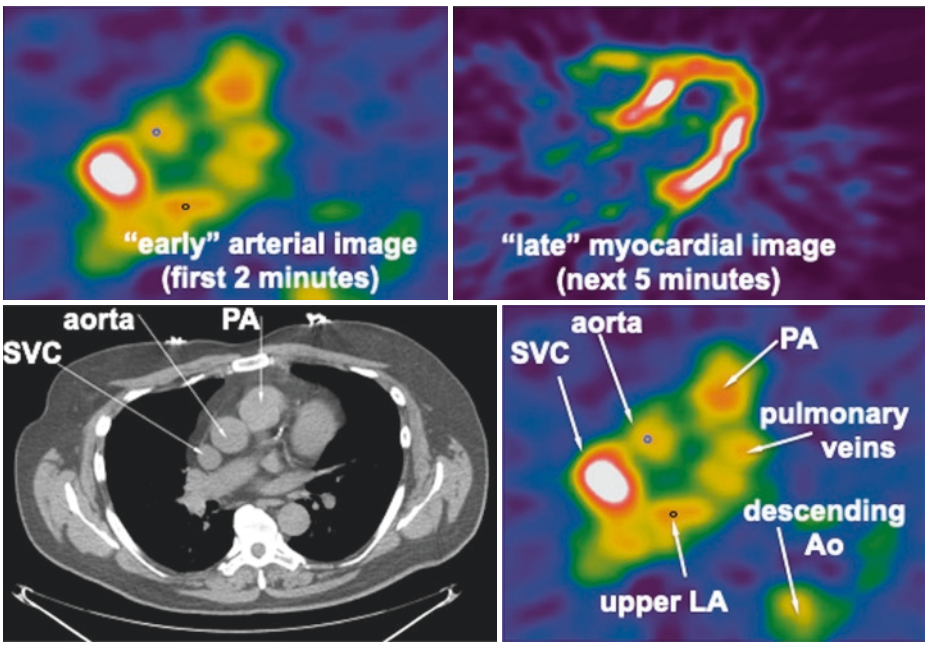

Fig. 6.35 PET and CT views of arterial activity and anatomy. Although not used for locating the arterial ROI, for teaching purposes the CT scan documents the structures as seen in slice B of Fig. 6.34 [2, 58]

Figure 6.36 illustrates experimental validation of our compartmental model and "simple" model for myocardial perfusion [14, 49, 57]. Both compartmental and simple flow models correlate with radiolabeled microspheres for Rb-82 and for N-13 ammonia.

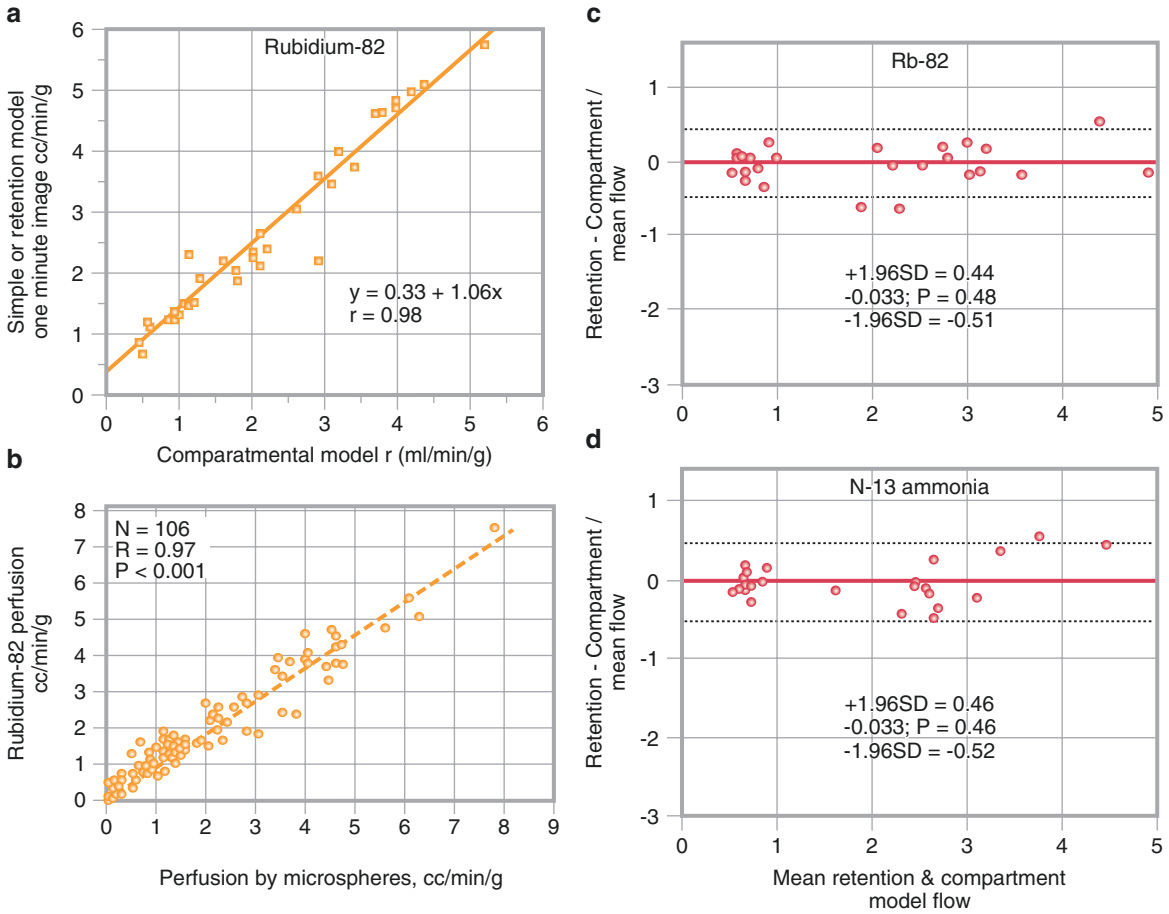

Fig. 6.36 Experimental validation of our compartmental model and "simple" model for myocardial perfusion. Both compartmental and simple flow models correlate with radiolabeled microspheres for Rb-82 (**a**) and for N-13 ammonia (**b**). The Bland Altman plots for variability between serial PET perfusion measurements for Rb-82 (**c**) and N-13 ammonia (**d**) are shown from the literature [60]. (**a** and **b**, *From* Yoshida et al. [57], with permission from the Society of Nuclear Medicine and Molecular Imaging, and from Gould et al. [49], with permission from McGraw-Hill Education. **c** and **d**, *From* Renaud et al. [60], with permission from Mosby)

Figure 6.37 shows experimental validation of perfusion using the oxygen-15 method compared with microspheres [61, 62]. Oxygen-15–labeled water from an onsite cyclotron is a freely diffusible radionuclide that requires a different model because it is not extracted or trapped by myocardium. The upper plot on this figure shows some scatter about the regression line due to variability on the PET-acquired arterial input. In the lower plot, on the other hand, the arterial input was measured by rapid serial blood samples drawn during the PET imaging. The validation of the three different radionuclides (O-15 water, N-13 ammonia, Rb-82) with their own specific acquisition protocols and models for calculating perfusion indicates that they provide equivalent perfusion measurement despite widely different behavior in the myocardium.

Image arterial and myocardial time activity curves were fitted to a single tissue compartment tracer kinetic model to estimate MBF in each myocardial region using O-15 water.

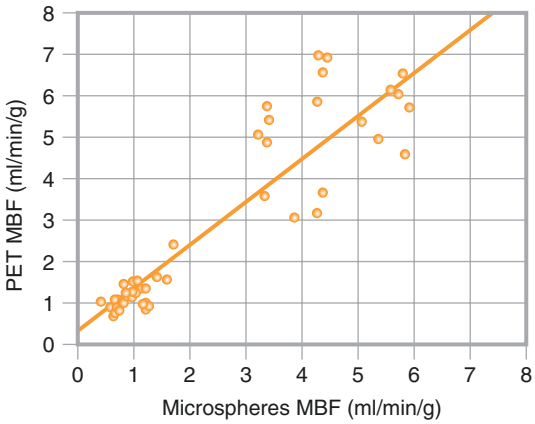

Image myocardial and blood sample time activity curves fitted to a single tissue compartment tracer kinetic model to estimate MBF in each myocardial region.

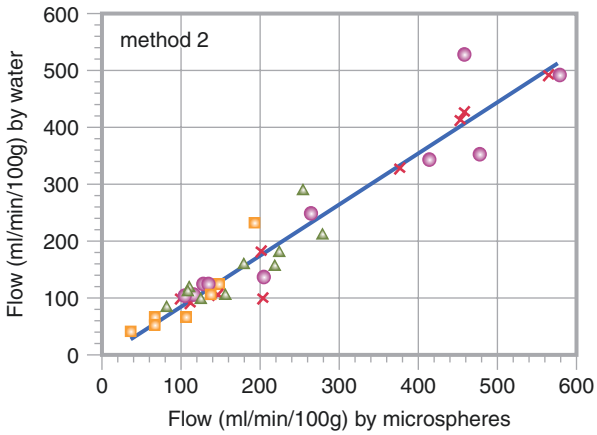

Fig. 6.37 Experimental validation of perfusion using the oxygen-15 method compared with microspheres. MBF myocardial blood flow. (*Upper panel from* Araujo et al. [61] and *lower panel from* Bol et al. [62]; with permission from the American Heart Association)

Myocardial perfusion reported in the literature was derived using two-dimensional (2D) PET scanners with a measured resolution of 1.0–1.5 cm [63]. Consequently, for constant myocardial activity corrected for time decay, activity recovery is substantially better during systole than during diastole because of the greater wall thickness during systole (Fig. 6.38). Diastolic images therefore are commonly heterogeneous owing to varying partial volume loss at different segments of the same slice, with anatomic wall thickness varying among the free wall, the papillary muscles, and the septum. The wall in systole is thicker and more anatomically uniform than in diastole. At resting heart rates, systole typically comprises one third of the cardiac cycle, but during tachycardia of stress, systole may comprise half of the heart cycle. Therefore, the partial volume loss changes dynamically with heart rate, as we have systematically demonstrated in clinical PETs with greater partial volume loss during bradycardia than tachycardia [63].

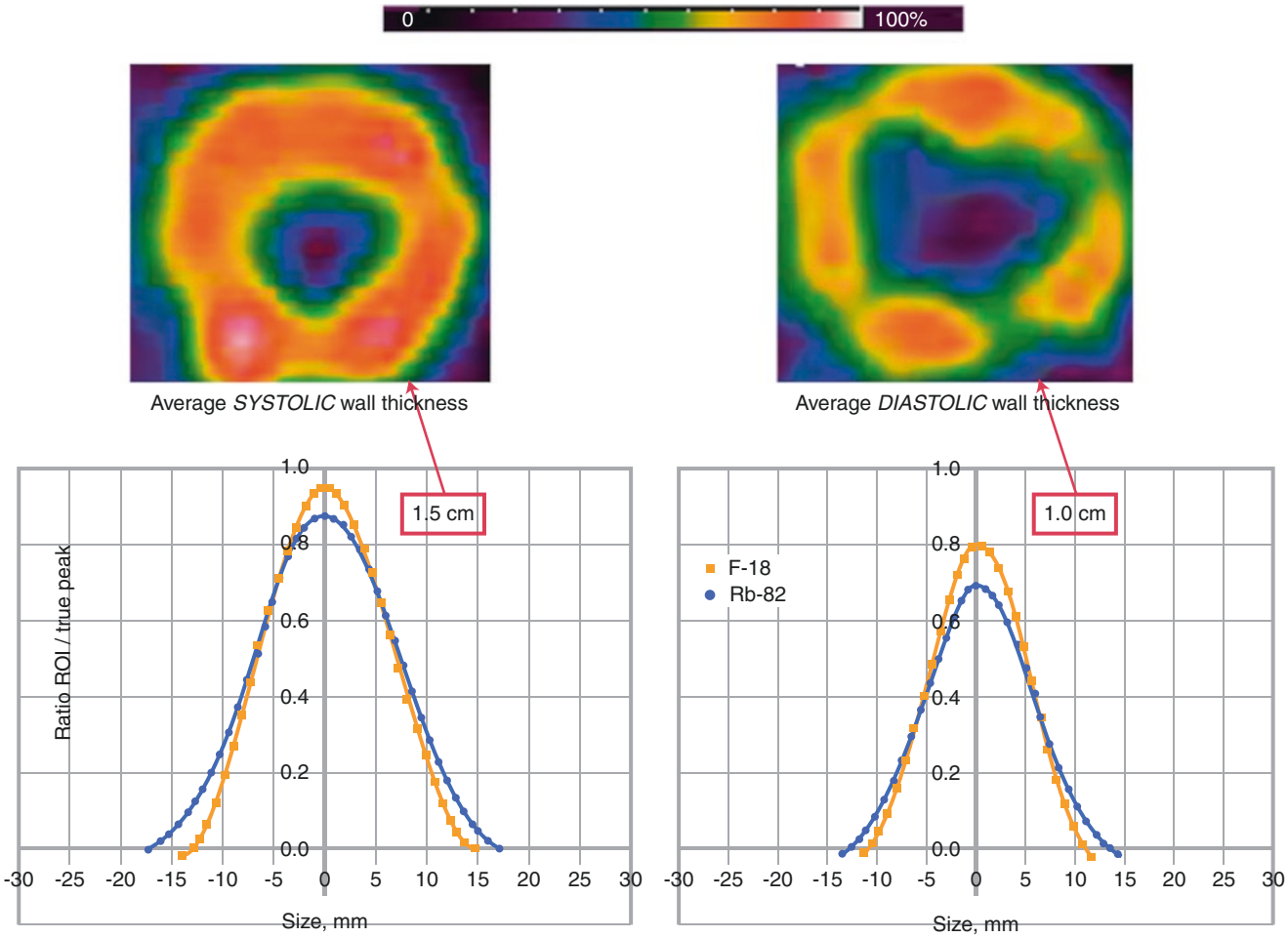

Fig. 6.38 Partial volume loss of activity recovery during systole and diastole

Activity recovery is so much greater in systole than in diastole that the average systolic activity dominates the cumulative myocardial activity over the time of acquisition [63]. Our "simple" model summarizes these complex time-varying partial volume losses by using a fixed partial volume correction based on average wall thickness derived from a branching phantom of various thickness in the one dimension of LV wall thickness for each specific scanner and radionuclide (Fig. 6.39). The correction of myocardial activity recovery in our model accounts for the longer positron ranges of Rb-82 than F-18 seen in this figure.

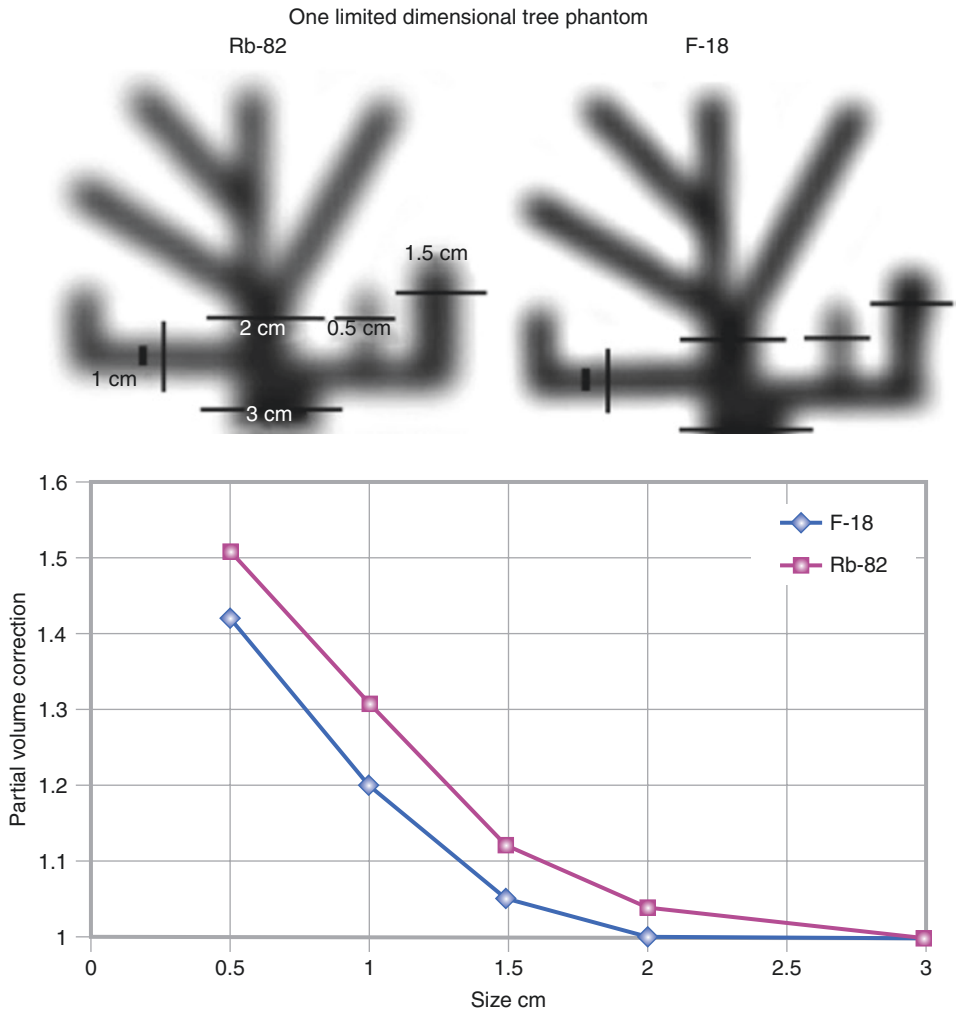

Fig. 6.39 Partial volume correction for perfusion measurements

The widely used compartmental modeling using multiple serial images calculates a partial volume correction as a term in the model equations by curve fitting time-activity curves to the model equations. However, the resulting partial volume corrections have never been extracted and published, to our knowledge. Given the low count density (statistical content) of the short serial images in a dynamically moving heart, the time-activity curves at the per-pixel level preclude the high precision and statistical pixel content required for curve-fitting the data to the model for determining the many unknowns, including partial volume correction and perfusion at the per-pixel level.

Our test-retest repeatability of PET perfusion in the same patient within minutes, ±10%, is the smallest variability reported in the literature, attesting to the validity of our simplified perfusion model and protocol [47], its good correlation to microsphere measurements experimentally [57], and its association with clinically relevant outcomes based on quantitative severity and size as a percentage of the LV [39].

Figure 6.40 shows the different positron ranges for the flow model of perfusion using Rb-82 and N-13 ammonia. On short-axis views of Rb-82, the LV wall appears thicker than for N-13 ammonia because of the longer positron range of Rb-82 [60, 63]. As shown in Fig. 6.41, this thicker appearance has no impact on our perfusion measurements based on maximal activity on radii from the LV center to the outside the myocardium. Both radionuclides provide similar validated perfusion despite differences in positron range, which is accounted for in their respective perfusion models.

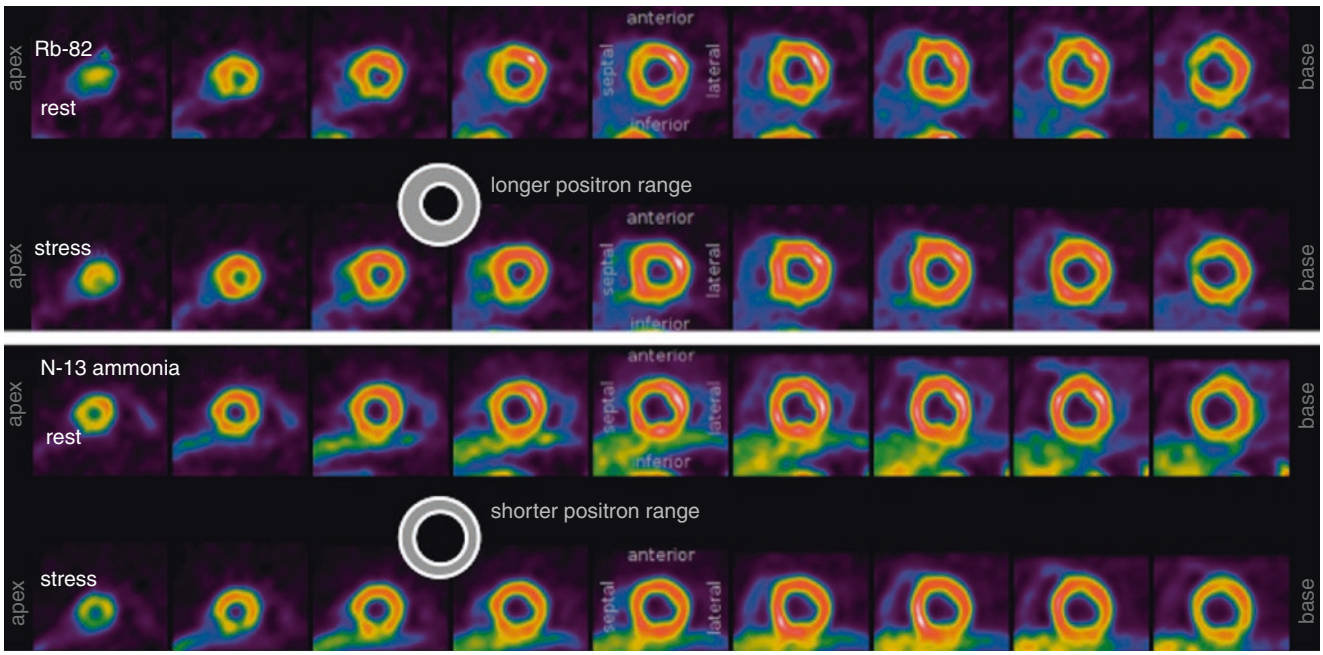

Compared to multi-compartmental analysis of sequential images (Ottawa), the simple retention model (Texas) was reported to have the following advantages:

- Values comparable to multi-compartmental analysis.
- Least variability of stress flow and coronary flow reserve.
- Most efficient simple acquisition and computation.
- Optimal ROI for arterial input.
- "Higher sensitivity for detection & localization of abnormal flow & myocardial perfusion reserve". (reference 62 Ottawa).

Fig. 6.40 Different positron ranges for the flow model of perfusion using Rb-82 and N-13 ammonia

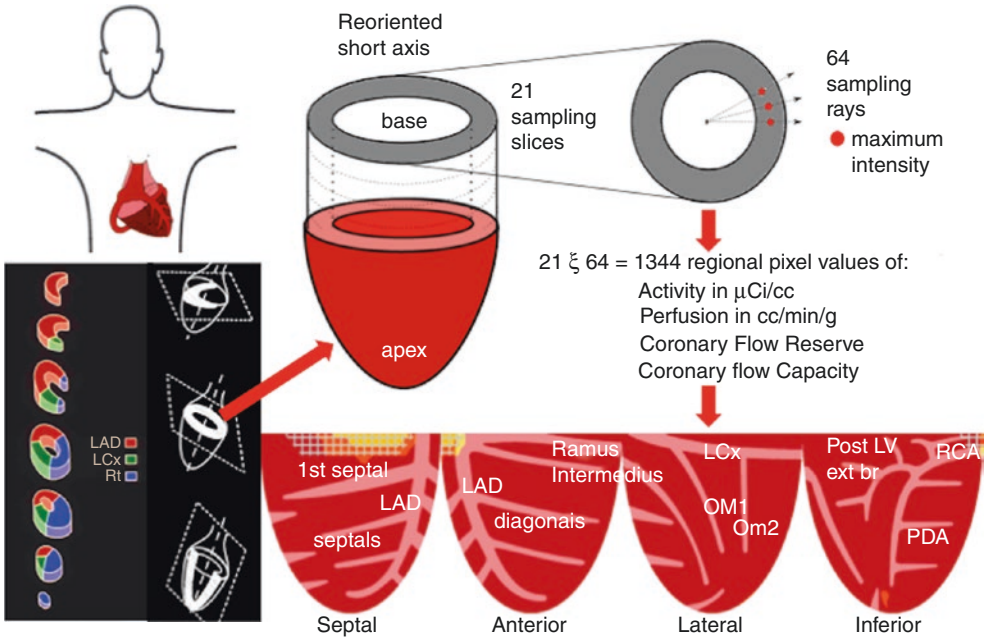

Fig. 6.41 Radial pixels—The secret for measuring pixel distribution of activity and perfusion for LV mapping in our cardiac PET processing software (FDA 510(k) 171,303)

In current literature using 2D quantitative PET, myocardial images are acquired at oblique angles to the LV long axis, are re-oriented into long- and short-axis tomographic slices in which the LV cross-section looks like a doughnut and the long axis looks like a U. In most commercial perfusion software, epicardial and endocardial borders of the long- and short-axis images are outlined automatically or manually, and average activity is calculated within these boundaries in predefined segments of the LV wall (as shown in Figs. 6.24 and 6.25, subdivided into the 17-segment model). In our view, this approach has several disadvantages (if not basic flaws) that explain some of the great variability within or among different PET sites, which undermines their clinical use.

As shown in the activity profile plots of Fig. 6.38, the smearing effect or point spread function of the scanner (due to the LV wall thickness being smaller than scanner resolution) make the location of both endocardial and epicardial borders highly uncertain at the low activity levels with variable spatial activity gradient. Every border definition method will be limited at these statistically poor, spatially changing border zones, thereby incurring comparable uncertainty of the average activity per region selected and the corresponding perfusion.

This border uncertainty contrasts with the maximal activity having the greatest statistical certainty of peak activity along each radius from LV center to outside the myocardium (*see* Fig. 6.41), which automatically by definition tracks motion and avoids uncertain border recognition. Maximal radial activity is optimally reproducible with clean partial-volume correction for every radial pixel, thereby providing maximal statistical content for efficient, robust automated spatial mapping of pixel perfusion in the LV for every artery and branch as it actually is in each individual.

The heart moves inferior and medially with the recoil of systolic ejection. It also reorients vertically, with a changing long-axis angle to the long axis of the body and scanner as the diaphragm moves vertically during respiration, which is augmented by hyperventilation during vasodilation stress. In addition, there is a slow plastic shift of the abdominal contents and diaphragm cephalad during the 15 minutes after lying supine during resting to stress imaging. These moving structures attenuate emission images over their average spatial range, in contrast to the seconds-long helical CT scan acquired unpredictably during some phase of heart and respiratory cycles during further rest and stress changes. The time-changing thoracic attenuation structures commonly cause errors in attenuation correction by either rotating rod or CT transmission scans with resulting large, severe perfusion abnormalities, for which we developed the first shift software to co-register transmission and attenuation data [64–66] (Fig. 6.42).

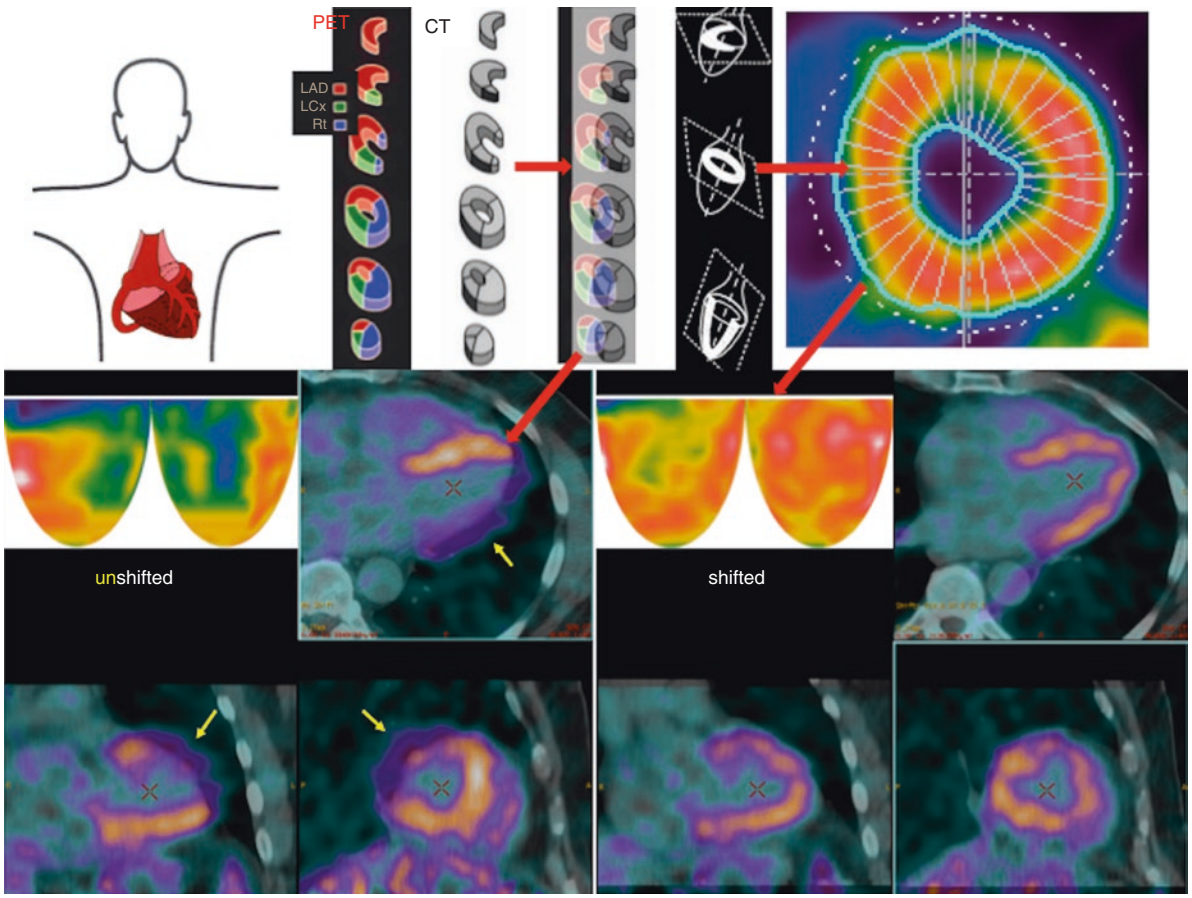

Fig. 6.42 Attenuation correction of imaged activity. This figure shows a schematic sequence (*red arrows*) of acquisition images, their rotation into short-axis and long-axis views, co-registration of schematic emission in color and CT data in black and white, and the radial maximal activity and topographic LV activity maps with a severe anterior defect (*yellow arrows*) due to erroneous attenuation correction caused by emission-transmission misregistration. After manually shifting the data to achieve co-registration, the LV activity map has only a mildly reduced activity

Figure 6.43 shows an example of fast helical CT emission-transmission mis-registration during normal inspiratory breath holding versus co-registration during normal expiratory breath holding. The double right diaphragm indicates diaphragmatic motion with a corresponding basal inferior abnormality that is mis-registration artifact propagated to the short-axis images in Fig. 6.44 and the topographic LV maps in Fig. 6.45.

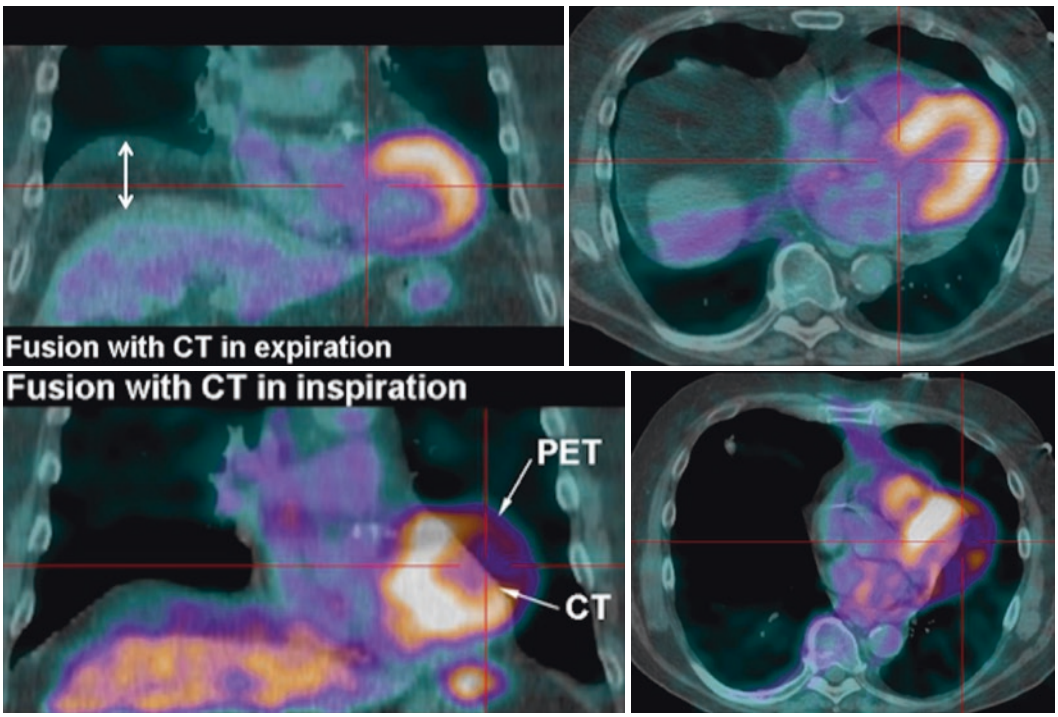

Fig. 6.43 Respiratory variation of attenuation data; an example of misregistration

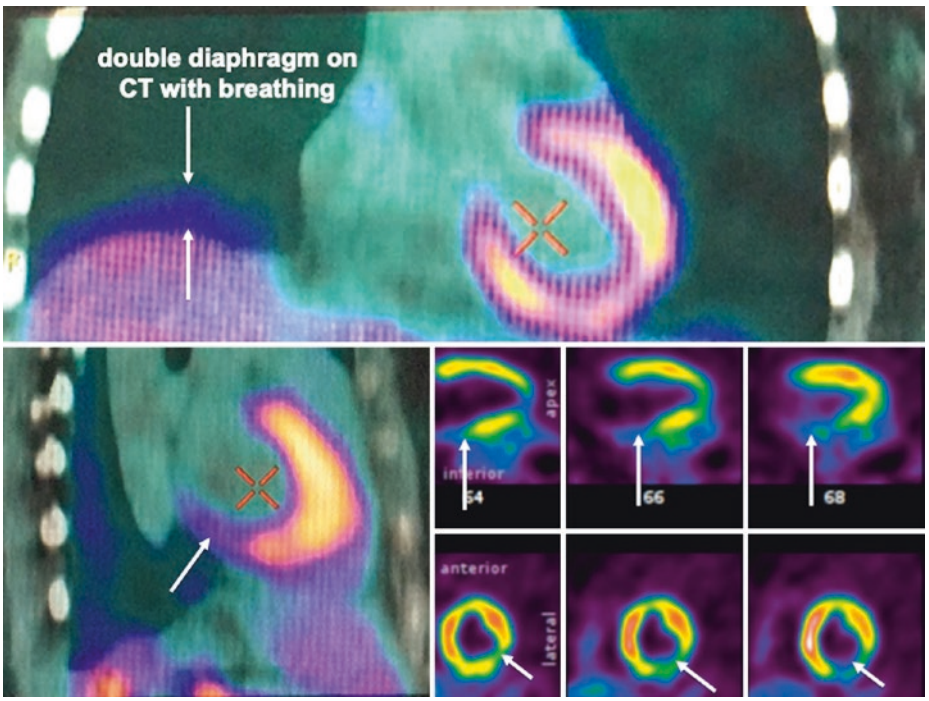

Fig. 6.44 Residual attenuation error despite cardiac emission-transmission co-registration

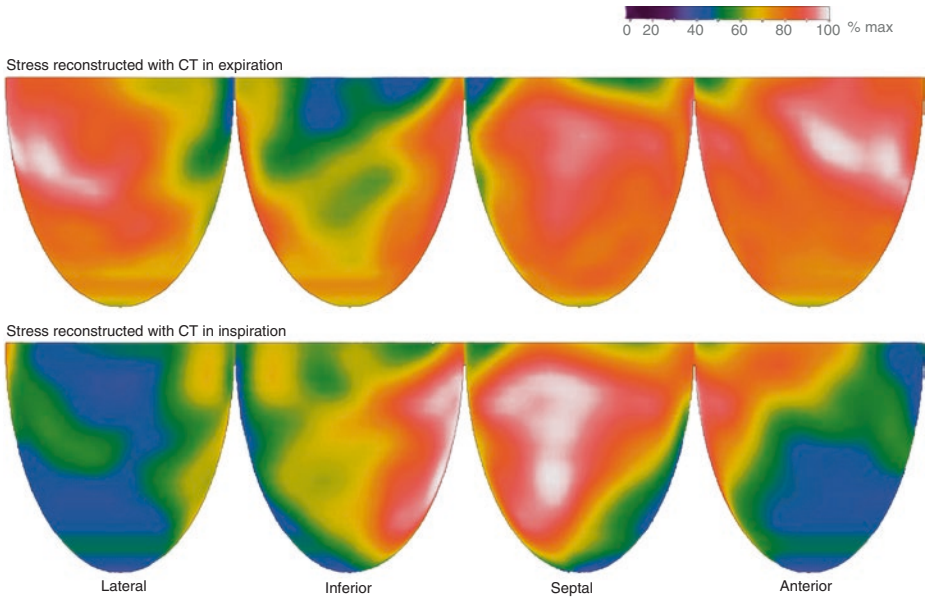

Fig. 6.45 Topographic LV maps with severe abnormalities due to erroneous attenuation correction

Figure 6.44 shows the same double diaphragm on the fast helical CT scan as in Fig. 6.43 (as well as liver activity) due to diaphragmatic motion during an intended normal expiratory breath hold. Despite correct co-registration of cardiac emission and transmission data, the double diaphragm of the fast helical CT causes a defect not correctable by shifting emission-transmission data. The defects due to emission-transmission mis-registration are least with low-dose cine CT imaging for attenuation correction acquired over 2.5 minutes and approximately two breath cycles paralleling emission acquisition during breathing.

In Fig. 6.45, the lower row shows the LV activity map before shifting rapid helical CT emission-transmission data to achieve co-registration. The upper row shows the map after manual co-registration. The residual basal inferior defect may be residual attenuation artifact due the double diaphragm or due to a small region of reduced stress perfusion. To minimize attenuation correction errors using fast helical CT scans beyond manual co-registration, we developed a protocol using a 2.5-minute cine CT scan over two normal respiratory cycles at reduced radiation dose, in order to acquire time-averaged attenuation corrections most comparable to the time-averaged acquisition of emission data without the common mis-registration on fast helical CT scans.

Figure 6.35 described placing the ROI in the left atrium or ascending aorta. Figures 6.46 and 6.47 show the consequences of erroneous arterial input on LV maps of CFC [58, 59]. In the upper row of Fig. 6.46, the ROI is outside the left atrium and a severe stenosis is not identified. With the correct ROI, the CFC maps show a severe infero-lateral defect due to severe stenosis of a dominant RCA.

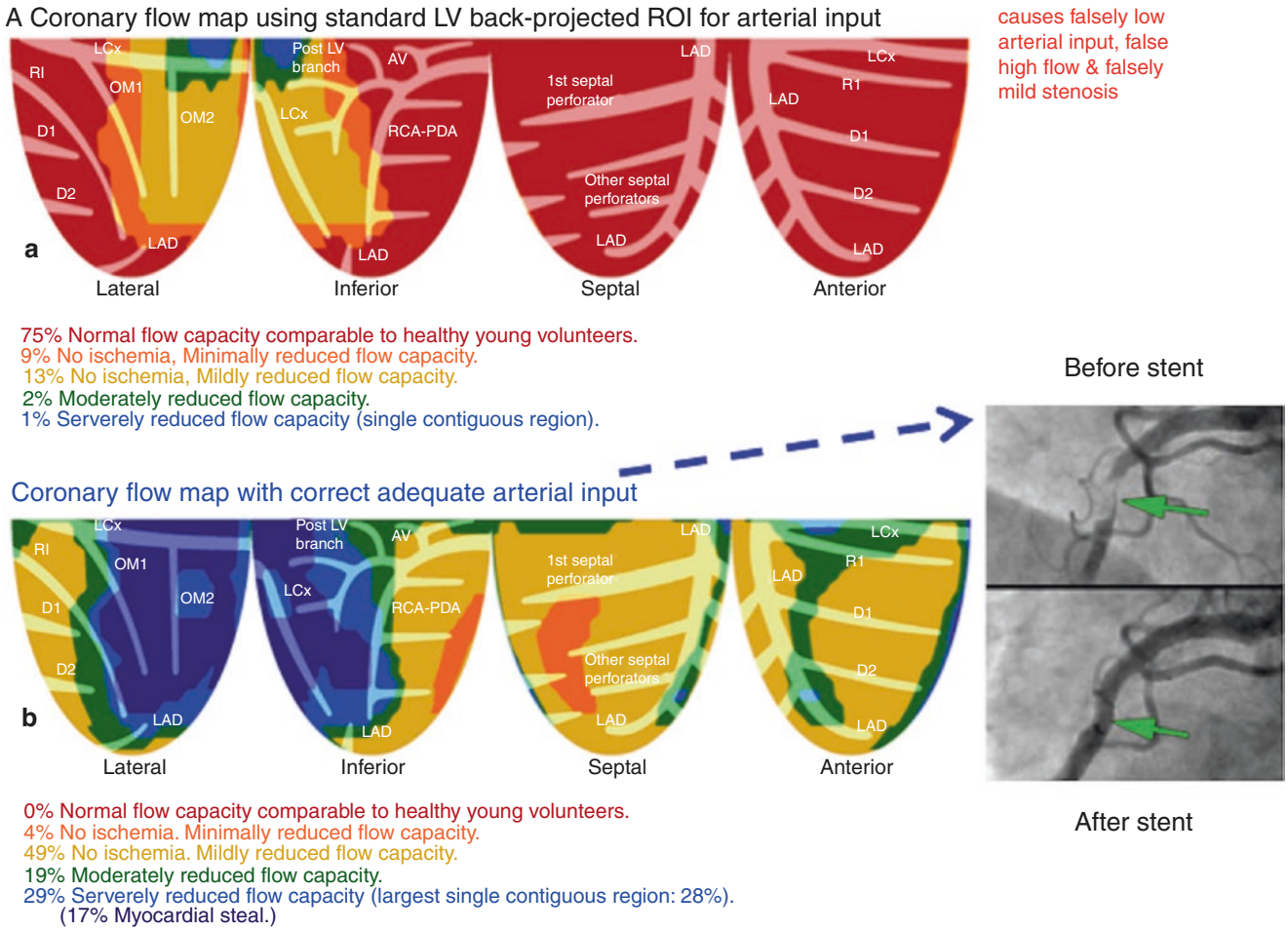

Fig. 6.46 Placement of ROI for time-activity arterial input function. For the CFC maps in the upper row, the ROI for arterial input was estimated for the left atrium just above the AV ring back, as back-projected from late LV myocardial images. This back projection from late myocardial phase images to locate the LA ROI is necessary for compartmental modeling using serial 10- to 15-second arterial phase images of such poor statistical quality that the left atrium cannot be visually located. The estimated back-projected location may not be centrally located in the left atrium, so that with heart motion, the ROI is outside the left atrium with consequent low arterial activity. In this case, the arterial activity was lower than actual arterial activity; perfusion values were increased to near-normal levels, thereby failing to identify a severe stenosis. An arterial ROI located directly on the high-quality 2-minute arterial phase images provides the correct higher arterial input, correct low perfusion, and correct CFC maps showing a severe stress abnormality, confirmed on angiography. (*From* Vasquez et al. [58]; with permission from Elsevier)

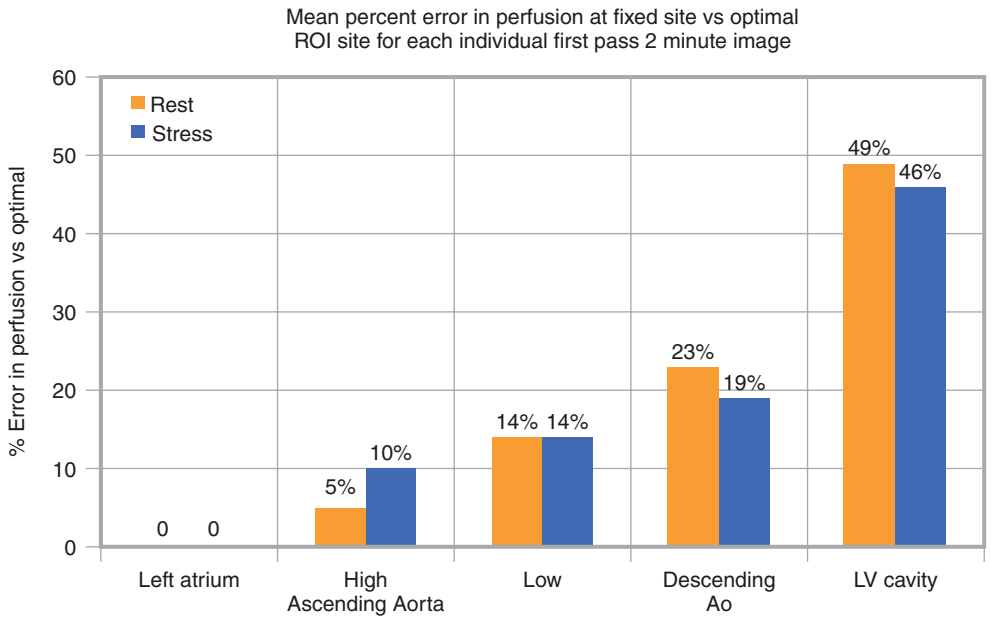

Fig. 6.47 Optimal arterial ROI site

We systematically tested for the optimal arterial ROI on multiple sites in the ascending and descending aorta, the LV cavity, and the high, mid, or low left atrium in each patient in a large series [49, 58, 59]. The optimal site was defined as the site with the highest activity without spillover from adjacent right atrium or pulmonary arteries, and the corresponding error in perfusion measurement was determined for all sites, compared with the optimal site. As shown in Fig. 6.47, the optimal site varied for individuals, but the central left atrium had the least error, with errors progressively increasing for ROIs placed in the ascending aorta, descending aorta, and LV. An ROI project to the estimated AV ring of LV is commonly used for the arterial input but causes the greatest errors in perfusion measurement because of its motion and activity spillover from the myocardium into the LV cavity. Equations purporting to correct for this spillover fail to recognize or account for cardiac motion and translation during the cardiac cycle, which may move the LV activity out of an estimated fixed LV cavity ROI.

Clinical Coronary Physiology by PET to Guide Cardiac Care

Although standard protocols call for abstinence from caffeine for at least 12 hours before vasodilator stress PET, the literature reports that 20% of subjects have caffeine in their blood (Fig. 6.48). Accordingly, we strongly emphasize 24-hour abstinence verbally, in written instructions, and with a phone call reminder 2 days before the scheduled PET. We also check serum caffeine in every patient, and have found that 6% have measurable caffeine levels despite the serial reminders about caffeine abstention. Even low caffeine levels may inhibit vasodilator stress; repeat PET without caffeine can show significant abnormalities that were missed when caffeine levels were higher.

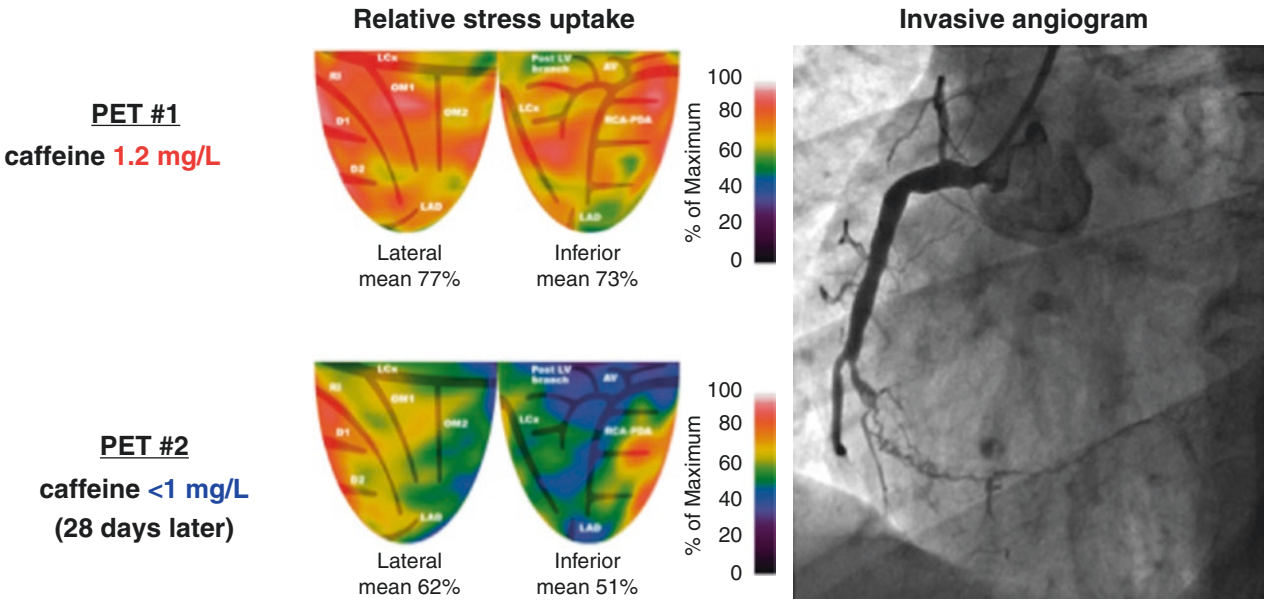

Fig. 6.48 Maximal vasodilator stress is essential. Even low caffeine levels, as in this case, may inhibit vasodilator stress. Repeat PET without caffeine can show significant abnormalities that may explain symptoms or clinical issues

Some patients have very high resting perfusion (Fig. 6.49a) with normal to high stress perfusion (Fig. 6.49b), thereby causing low, apparently abnormal CFR (Fig. 6.49c). Others may have low resting perfusion (Fig. 6.49e) with reduced stress perfusion (Fig. 6.49f) but excellent CFR (Fig. 6.49g) owing to the low resting levels. Figure 6.49 shows two topographic views of three common patterns of quantitative myocardial perfusion for which either CFR or stress perfusion alone fails to provide definitive information for clinical management that is provided by both together. These global differences in resting perfusion and CFR between individuals are called *global heterogeneity* among different subjects. *Regional heterogeneity* of resting and CFR images also is common and is largely due to endothelial dysfunction associated with risk factors. High regional rest flow (I) with uniform stress flow (J) may cause apparent regional stress defect (K). However, as illustrated in Fig. 6.49, perfusion heterogeneity is accounted for as normal (D and H) or mild diffusely reduced CFC due to non-obstructive CAD (L) that is differentiated from true segmental perfusion abnormalities on the CFC maps [2, 25, 27, 39–49], shown in Figs. 6.2, 6.5, 6.26, and 6.46, and quantitatively documented in Figs. 6.50, 6.51, and 6.52.

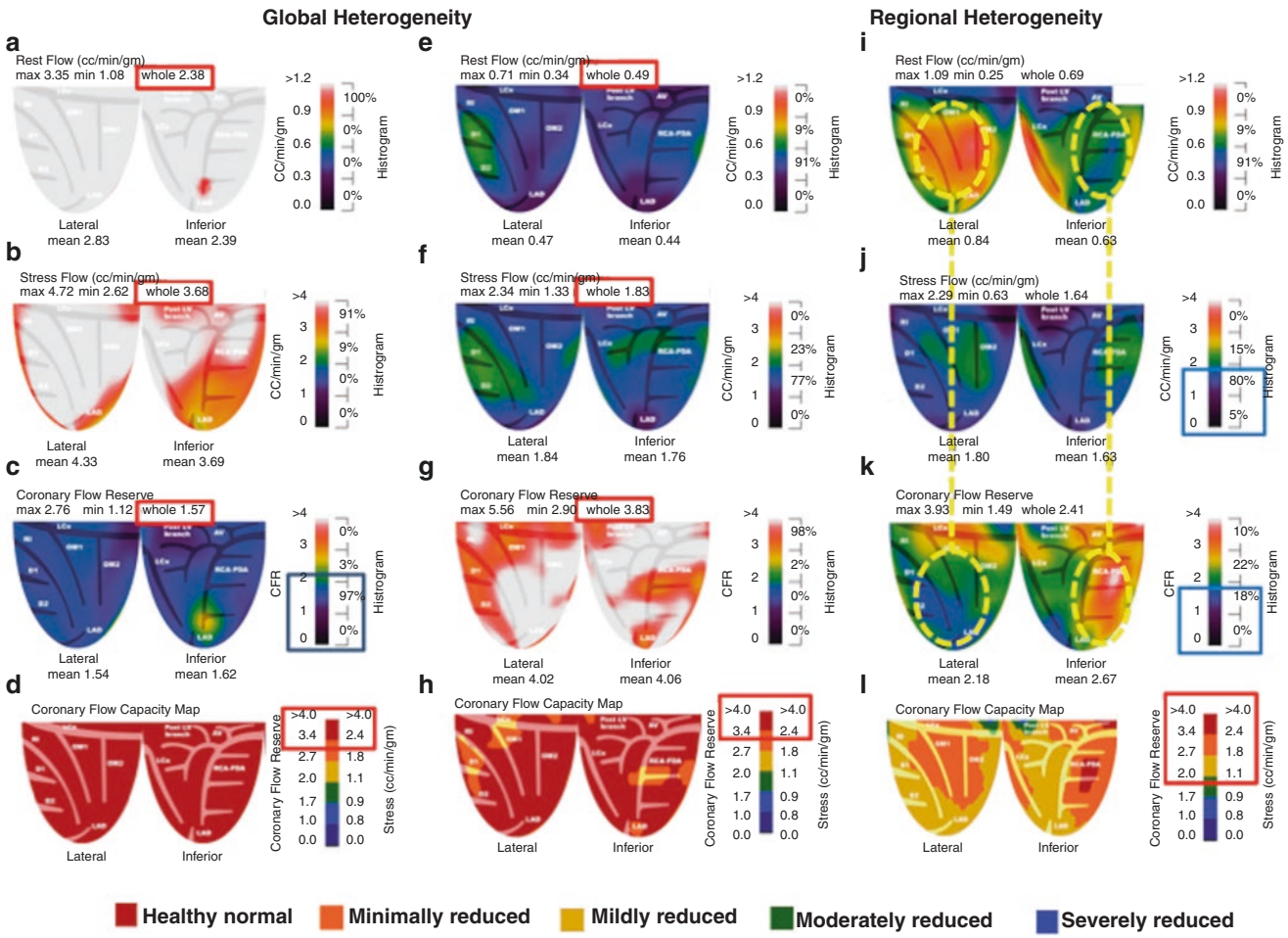

Fig. 6.49 Perfusion heterogeneity may cause misinterpretation of PET perfusion, which can be resolved by CFC maps of comprehensive clinical physiologic severity. This figure shows two topographic views of three common patterns of quantitative myocardial perfusion for which either CFR or stress perfusion alone fails to provide definitive information for clinical management that is provided by both together. For efficiency of comparisons, only two of the four topographic views are displayed, with CFR and stress perfusion scaled according to the color bars. In the first patient (**a–d**), rest perfusion is very high (**a**), stress perfusion also high (**b**), and CFR is very low (**c**) because of the high rest flow, as commonly seen with anxiety, high blood pressure, and in women. Alternatively, in another patient (**e–h**), rest perfusion may be very low owing to beta blockers (**e**), and stress flow is also low (**f**), but CFR is excellent (**g**) and well above the ischemic threshold. These global differences in resting perfusion and CFR between individuals are called *global heterogeneity* among different subjects. The integrated CFC maps (**d** and **h**) of these two subjects accounts for both CFR and stress perfusion together. For these two examples, the red regions of **d** and **h** indicate CFC comparable to that of young, healthy volunteers without risk factors. These examples show that because of the common global perfusion heterogeneity among different patients, CFR alone or stress perfusion alone may fail to characterize coronary perfusion adequately

In the third patient (**i–l**), the rest perfusion image is regionally heterogeneous (**i**) and stress perfusion images are uniformly adequate, without ischemia (**j**). As a result of the resting perfusion heterogeneity, CFR is also heterogeneous, with what appears to be a severe inferolateral stress defect due to the high inferior resting perfusion (**k**), but the CFC map (**l**), which accounts for CFR and stress perfusion, incorporates this heterogeneity and indicates only mildly reduced CFC diffusely, which is due to mild, diffuse, nonobstructive CAD with no regional stress defect or flow-limiting stenosis

Coronary Flow Capacity Color Thresholds For Clinical Groups of PETs			7-7-17			
ROC threshold between clinical groups	Normals	Norm vs no CAD	No CAD vs CAD	No isch vs prob isch	No isch vs ischemia	Steal
Stress with pet defect, angina, ECGΔ*	0 of iii	0 of iii	0 of iii	i of iii	ii of iii	CFR < 1
Clinical class (without PET data)	Normals	Risk Factors	All CAD	Probable ischemia	Stress angina/STΔ	subset steal
Number PET cases	212	2171	979	548	278	subset 218
ROC threshold between color groups	Normals	red vs orange	orange vs yellow	R,O,Y vs green	R,O,Y vs blue	steal CFR<1.0
Ordinal id number	4	3	2	1	0	Subset included
stress flow original ROC threshold cc/min/g		2.17 original	1.82 original	1.09 original	0.83 original	in the 4188
Coronary Flow Reserve original ROC threshold		2.90 original	2.38 original	1.60 original	1.27 original	CFR < 1.0
CFR AUC		0.81	0.61	0.8	0.97	
CFR Sensitivity = Specificity		74%	58%	72%	91%	
CFR 95% CI (upper - lower median)		0.84 - 0.79	0.63 - 0.59	0.83-0.78	0.98 - 0.96	
CFR - P value for AUC		< 0.001	< 0.001	< 0.001	< 0.001	
CFR standard error		0.015	0.01	0.01	0.005	
stress flow cc/min/g AUC		0.63	0.68	0.76	0.94	
stress flow Sensitivity = Specificity		60%	64%	69%	87%	
str flo 95% CI (upper - lower median)		0.66 - 0.59	0.7 - 0.66	0.78 - 0.73	0.96 - 0.93	
stress flow P value for AUC		< 0.001	< 0.001	< 0.001	< 0.001	
stress flow standard error		0.018	0.01	0.01	0.008	
Total 4188 where the subset of 218 with steal defned as CFR < 1.0 (dark blue) is already included in the 4188 PETs						

Fig. 6.50 CFC thresholds for clinical groups of PETs—an essential physiologic measurement for guiding patient care and reducing mortality. This table shows specific clinically defined groups with the number of rest-stress PET studies in each group, classified independently of and separately from any PET images or data. In order to integrate stress perfusion in mL/min/g and CFR, patients or volunteers had 4188 rest stress quantitative dipyridamole stress perfusion PET studies using Rb-82 with a DST-16 GE PET CT scanner. The wide range of stress perfusion and CFR values for each of 1344 radial pixels in 4188 studies comprises a vast number of combinations that are difficult to display and interpret. Accordingly, this huge number of possible stress perfusion and CFR pixel combinations were reduced by ROC analysis for the optimal thresholds of CFR and stress perfusion in mL/min/g that differentiated the five clinically defined groups with highest area under the curve (AUC). Stress perfusion and CFR combinations were thereby reduced to five color ranges for the clinically defined groups*, as detailed in this table and plotted in Fig. 6.51:

Red: Healthy Young Volunteers (n = 212): Healthy young volunteers under 40 years old with no vascular risk factors, normal measured lipid profile, no obesity, no measurable caffeine on blood samples for every PET, and no blood or urine cotinine levels measured for every PET

Orange: Risk Factors Only (n = 2171): Subjects with one or more vascular risk factors but no known CAD pre-PET, as defined by no history of MI, PCI, coronary artery bypass (CAB), abnormal coronary angiogram, or angina; no dipyridamole stress–induced ischemia at PET; and no myocardial scar as defined below

Yellow: Established Coronary Artery Disease (CAD) (n = 979): Subjects with CAD defined by pre-PET history of MI, PCI, CAB, or abnormal coronary angiogram. Subjects with definite or possible ischemia during dipyridamole stress, as defined below, are excluded from this group; they are classified in the next two groups. Subjects with significant myocardial scars defined as a severe fixed relative defect with rest flow ≤0.2 cc/min/g were also excluded in order to avoid the downward bias in thresholds of perfusion and CFR due to low flow of scars unrelated to stress

Green: Possible Ischemia During Dipyridamole Stress PET (n = 548): Subjects meeting any *one* of the following three criteria during dipyridamole stress PET:

A significant perfusion defect on stress images with >5% rest-to-stress change in the percentage of LV with ≤60% maximum on relative uptake stress images that is >3 SD below the mean of rest and stress relative PET images of normal young volunteers, *or*

ST depression >1 mm on ECG not present on resting ECG, *or*

Definite angina requiring reversal by aminophylline, nitroglycerin, or IV metoprolol

Blue: Definite Ischemia During Dipyridamole Stress PET (n = 278): Subjects with definite ischemia are defined as having:

A significant perfusion defect on stress images with >5% rest-to-stress change in percentage of LV with ≤60% maximum on relative uptake stress images that is >3 SD below the mean of rest and stress relative PET images of normal young volunteers, *plus* one or both of the following:

ST depression >1 mm on ECG not present on resting ECG

Definite angina requiring reversal by aminophylline, nitroglycerin, or IV metoprolol as we have previously published with AUC of 0.97 [42, 43]

Subjects with myocardial scar are excluded from this group and classified separately below so that the thresholds for stress flow and CFR would reflect the true stress perfusion and CFR changes without the downward bias due to low flow of scars unrelated to stress

* The numbers iii, ii, I, or 0 indicate the number of the following criteria of ischemia met during dipyridamole stress perfusion imaging: ECG ST depression >1 mm, definite angina requiring aminophylline reversal, relative stress defect ≤60% of maximum for >5% of LV

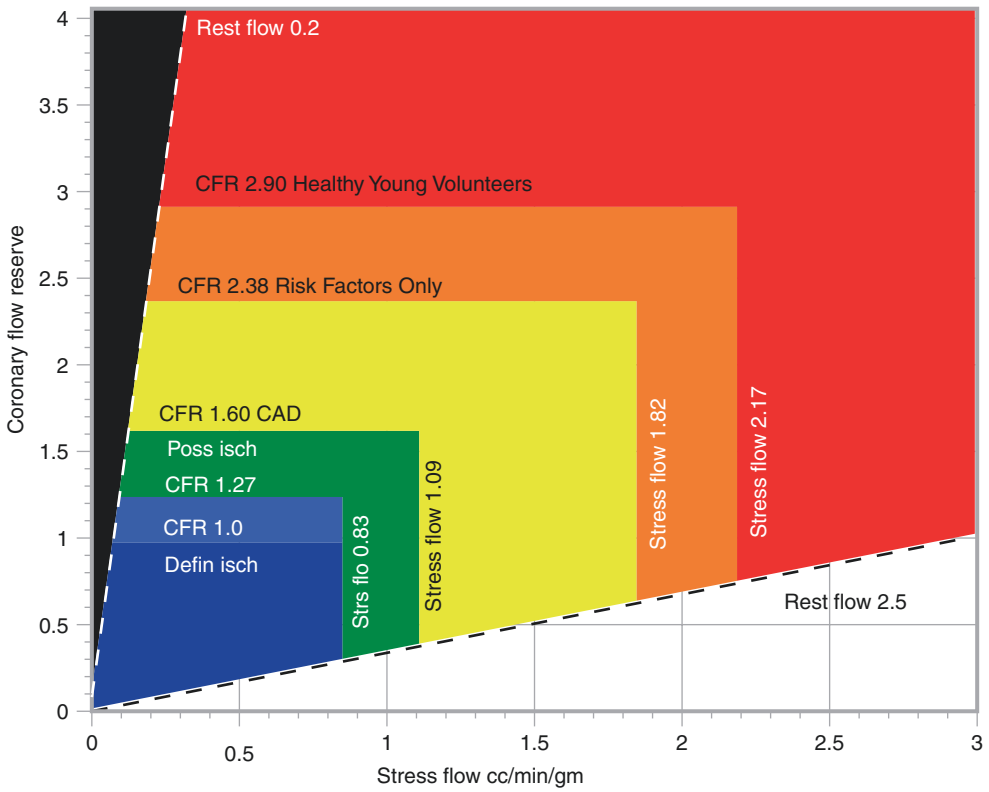

Fig. 6.51 Schema for color-coding each pixel of the CFC map. The color-coded ranges of CFR and stress perfusion for each pixel of the CFC map are based on the objective, predefined clinical groups listed in Fig. 6.50. The perfusion boundaries between the clinical groups were determined by objective ROC analysis for optimum CFR and stress-perfusion separation of the groups

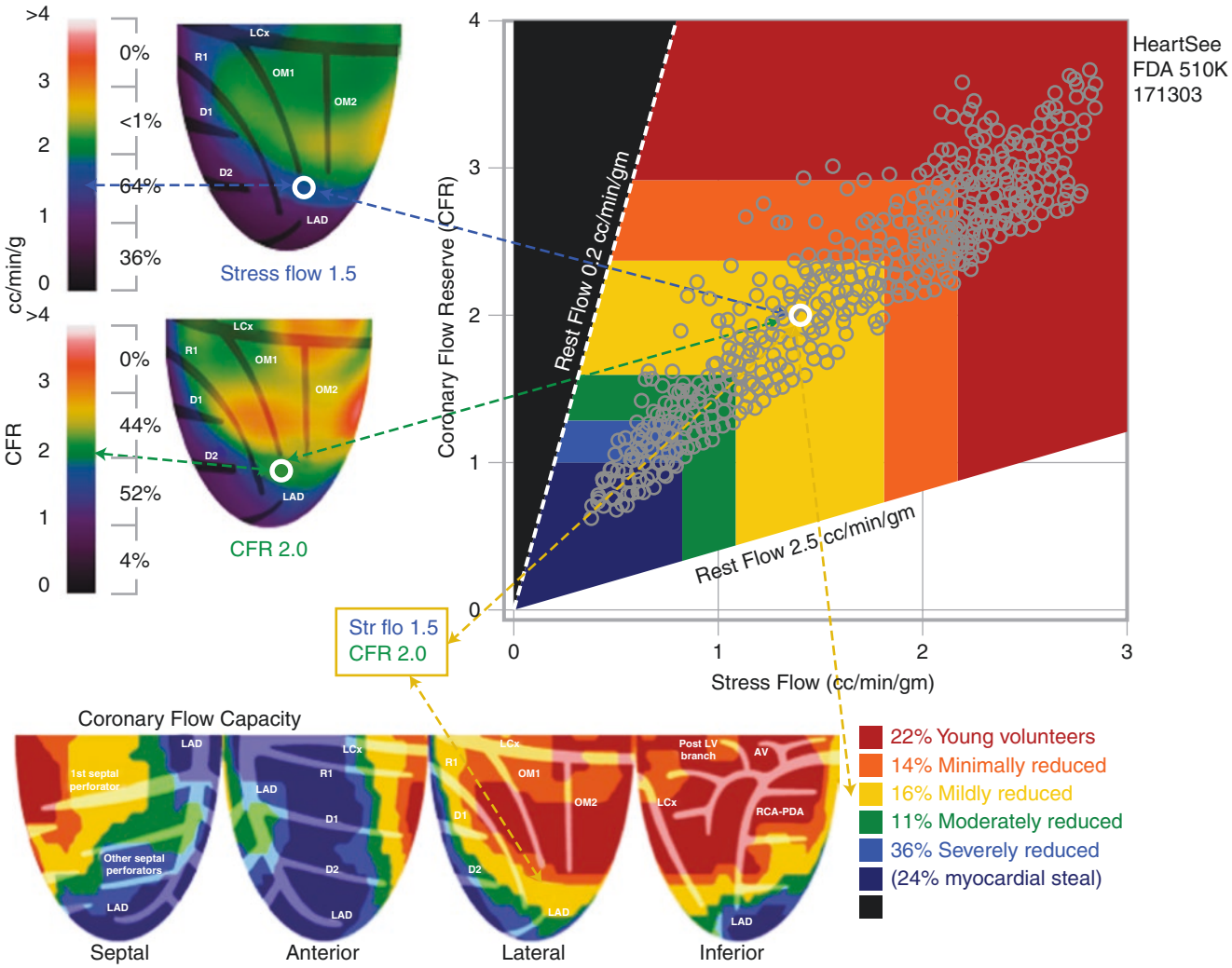

Fig. 6.52 The CFC map in this figure color-codes each pixel within five color ranges for combined CFR and stress perfusion values of each pixel, spatially maps each pixel back into its LV location with corresponding stress perfusion and CFR values, and calculates the percentage of LV for each range of combined *both* CFR *and* stress perfusion values listed in the CFC color histogram bar. The LV CFC map incorporates all perfusion metrics into a comprehensive, easily understood clinical guide derived from in-depth coronary physiology and imaging physics. (*From* Gould and Johnson [25]; with permission from Elsevier)

The table in Fig. 6.50 gives details of the CFC thresholds for clinical groups of PETs—an essential physiologic measurement for guiding patient care and reducing mortality [2, 25, 27, 39–49]. This table shows specific clinically defined groups with the number of rest-stress PET studies in each group (total 4188) classified independently of and separately from any PET images or data. The wide range of stress perfusion and CFR values for each of 1344 radial pixels in 4188 studies comprises a vast number of combinations that are difficult to display and interpret. Accordingly, this huge number of possible stress perfusion and CFR pixel combinations were reduced by ROC analysis for the optimal thresholds of CFR and stress perfusion in cc/min/g that differentiated the five clinically defined groups with highest area under the curve (AUC). Stress perfusion and CFR combinations were thereby reduced to five color ranges for the clinically defined groups, as detailed in this table and plotted in the Fig. 6.51. *CFR* is used as a synonym for *myocardial perfusion reserve* to emphasize the original physiological concepts.

Pixel values of rest-stress relative images, quantitative perfusion, and CFR comprise infinite numbers of values and combinations reflecting true perfusion heterogeneity that must be compressed into clinically relevant ranges and regional distribution for clinical utility. Figure 6.52 shows the threshold values of stress perfusion and CFR for the color-coded ranges from the above table for the CFC map incorporating all perfusion metrics into a comprehensive, easily understood clinical guide derived from in-depth coronary physiology and imaging physics to guide clinical management [2, 25, 27, 39–49].

The pixel measures of absolute and relative activity, perfusion in cc/min/g, CFR, and CFC map the distribution of perfusion metrics as they actually are in each individual with a color-scale bar (Fig. 6.53). Each map provides the following metrics for size and severity of abnormalities:

- The visual size and severity of quantitative perfusion abnormalities for each artery and its branches as they actually are, undistorted by arbitrarily selected regions or bulls-eye displays as shown in Fig. 6.27.
- The histogram for percent of LV in each severity range, located on the right edge of the color-scale bar or at the bottom of the CFC maps.
- Average values for each quadrant in the distribution of each coronary artery.
- The automated severity contour selection option, to determine the size and severity of any specifically selected defect (*see* Fig. 6.54).
- These same four metrics for abnormalities of relative myocardial activity distribution.

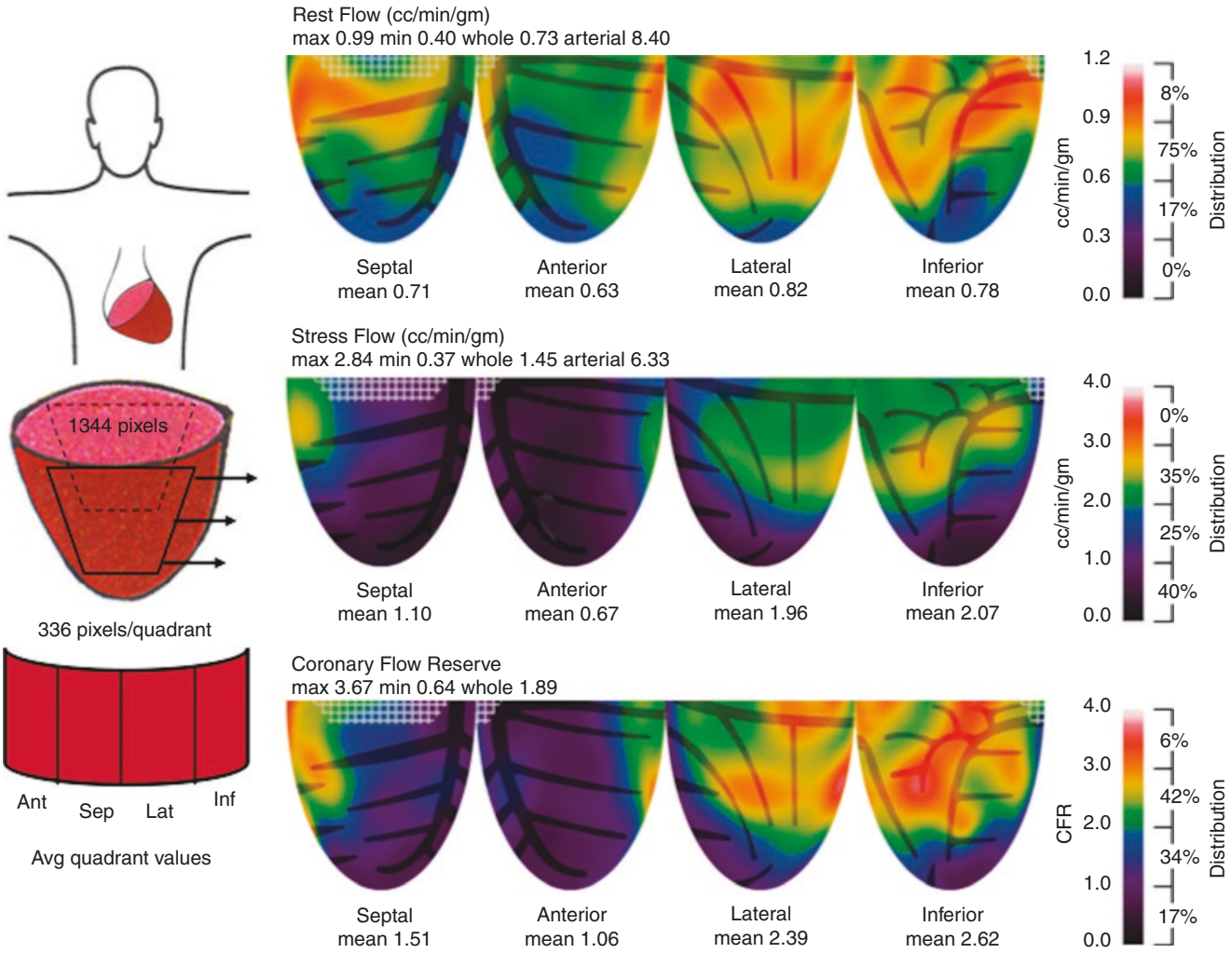

Fig. 6.53 Size and severity of perfusion abnormalities, as shown by several different metrics

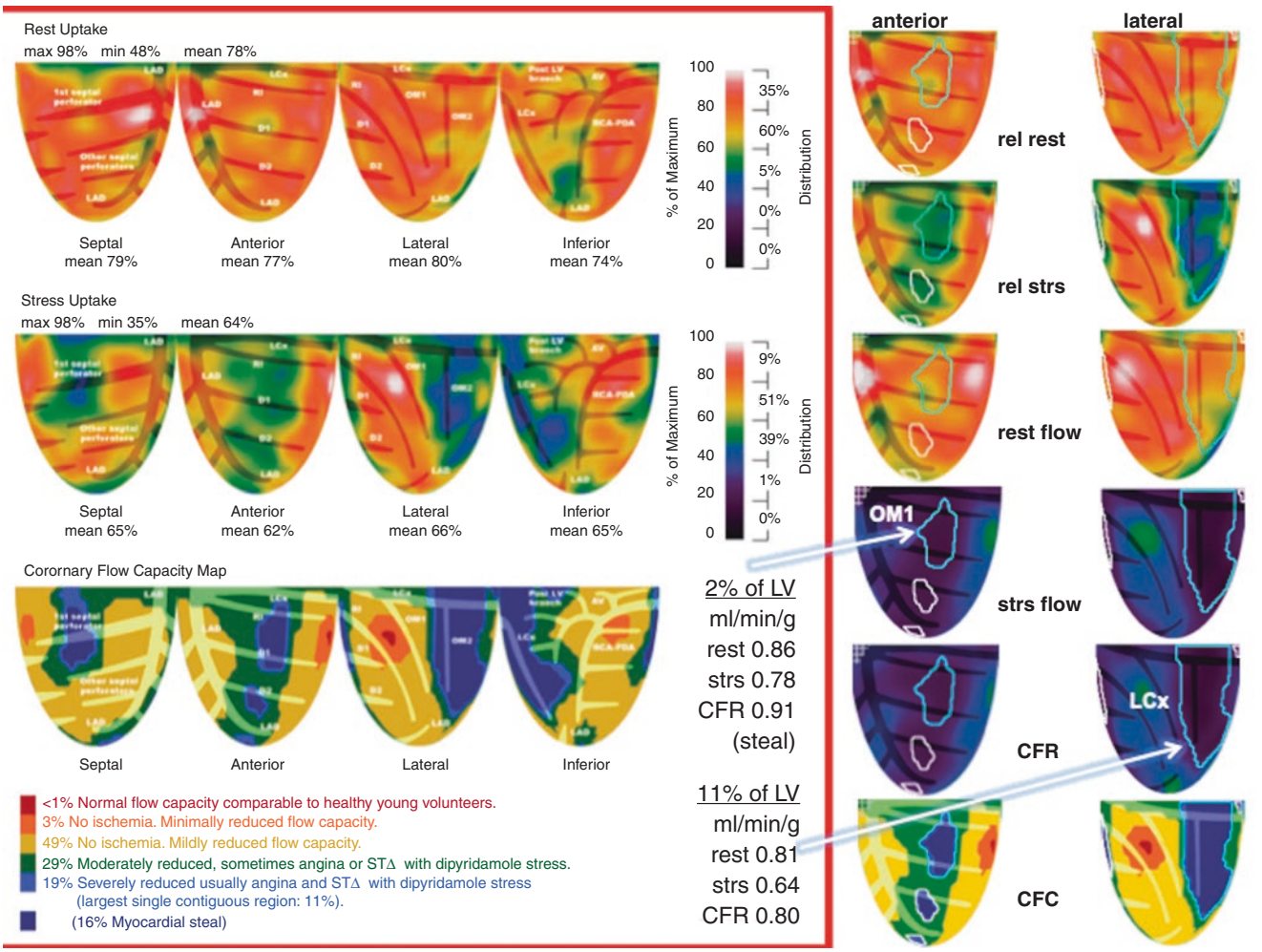

Fig. 6.54 Optional additional size-severity quantification. The three-row display at left is our routine report. The two views of all perfusion metrics for this patient (*right*) demonstrate additional size-severity quantification by iso-contour, selected by the reading physician in order to refine the visual impression

A complete set of perfusion images includes relative rest-stress tomograms, relative rest-stress LV topographic maps, rest-stress perfusion maps, and CFR and CFC maps. Because perfusion heterogeneity makes the rest-stress-CFR maps (Fig. 6.53) difficult to understand and interpret, our final report (Fig. 6.55) consists of the relative rest-stress maps as the primary data, with the CFC map as the summary of quantitative perfusion metrics; the rest-stress-CFR display (Fig. 6.53) can be added to the report as needed for each case [2, 25, 27, 39–49].

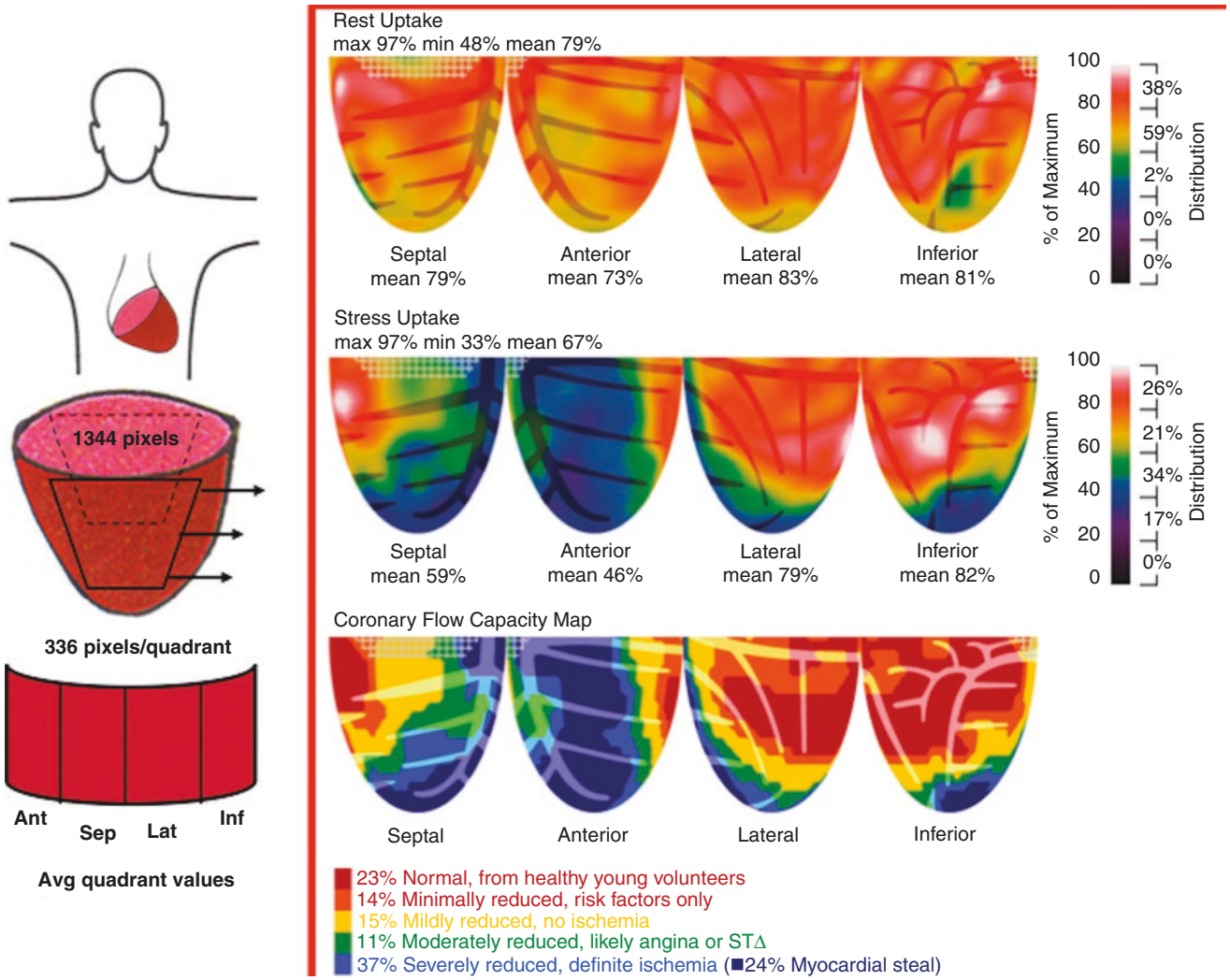

Fig. 6.55 The Primary Clinical Report summarizing coronary physiology, comprising primarily the relative rest-stress maps and CFC map

Figure 6.54 (right panel) illustrates optional, additional size-severity quantification for two of the four quadrant views for a patient to help the reading physician refine the visual impression.

In the same patient imaged serially minutes apart, the stress perfusion, CFR, and CFC maps are highly reproducible, with test-retest precision in the same patient of ±10% within minutes [47]. Indeed, even on a different day, the values remain highly reproducible, as illustrated in Fig. 6.56. Figures 6.57 and 6.58 demonstrate reproducibility by the Kolmogorov–Smirnov test comparing serial CFC histograms in the same subject [47, 48].

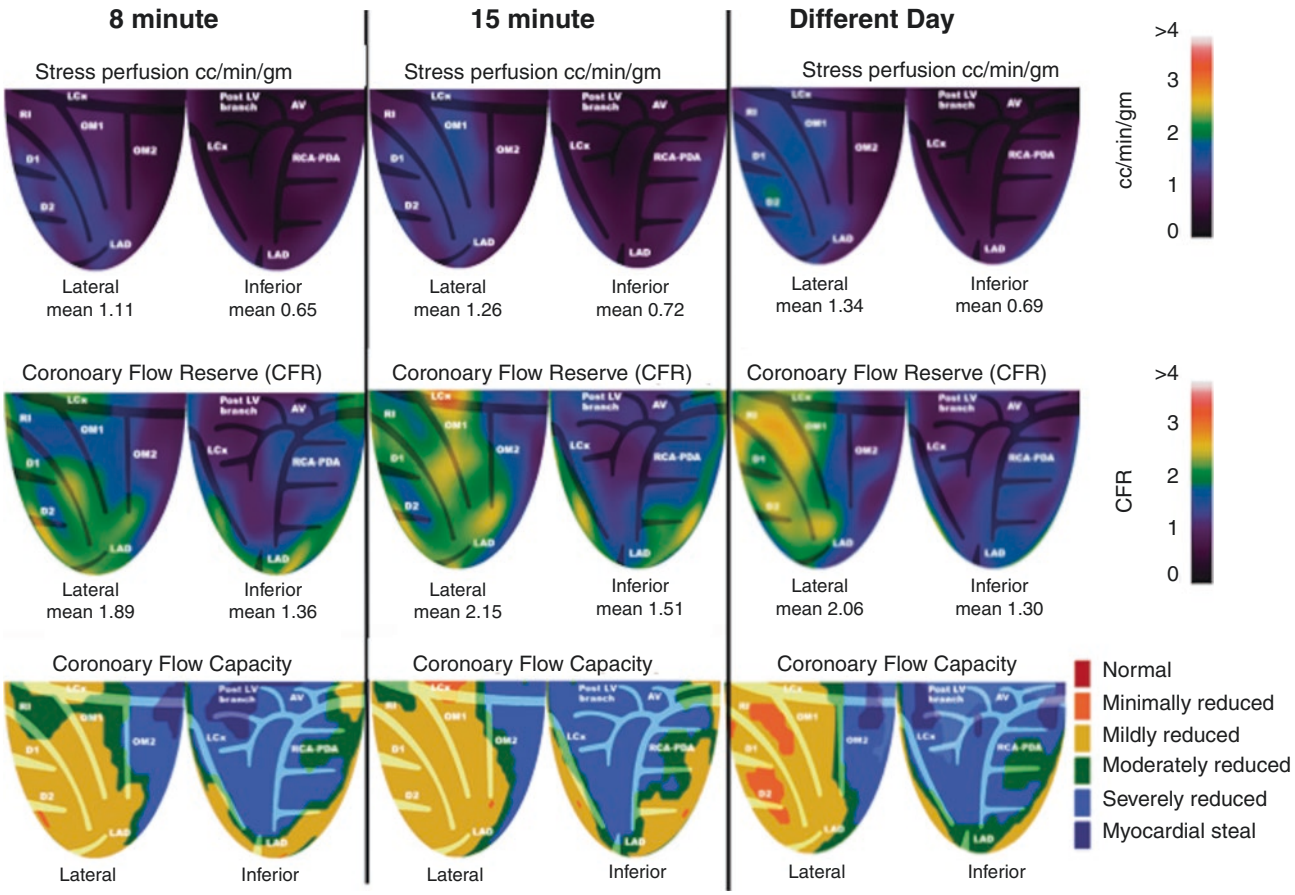

Fig. 6.56 Reproducibility of CFC maps. (*From* Kitkungvan et al. [47]; with permission from Elsevier)

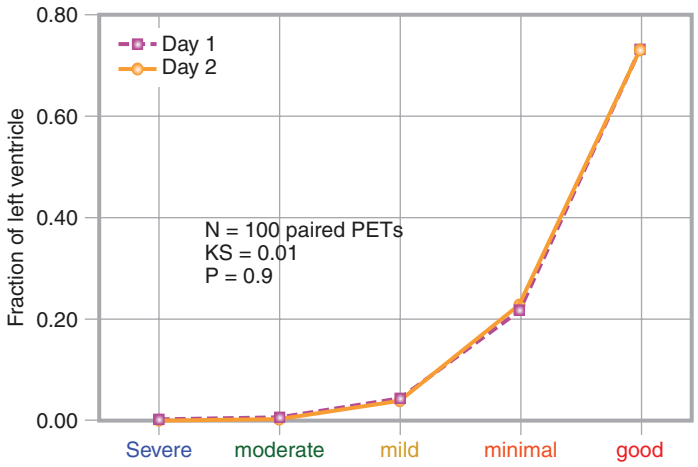

Fig. 6.57 Reproducibility by the Kolmogorov–Smirnov test for comparing two serial CFC histograms in the same subject, from 100 healthy volunteers without risk factors. (*From* Kitkungvan et al. [48]; with permission from Elsevier)

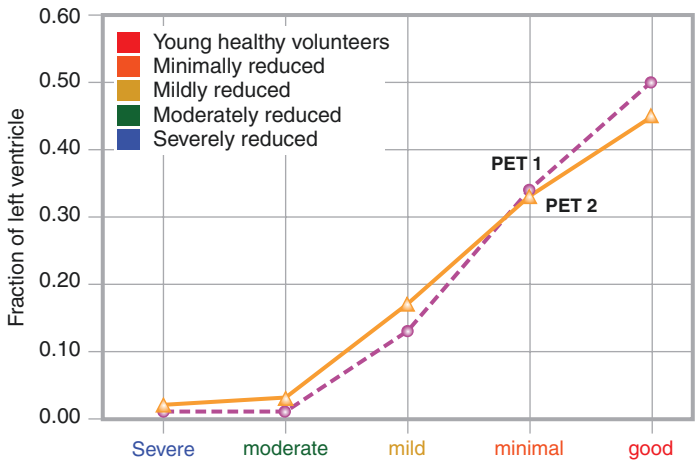

Fig. 6.58 Reproducibility by the Kolmogorov–Smirnov test for comparing two serial CFC histograms in the same subject, from 120 volunteer patients with CAD or risk factors. (*From* Kitkungvan et al. [47]; with permission from Elsevier)

The table shown in Fig. 6.59 demonstrates the reproducibility of our method of stress perfusion compared with other cardiology metrics, using the coefficient of variation (standard deviation divided by mean) [27, 44, 47].

Variability of cardiovascular measurements

Test re-test measurement	Coefficient of variation
PET flow cc/min/gm	10%
Angiogram % diameter stenosis	17%
LDL cholesterol	9.5%
ECHO ejection fraction	15%
SPECT ejection fraction	17%
SPECT sum stress scores (SSS)	29%
C reactive protein	46%

Fig. 6.59 Variability of cardiovascular measurements using the coefficient of variation (standard deviation divided by mean)

Severity of true pressure-derived FFR reduction is directly related to the risk of MI or death (Fig. 6.60). For severely reduced FFR, revascularization may be associated with reduced risk of death or MI. At high FFR, revascularization provides no improvement over medical treatment. The curve for the natural history of severity-risk may be improved by revascularization only for severely reduced FFR, below 0.65. Although the FFR threshold for PCI is commonly 0.8, this threshold is rarely associated with angina or STΔ during adenosine infusion since it reflects only relative flow reserve, not ischemia sufficient to benefit from revascularization.

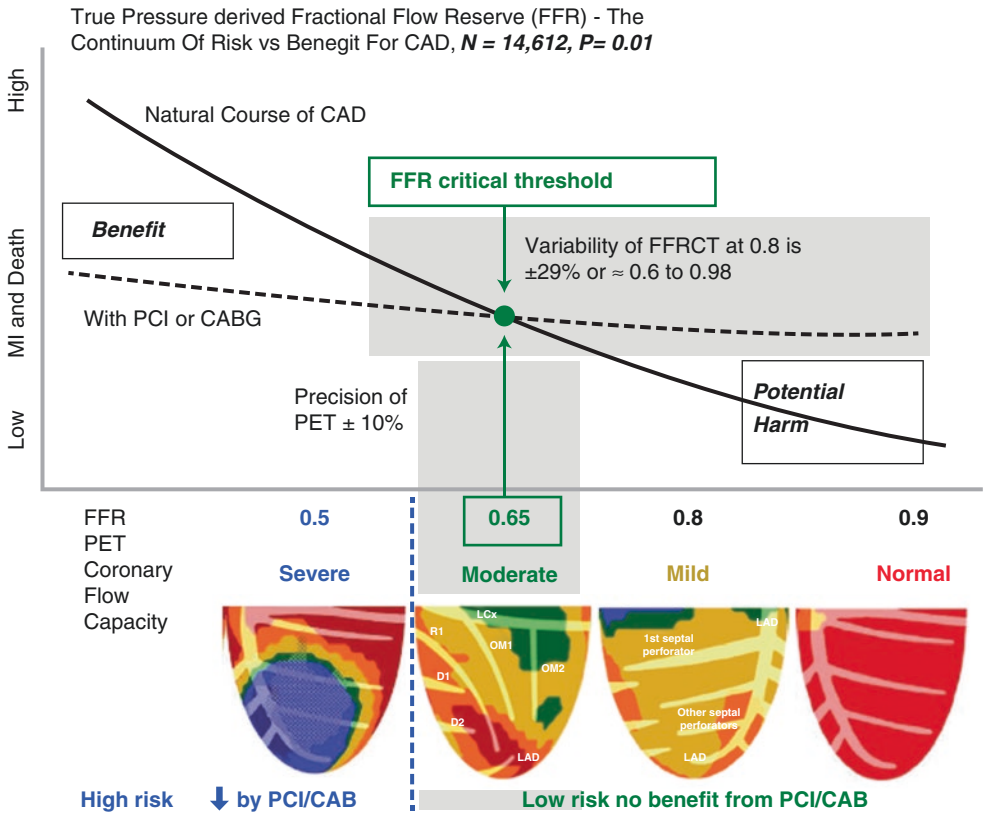

Fig. 6.60 Severity–risk continuum for FFR, PET, and FFR_{CT}

The crossover of the average statistical FFR severity-risk curves with and without PCI is FFR = 0.65. For PET, this threshold range of severity-risk for benefit of revascularization is severely reduced CFC for >0 to 3% of LV, with a precision for stress perfusion of ±10%. By comparison, at the current pressure-derived FFR threshold of 0.8, the variability for simulated FFR_{CT} ranges from 0.62 to 0.98, reflecting its Bland-Altman limits of agreement with pressure-derived FFR of 0.23 FFR units in Fig. 6.21. Simulated FFR_{CT} variability is due to the limited resolution of 0.5 mm for CT for arterial diameter of typically 3–4 mm, where blood flow is a function of radius raised to the fourth power, as well as heterogeneity among subjects regarding vasodilator capacity. This variability likely explains why PET is superior to CTA and simulated FFR_{CT} by directly assessing coronary physiologic severity, as shown in Figs. 6.19, 6.20, and 6.21.

Physiologic Severity, Revascularization, and Outcomes

Figure 6.61 demonstrates that global CFR <2.0 predicts increased major adverse cardiac events or mortality, compared with CFR >2.0 [67–69]. For global CFR <1.5, bypass surgery may be associated with improved survival in a nonrandomized cohort, but global CFR fails to account for regional or segmental quantitative perfusion or stenosis from diffuse CAD (*see* Fig. 6.62) needed to guide interventions.

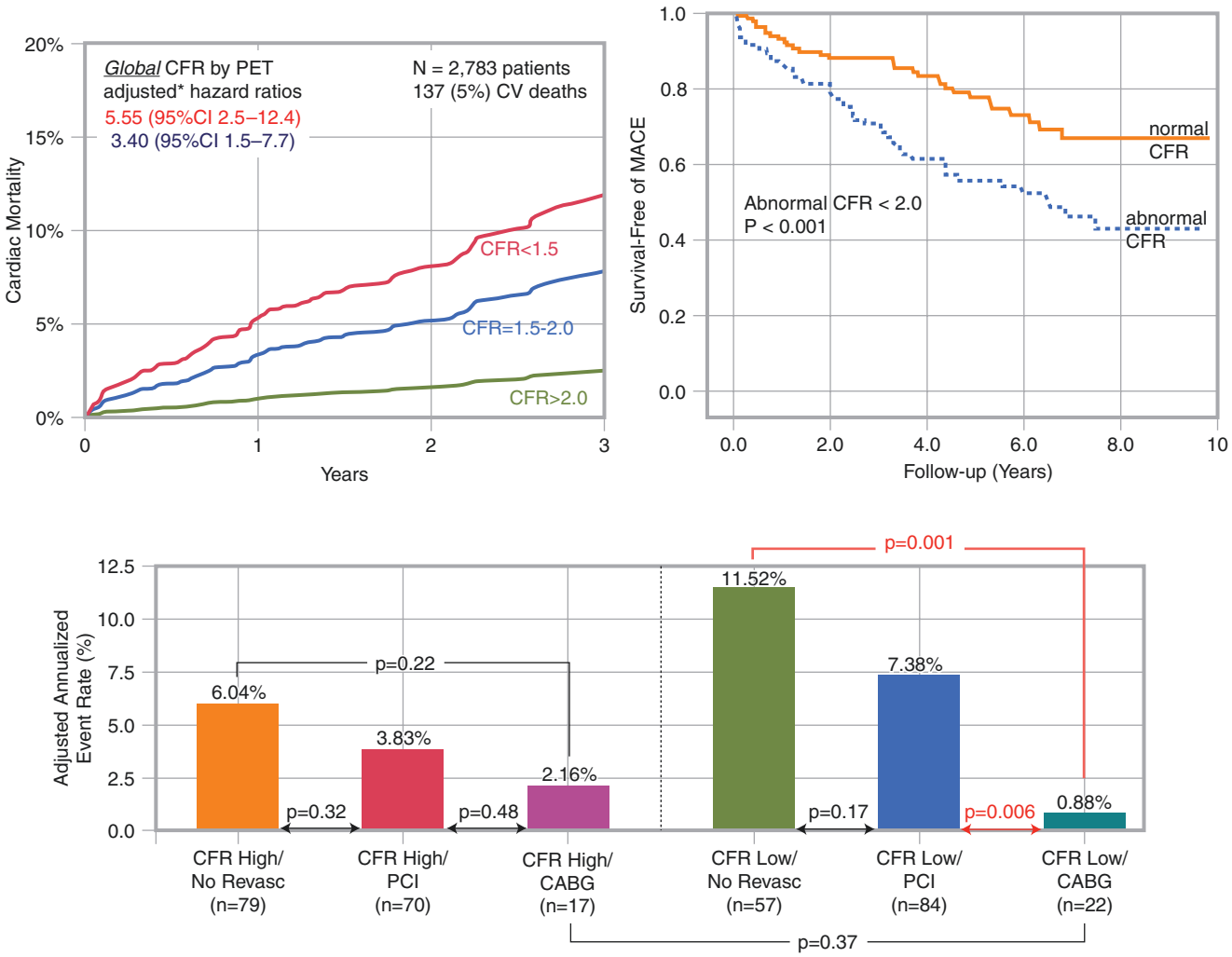

Fig. 6.61 Literature on CFR predicting major adverse cardiac events (MACE) or mortality. (*Left upper graph from* Murthy et al. [67] and *lower graph from* Taqueti et al. [69], with permission of the American Heart Association; *Right upper graph from* Herzog et al. [68], with permission of Elsevier)

Figure 6.62 shows that the failure to quantify regional physiologic severity due to stenosis as well as diffuse disease makes global CFR of little clinical value for guiding management of CAD [25]. High global CFR of 3.0 (Fig. 6.62a) fails to quantify a severe inferior stress defect. Low global CFR of 1.9 also fails to identify a severe stress defect in LAD distribution large enough to reduce global CFR (Fig. 6.62b) associated with myocardial steal indicating collaterals to viable myocardium. Thus, global CFR fails to quantify significant physiologic severity of focal stenosis needed for optimally guiding personalized clinical management in an individual patient and predicting risk or outcomes.

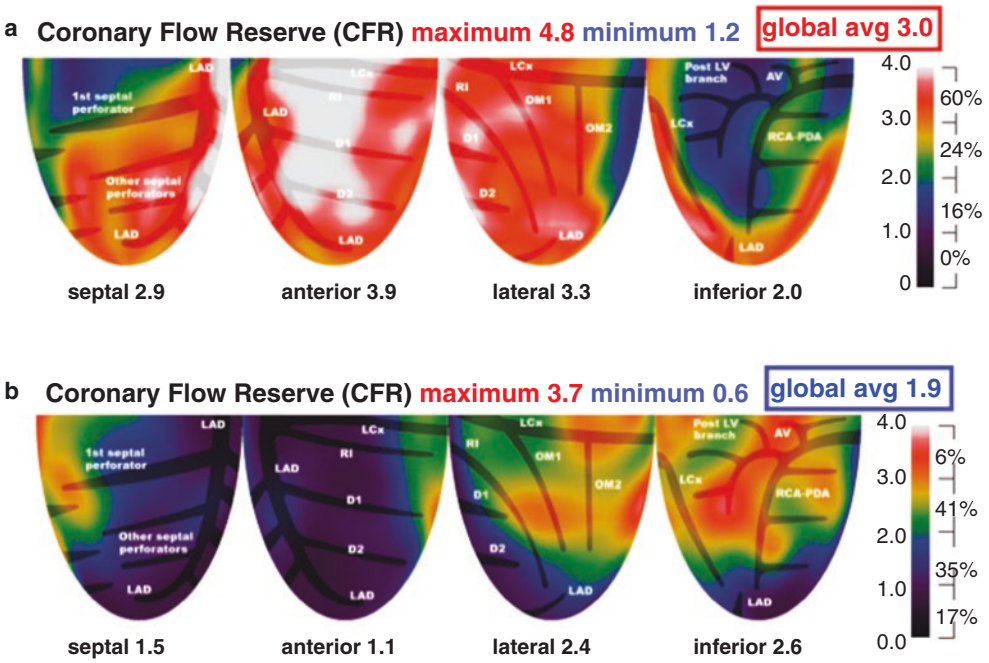

Fig. 6.62 Global CFR versus regional CFR to guide clinical management. (**a**) Global CFR is excellent at 3.0 but fails to account for a severe, high-risk inferior stress defect. (**b**) A low global CFR fails to differentiate diffuse CAD from a high-risk, severe stenosis of the LAD proximal to the first septal perforator and wrapping around the apex. Thus, both high and low global CFR fail to quantify significant focal physiologic severity needed to guide clinical management and predict risk or outcomes relevant to individual patients. (*From* Gould and Johnson [25]; with permission from Elsevier)

Figure 6.63 illustrates another case of a patient in whom global CFR is excellent at 2.97 which fails to account for the severe, high-risk, inferior abnormality because of the surrounding excellent CFR. In addition, the global CFR fails to identify inferior myocardial steal, indicating collateral perfusion beyond total or subtotal occlusion of a dominant RCA, as the CFR is excellent in the proximal LCx and OM1 distributions. The CFC map correctly quantifies this inferior abnormality in the face of excellent surrounding CFC that averages the global CFR to 2.97.

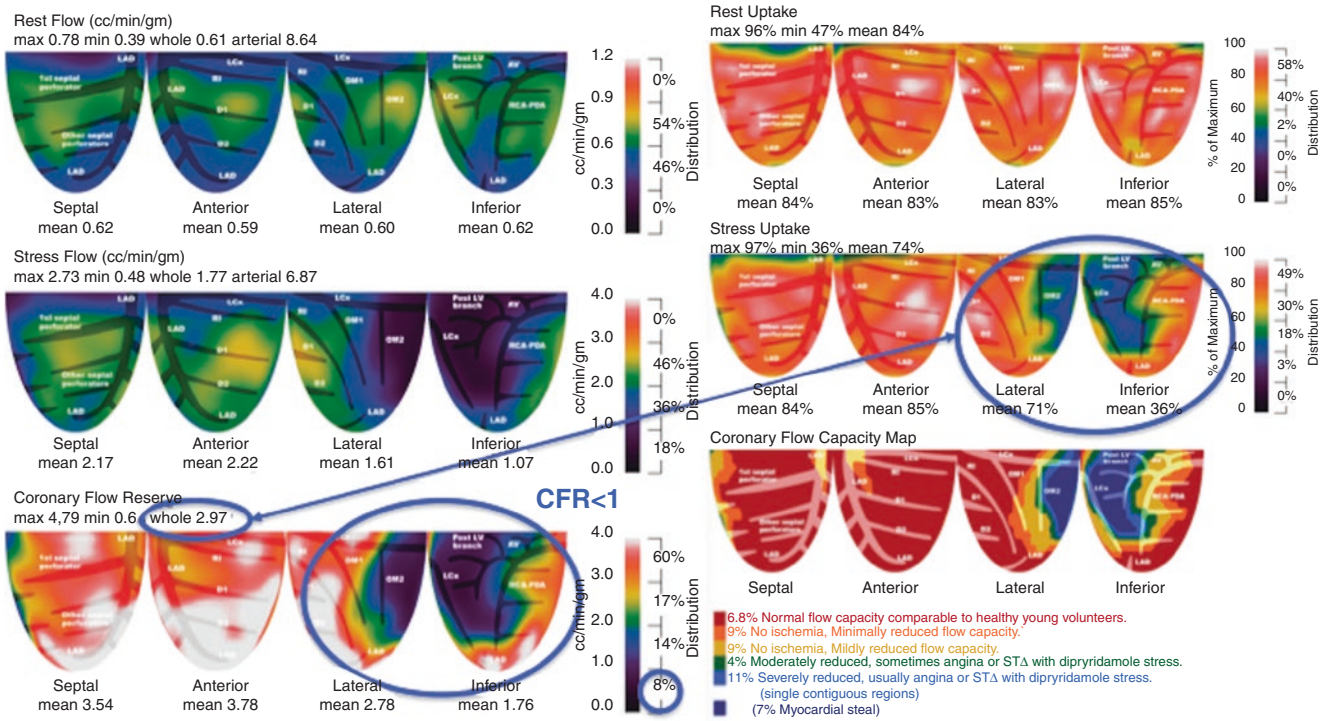

Fig. 6.63 Global CFR versus CFC to guide clinical management. The excellent global CFR in this patient fails to account for a severe, high-risk, inferior abnormality, and the global CFR also fails to identify inferior myocardial steal, indicating collateral perfusion beyond total or subtotal occlusion of a dominant RCA, as the CFR is excellent in the proximal LCx and OM1 distributions. The CFC map correctly quantifies this inferior abnormality

Figure 6.64 compares the probability of MACE-free survival over 9 years in patients with severely reduced CFC on PET versus those with no severe CFC reduction. For severe CFC abnormalities, the risk of death, MI, or stroke is 60% over the 9 years of follow-up, but the risk is low for the non-severe group. The PET scans to the right show representative severely reduced CFC (blue) or no severely reduced CFC (no blue).

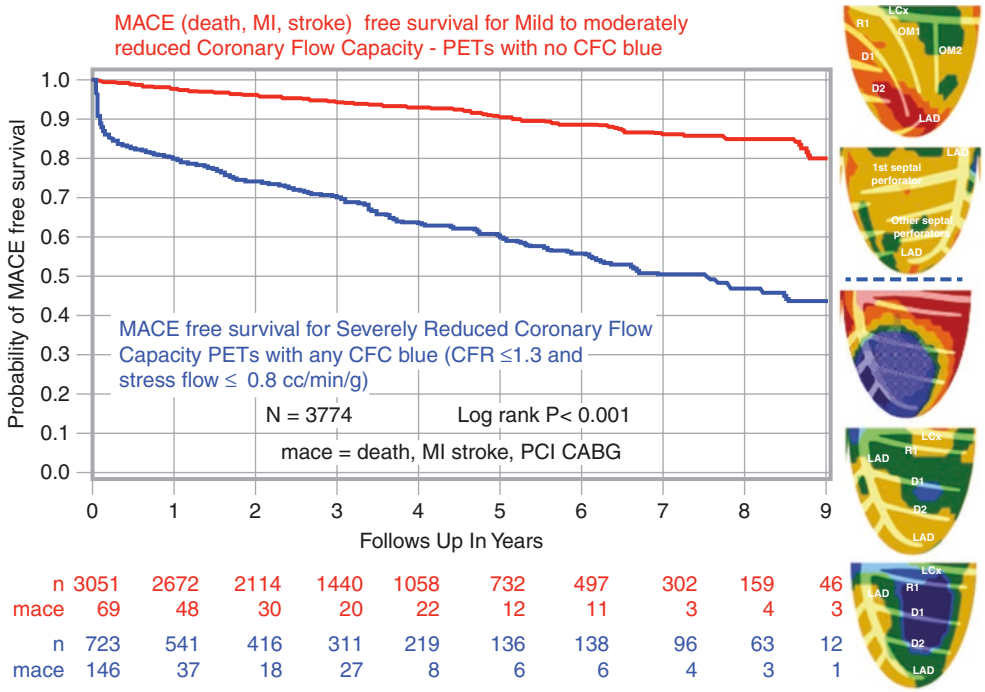

Fig. 6.64 Risk of death, MI and stroke (MACE) during 9 years of follow-up in patients with severely reduced CFC (*blue*) compared with no severe CFC abnormalities (*no blue*). The top two single CFC views (from different patients show) the range of non-severe CFC (*no blue*) associated with low risk. The lower three single views show the range of severely reduced CFC [39]

Figure 6.65 demonstrates that revascularization within 90 days after PET is associated with 54% reduced risk of death, MI, or stroke in patients with severe CFC abnormalities, compared with similar severely abnormal CFC without revascularization ($P = 0.0396$). Among patients with only mild or moderate CFC impairment, however, rates of MACE were insignificantly *higher* ($P = 0.45$) in the revascularization group. The lack of benefit with revascularization in these patients reflects their diffuse, nonobstructive CAD without severe focal stenosis by PET.

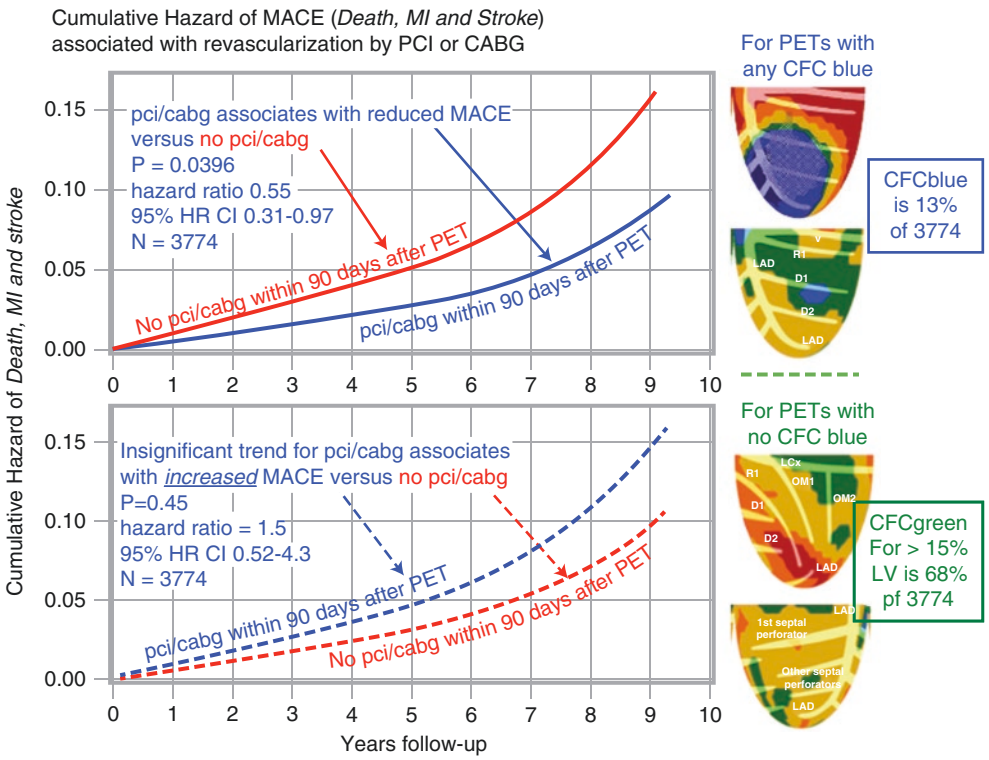

Fig. 6.65 Risk of death, MI, or stroke with and without revascularization for severely reduced CFC and for no severely reduced CFC. This figure plots cumulative hazard over 9 years showing reduced death, MI, or stroke after revascularization within 90 days after PET (*solid blue line*) versus no revascularization within 90 days after PET (*solid red line*) ($P = 0.0396$). For patients with mild or moderate CFC impairment, however, MACE was insignificantly more frequent in the revascularization group (*blue dashed line*) versus the no-revascularization group (*red dashed line*) ($P = 0.45$). The top two single CFC views (from different patients) show the range of severe CFC (*blue*) associated with high risk that is significantly reduced by revascularization. The lower two single views show CFC with no severe pixels (*no blue pixels*) associated with no benefit or increased risk with revascularization; the risk in this group reflects diffuse, nonobstructive CAD. (*From* Gould et al. [39]; with permission from the Society of Nuclear Medicine and Molecular Imaging)

In this population with high prevalence of CAD (89% with coronary calcium), PET identified 13% as severe enough to warrant coronary angiogram. Of quantitative PET-guided coronary angiograms, 80% had a revascularization procedure. Although prevalence of CAD was high in this population as confirmed by abnormal PET, the PET quantitative metrics showed mild to moderate CAD in 68% that would not benefit from angiogram or revascularization procedures but were best served by medical management alone. Thus quantitative PET was optimal and unique as the gatekeeper and guide to interventions compared to any other test reported in the literature.

As demonstration of its validity as a general concept in Fig. 6.66, invasive CFC as combined absolute coronary flow velocity reserve and CFR predicts a high risk of MACE paralleling PET CFC, from which the invasive measurements evolved [70–74].

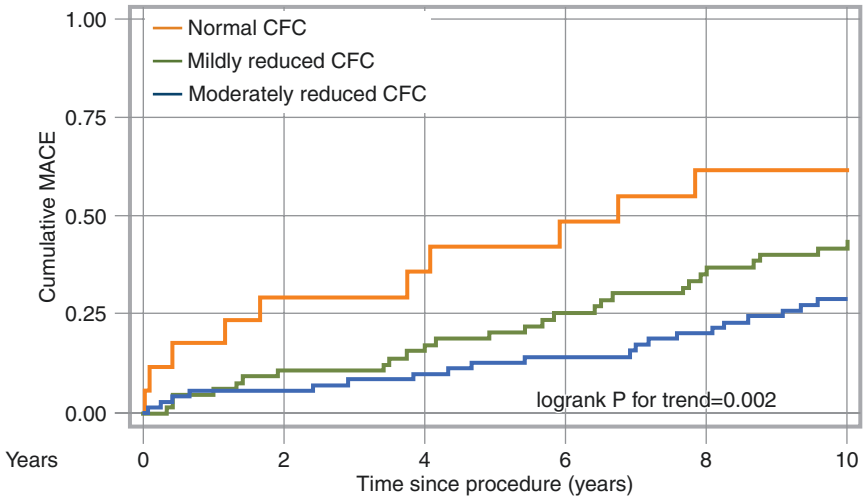

No. at. risk:

Normal CFC	70	66	63	60	55	47
Mildly reduced CFC	65	57	54	46	39	31
Moderately reduced CFC	17	11	10	8	6	5

Fig. 6.66 Invasive CFC with coronary flow velocity and MACE. (*From* van de Hoef et al. [70]; with permission from Elsevier)

As further demonstration of its validity as general concept, CFC determined as combined coronary flow by intracoronary bolus thermodilution reserve and CFR (Fig. 6.67) also a high risk of MACE paralleling PET CFC from which the invasive measurements evolved [72, 73].

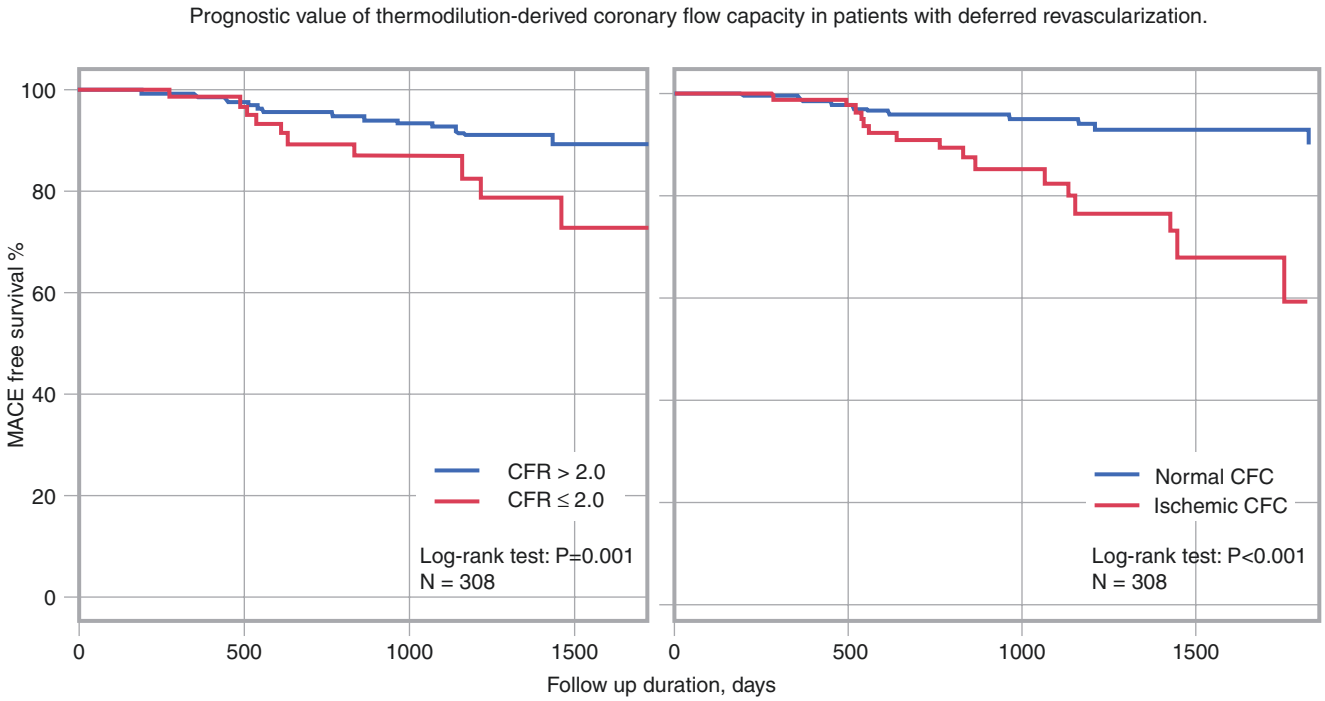

Fig. 6.67 Prognostic value of invasive CFC versus CFR with coronary thermodilution and MACE [72, 73]. (*From* Hoshino et al. [73]; with permission from from CongrHealth.com)

The pathophysiologic sequence of recurrent subclinical plaque ruptures leads to acute coronary syndromes (ACS) [75–77]. As illustrated in Fig. 6.68, 89% of acute fatal coronary events result from a series of preceding, subclinical, small plaque ruptures that heal with progressive narrowing to a severe stenosis. The last plaque rupture finally occludes the small remaining lumen, producing myocardial infarction. Most of these subclinical small plaque ruptures heal and stabilize without occluding the relatively large lumen. A large, nonstenotic lumen with an initial single occlusive plaque rupture explains only 11% of fatal infarctions at pathologic examination. This mechanism of serial plaque rupture to severe stenosis before an event explains why the most powerful or compelling indicator of high risk needing revascularization is severely reduced CFC.

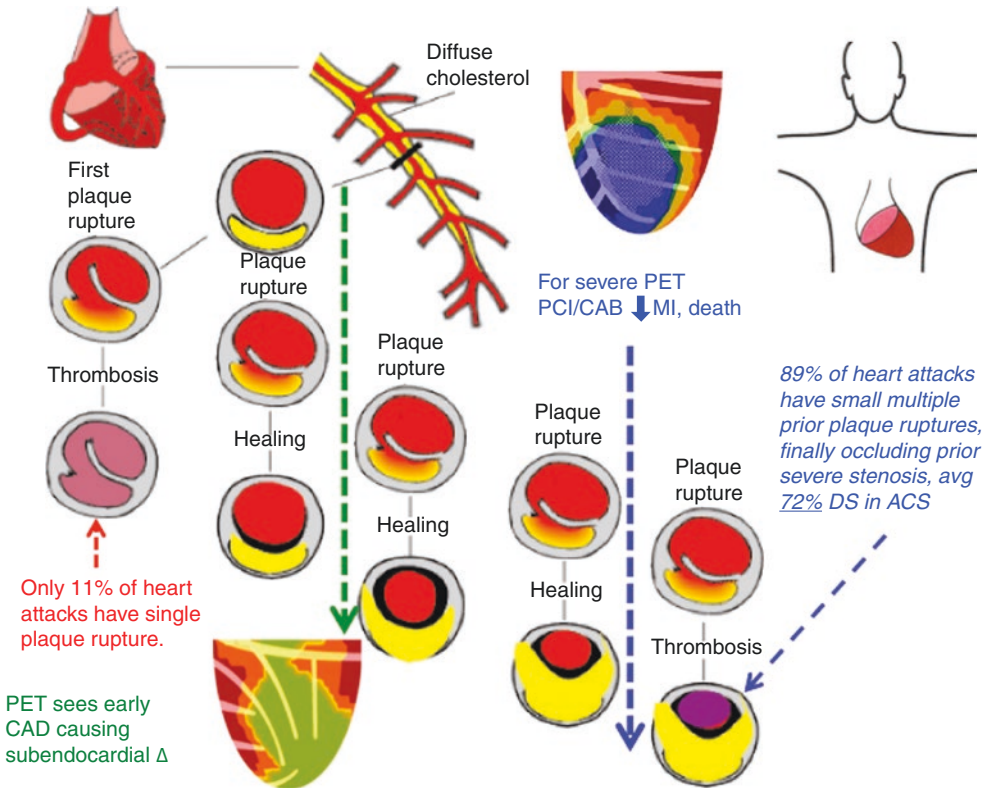

Fig. 6.68 Plaque rupture and quantitative PET perfusion [2]. DS diameter stenosis

Intracoronary optical coherence tomography–intravascular ultrasound (OCT-IVUS) in acute coronary syndromes (ACS) demonstrates severe focal lumen narrowing (averaging 72 ± 13% diameter stenosis) superimposed on varying severities of diffuse disease. This OCT-IVUS finding confirms in patients the high risk of severe stenosis superimposed on diffuse disease in ACS. This progression to severe stenosis by serial plaque ruptures may develop over days, weeks, months, or years thereby explaining the continuum of clinical manifestations from ACS to chronic "stable" CAD of varying severity.

The anatomic and physiologic severity of CAD associated with ACS defines the severity threshold at which revascularization may reduce MI and mortality in patients with chronic CAD. Quantitative PET identifies and quantifies this high-risk severity underlying ACS, thereby explaining the reduction of MACE after revascularization of severely reduced CFR (*see* Fig. 6.65).

During vasodilation stress, diffuse epicardial CAD may cause graded, base-to-apex longitudinal pressure and perfusion gradients [12–15, 78] (Fig. 6.69). In the absence of proximal stenosis, FFR measurement in the distal coronary artery correlated with PET-measured longitudinal perfusion gradients during vasodilation stress in 43% of patients in the study by Bom et al. [78]. Proximal stenosis may preclude longitudinal pressure and perfusion gradients. Longitudinal perfusion gradients do not substitute for CFC or CFR, but rather add insight on diffuse CAD that may moderate any potential benefit from stents.

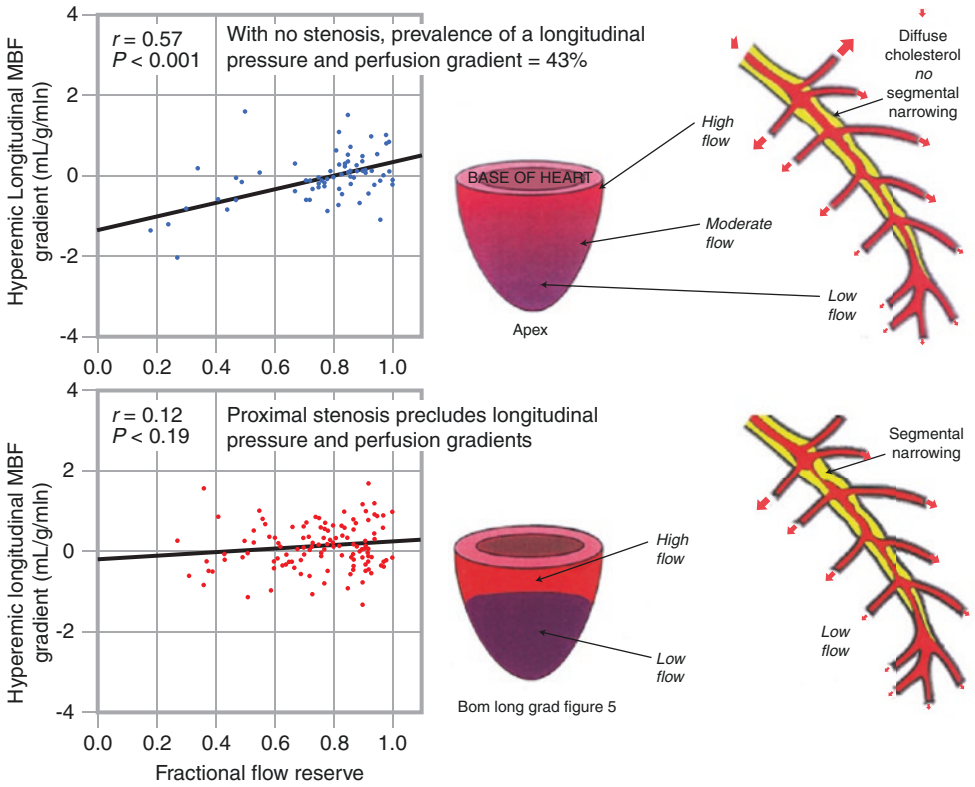

Fig. 6.69 Longitudinal perfusion gradients, another face of diffuse CAD. MBF myocardial blood flow. (From Bom et al. [78]; with permission from Oxford University Press)

Base-to-apex longitudinal pressure and perfusion gradients commonly reduce subendocardial perfusion during vasodilation stress, particularly at the apex because of cumulative pressure loss due to viscous friction along the length of the artery [2, 12, 13, 15, 25, 49, 78]. In the patient shown in Fig. 6.70, blood flow is shunted into proximal branches owing to pressure declining along the arterial length sufficient to reduce flow at the apex to values lower than resting values; this *branch steal* is documented experimentally and is clinically associated with angina.

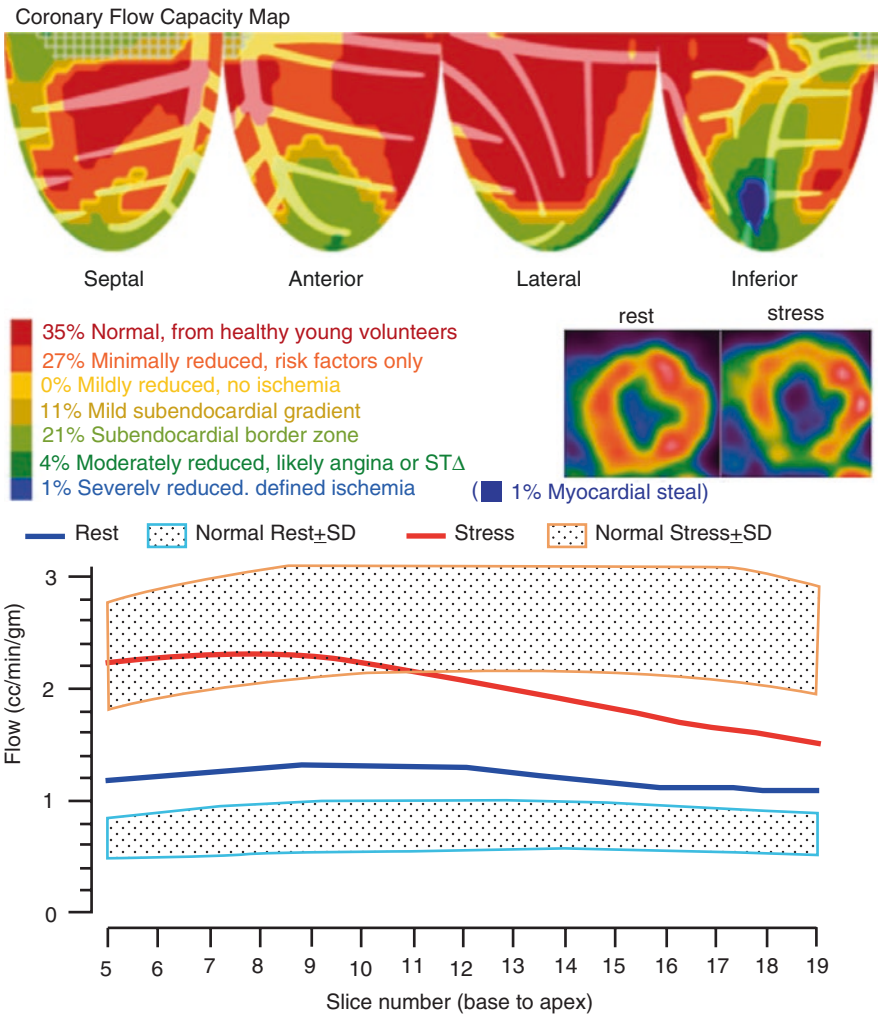

Fig. 6.70 Longitudinal perfusion gradients and subendocardial ischemia. In this patient, blood flow is shunted into proximal branches owing to pressure along the arterial length that is sufficient to reduce flow at the apex to values lower than resting values

Collaterals typically connect from a patent supply artery to an occluded artery through small distal anastomosis. Therefore, in many cases, the direction of collateral flow is from distal to proximal perfusion regions, thereby causing a reverse longitudinal gradient during vasodilation stress and myocardial steal (Fig. 6.71). In these patients, the worst perfusion defect is therefore at the base, where the occlusion is located; this area is the farthest away from the best perfusion, which is found at the source of flow through the distal collateral anastomosis.

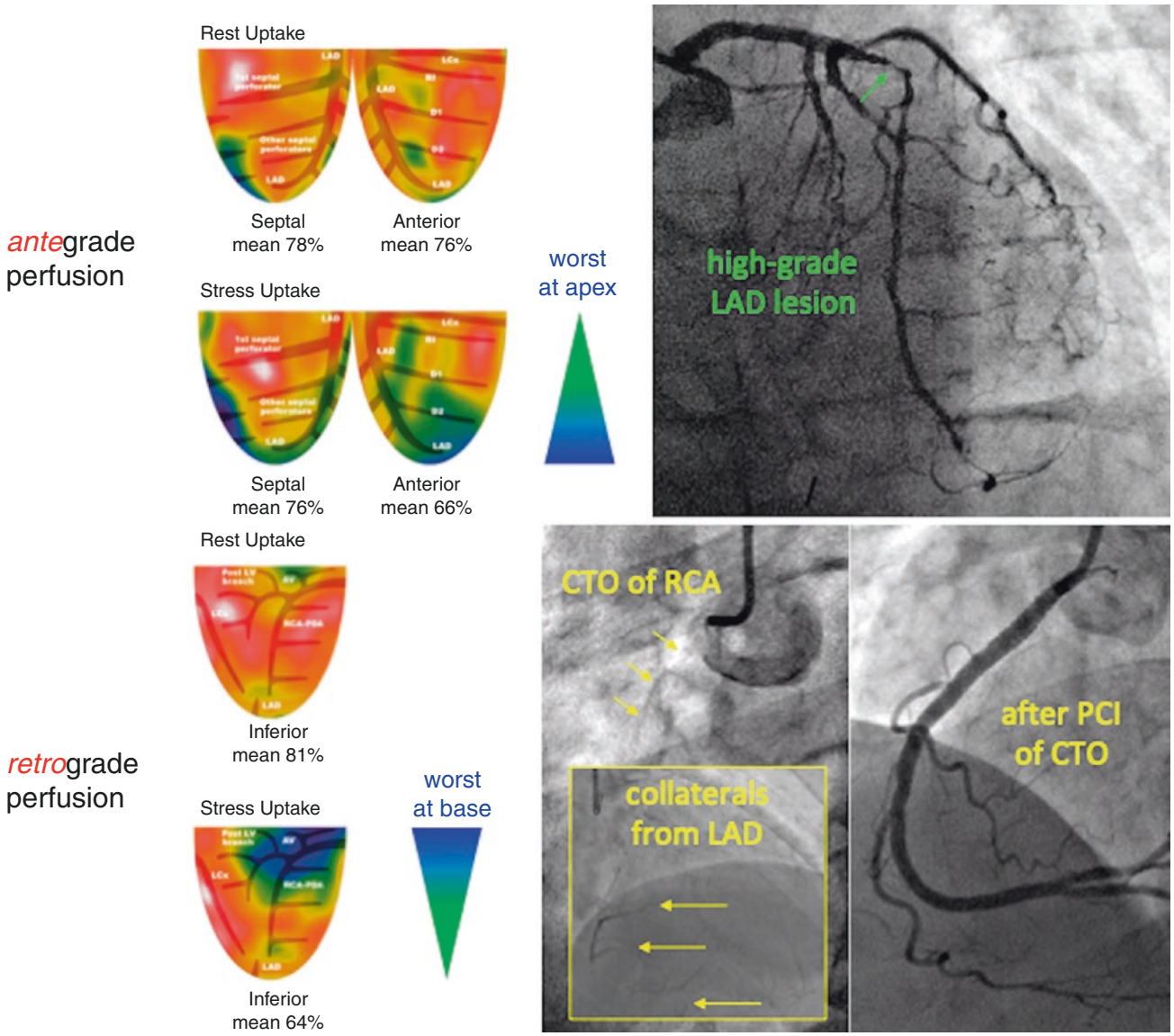

Fig. 6.71 Reverse apex-to-base longitudinal perfusion gradient: retrograde perfusion through a distal collateral anastomosis is worst at the base. CTO chronic total occlusion

Figures 6.72 and 6.73 compare phasic coronary blood flow, pressure, and transmural perfusion with normal coronary arteries versus CAD. With normal coronary arteries, systolic compression stops coronary blood flow, with post-systolic reactive hyperemia; diastolic flow is high in early diastole and falls during later diastole. This normal phasic coronary pressure and flow supply the LV with adequate transmural flow even during tachycardia and high flow demands. In patients with coronary artery narrowing or marked LV hypertrophy, however, the rapid diastolic flow cannot compensate for systolic compression, and the result is subendocardial or transmural ischemia, particularly with tachycardia of hypertension, which further impede subendocardial perfusion.

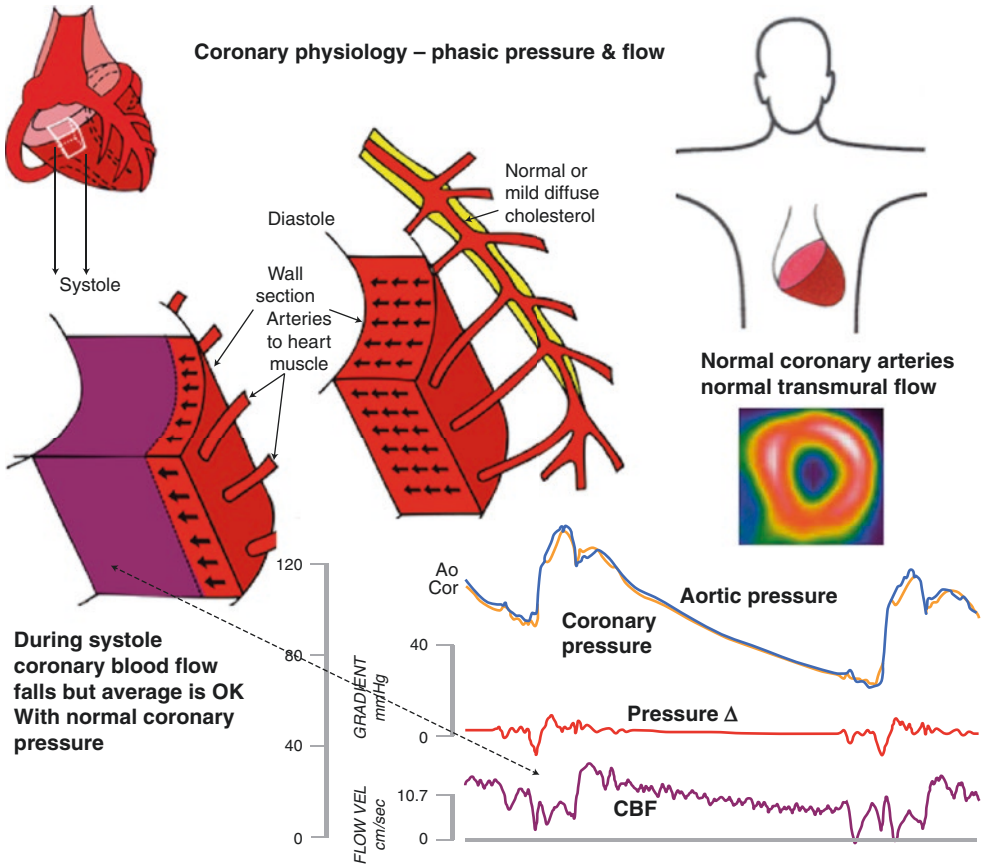

Fig. 6.72 Phasic coronary blood flow, pressure, and transmural perfusion with normal coronary arteries

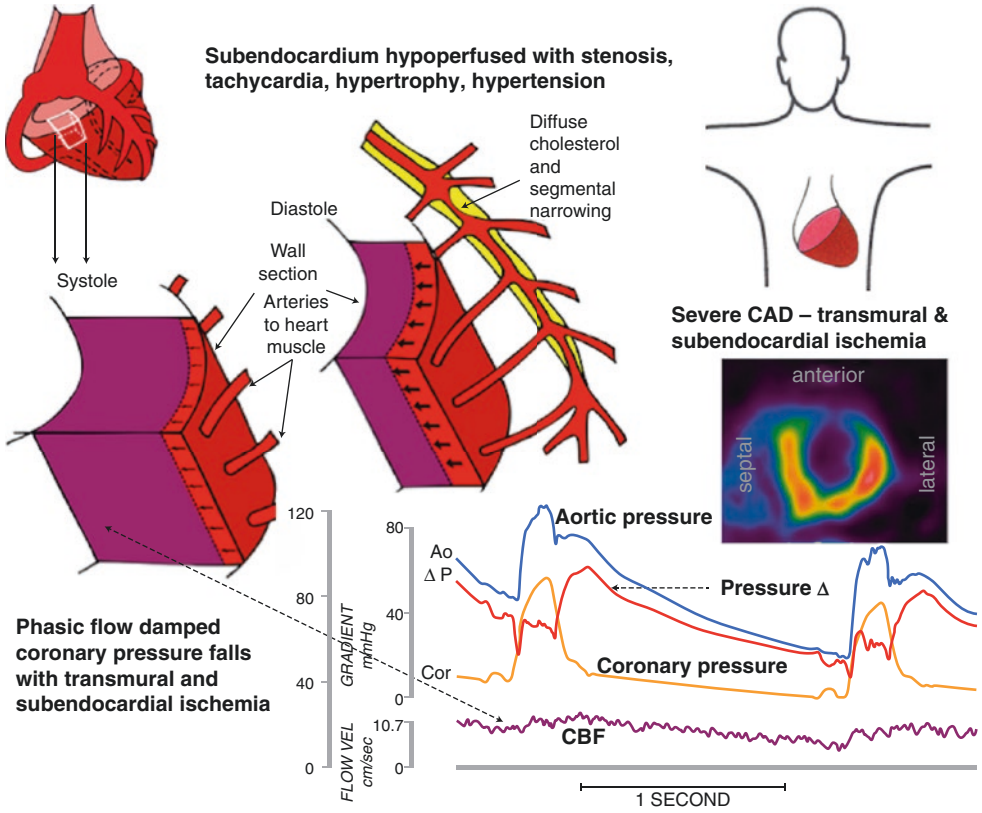

Fig. 6.73 Phasic coronary blood flow, pressure, and transmural perfusion with CAD

When patients complain of angina, we ask what size and severity of low subendocardial perfusion is causing it. In the example shown in Fig. 6.74, a large, severe LAD stress defect indicated severe stenosis or occlusion of the LAD proximal to the first septal perforator and proximal to large diagonal branches. After LAD stenting the patient still had angina, stress perfusion was much better, but a small area of mildly reduced subendocardial perfusion continued to cause moderate angina and STΔ >1 mm during dipyridamole stress, indicating subendocardial ischemia. Angina from this low-risk stress perfusion defect is explainable by the interrelated physiology of CFC (top panel of PET images), subendocardial perfusion (left tomograms and lower-right activity profiles), and FFR by PET expressed as the relative map of stress perfusion in cc/min/g (FFRpet, upper right black and brown color bar scale). The relative image of stress PET perfusion in cc/min/g is the original reference standard used to validate invasive pressure-derived FFR [79, 80], as further detailed below in Figs. 6.75, 6.76, 6.77, 6.78, 6.79, and 6.80.

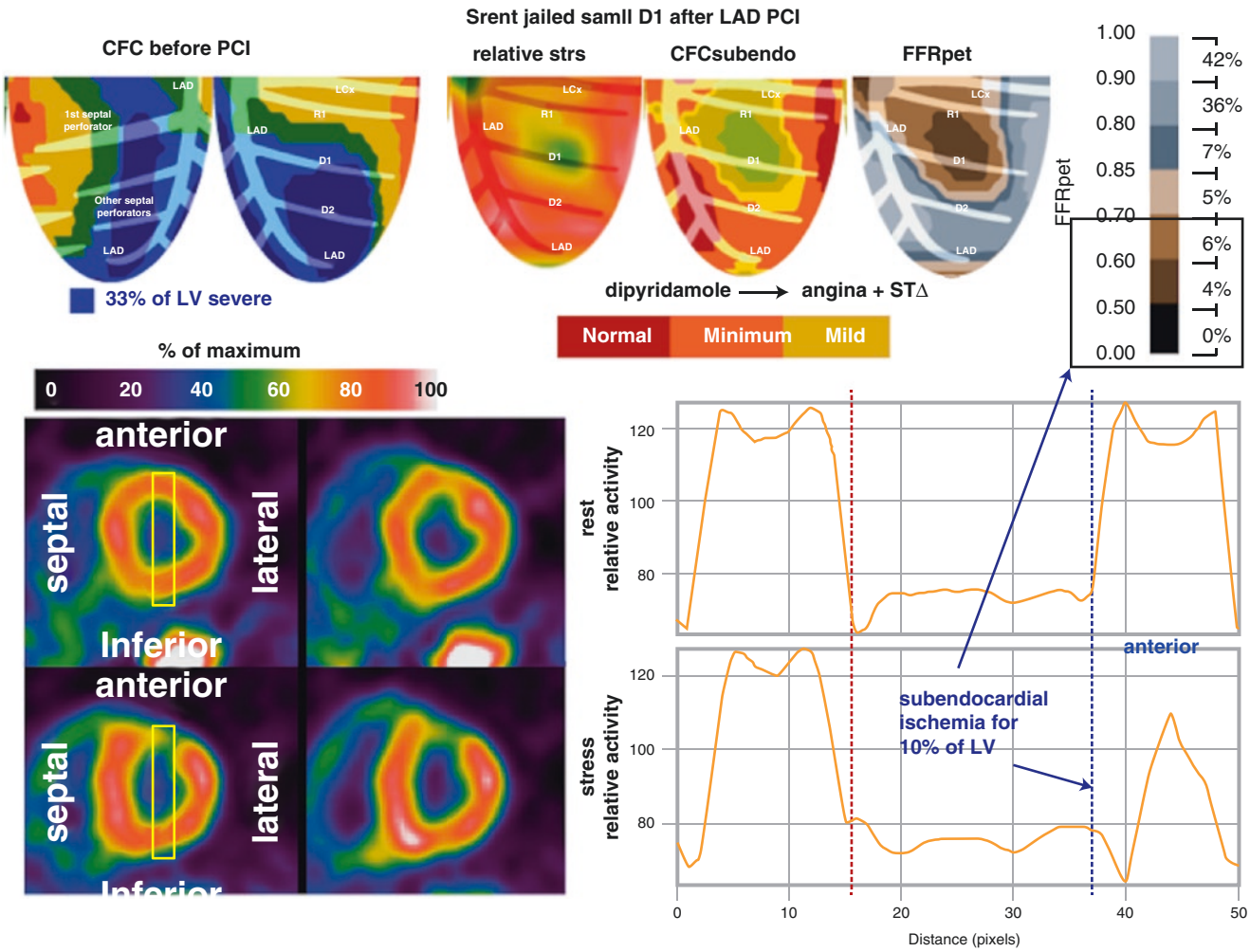

Fig. 6.74 Angina caused by reduced subendocardial perfusion. A large, severe LAD stress defect indicated severe stenosis or occlusion of the LAD proximal to the first septal perforator and proximal to large diagonal branches, but the angina continued (though it was less severe) after a stent was placed with PCI. At PET after the LAD stenting, stress perfusion is much better, with a small residual mid-anterior stress defect in a small D1 distribution caged by the LAD stent. This small area of mildly reduced subendocardial perfusion, comprising only 3% of LV (*light green* on the CFC map) caused moderate angina and STΔ >1 mm during dipyridamole stress, indicating subendocardial ischemia

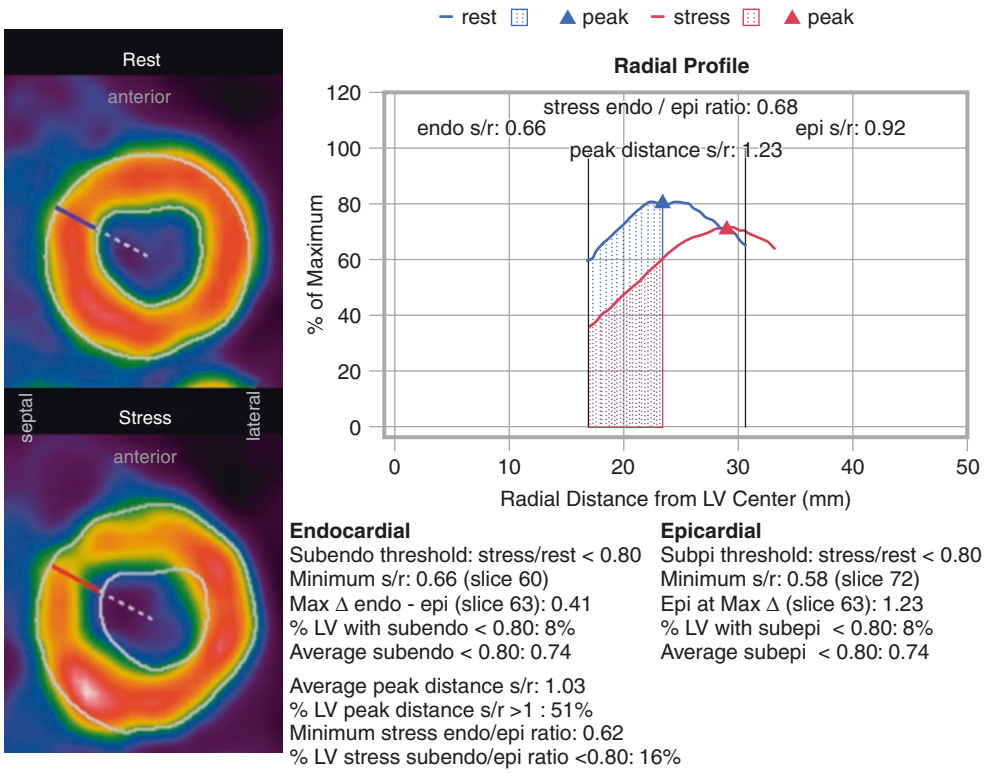

Fig. 6.75 Automated quantitative subendocardial analysis for the patient in Fig. 6.74. FFRpet below 0.7 for 10% of the LV associated with reduced subendocardial perfusion in the tomograms and activity plots is quantified as a minimum subendo/epicardial ratio of 0.62 and 16% of LV with a subendo/epicardial ratio <0.8. For each relative tomographic slice, the rest endocardial and epicardial boundaries are tracked in *white lines*. The rest endocardial boundary is projected onto the same stress slice and the stress epicardial boundary is outlined. Radial activity is tracked between these boundaries to determine the peak values at radial distance from the center of the LV (here the *blue line* for resting radial activity profile and the *red line* for stress activity profile of this tomographic slice). On each rest tomographic slice, the area from rest endocardial boundary to peak activity defines the subendocardium (*blue hatched area*) for comparison to stress activity within this same area (*red hatched area*) as the subendocardial stress/rest ratio (red area/blue area) for each of 64 radii in each of 20 tomographic slices. The subendocardial stress/rest ratio threshold of <0.8 was established from the mean ± 1.95 SD of 124 healthy volunteers under 40 years old without risk factors. This subendocardial stress/rest ratio is reported in several different ways, describing size and severity as follows: the minimum of all radii in the LV (here 0.66), the % LV with the subendocardial stress/rest ratio <0.8 (here 8%), the average subendocardial ratio <0.8 (here 0.74), and the maximum subendo-subepicardial difference of all radii (here 0.41). The final metric accounts for stress-induced LV dilatation as the radial distance from the center of the LV to the peak radial activity for each radius of each rest and stress tomographic slice, expressed for the whole LV as the average peak radial distance stress/rest (in this case, 1.03) and the % of LV with a peak radial stress/rest ratio >1.0 (here, 51%), indicating normal or minimal LV dilatation with stress

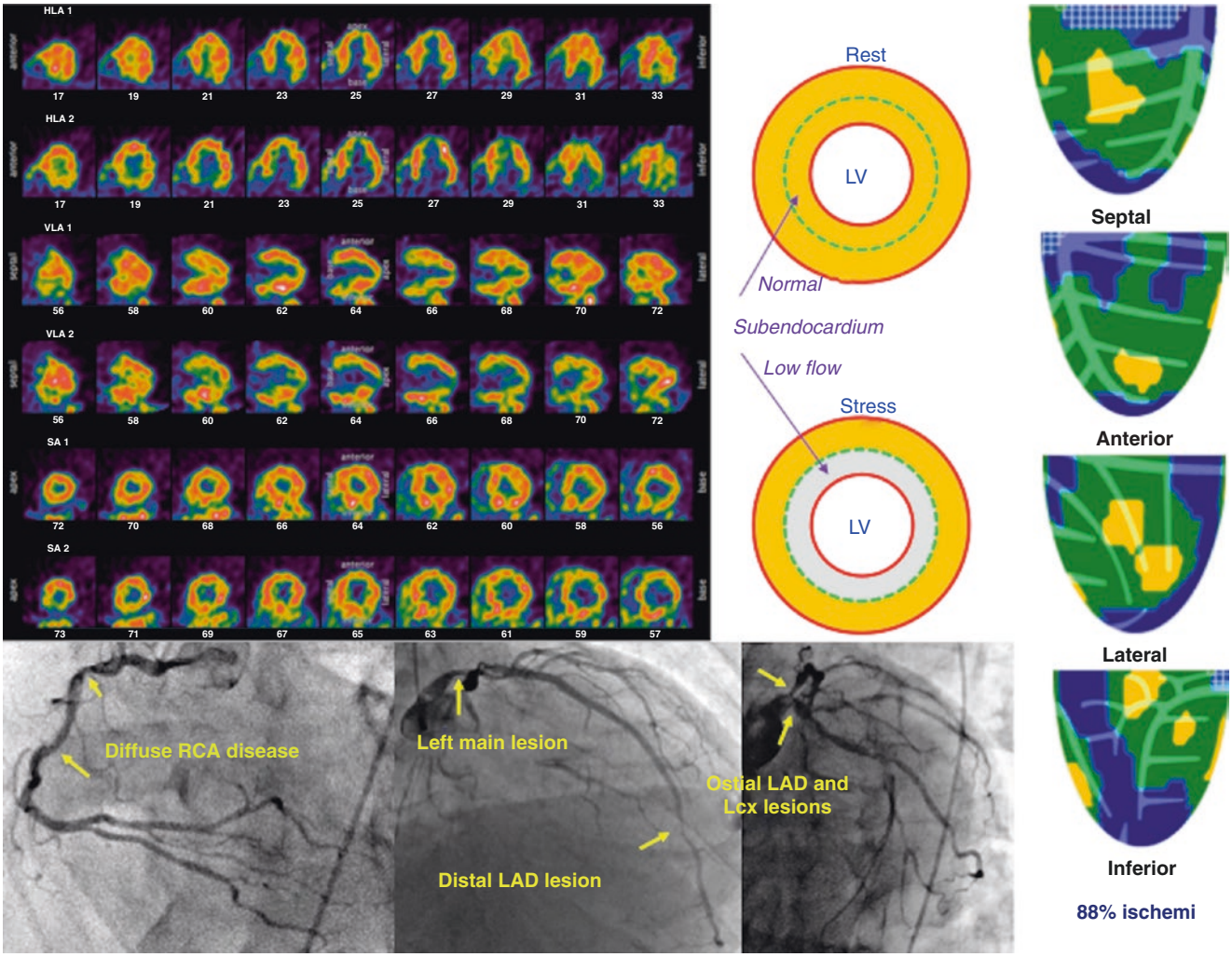

Fig. 6.76 Global subendocardial ischemia and angina

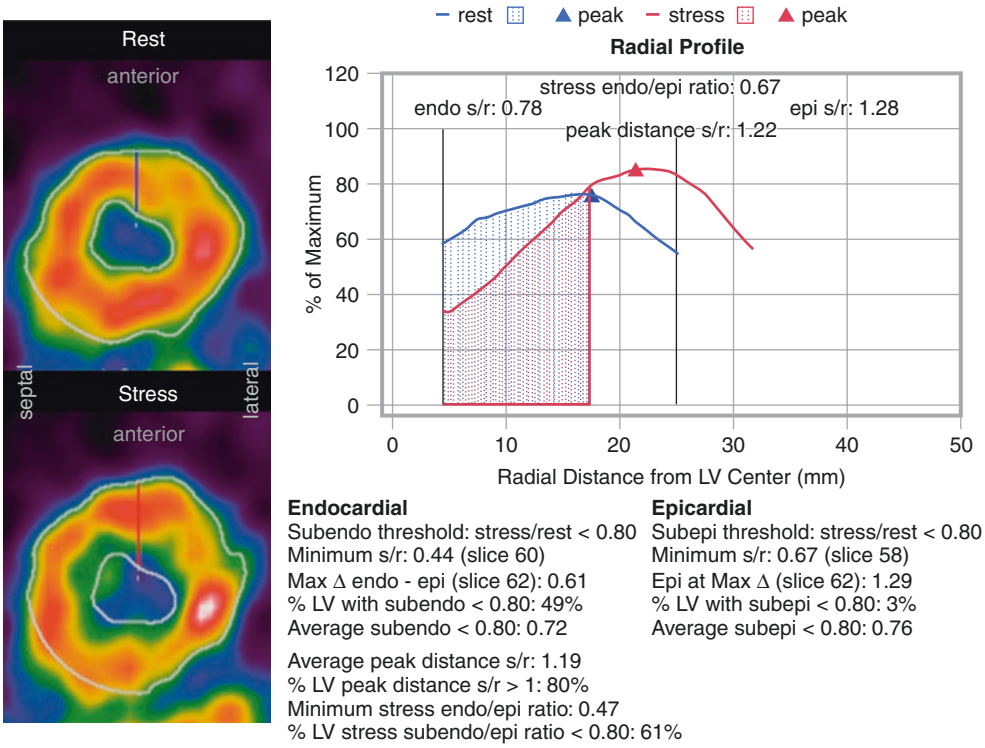

Fig. 6.77 Automated quantitative subendocardial analysis for the patient in Fig. 6.76. Using the same terms and methodology described for Fig. 6.75, the subendocardial metrics shown here include minimum subendocardial stress/rest ratio, 0.44; average subendocardial stress/rest ratio, 0.72; 80% of LV with subendocardial stress/rest ratio <0.8; minimum stress subendo/epicardial ratio, 0.47; 61% of LV with subendo/epicardial ratio <0.8; average radial peak distance stress/rest ratio, 1.19; and 80% of LV with peak distance stress/rest ratio >1.0—all results that indicate severe, diffuse subendocardial ischemia and ischemic LV dilatation

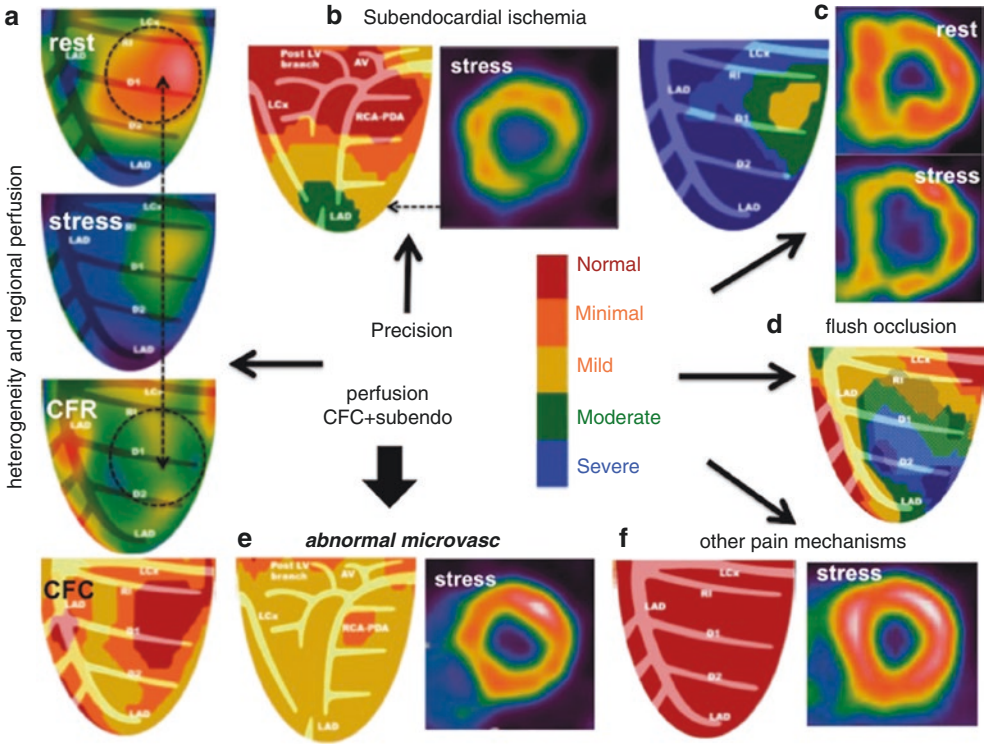

Fig. 6.78 CFC solutions for common clinical issues without angiographic stenosis, shown for efficiency in single views of CFC maps: (**a**), Abnormal CFR due to resting perfusion heterogeneity and only mildly diffusely reduced CFC; (**b**), Mild, diffuse epicardial CAD with good small-vessel function and high stress flow sufficient to cause a longitudinal perfusion gradient; (**c**), Severe, diffuse epicardial CAD with good small-vessel function (enough small-vessel function for stress flow to reduce coronary perfusion pressure, causing severe global subendocardial ischemia and LV dilatation); (**d**), Flush occlusion (chronic occlusion) of a large diagonal not seen on angiography; (**e**), Small-vessel disease with uniform regional and transmural reduction of CFC; (**f**), Angina during very high CFC with normal subendocardial perfusion, indicating altered pain mechanisms without ischemia. (*From* Gould and Johnson [25]; with permission from Elsevier)

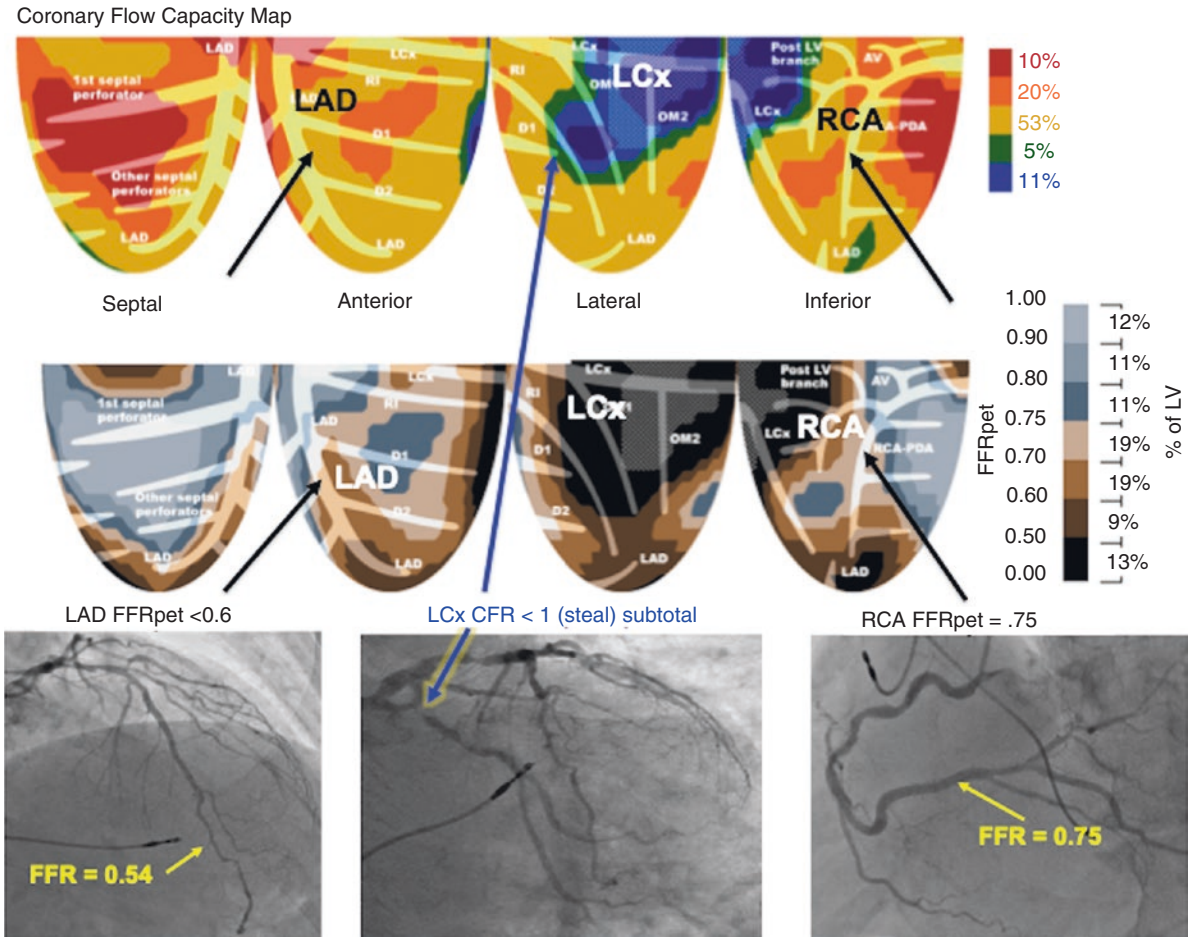

Fig. 6.79 Interrelated physiology—CFC, FFRpet, and FFR by pressure wire—in complex CAD. In this figure, CFC is mildly reduced in LAD and RCA distributions (*yellow*), indicating mild to moderate flow-limiting stenosis but severe stenosis or occlusion of the LCx (*blue*) in 11% of LV, with myocardial steal indicating collaterals. The relative map of stress FFRpet shows severe reduction to <0.6 in the LAD, to 0.7–-0.75 in the RCA (confirmed by FFRpressure) and to <0.5 in the LCx; a cumulative 41% of the LV has FFRpet <0.7

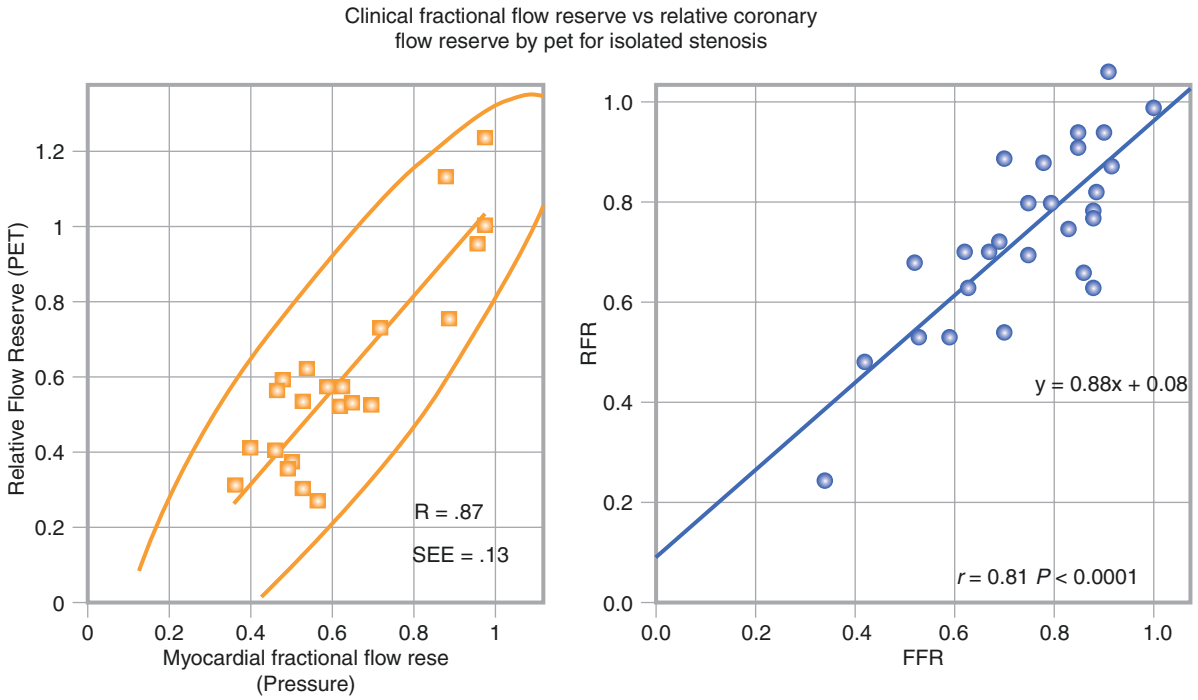

Fig. 6.80 Interrelated physiology—FFR based on intracoronary pressure. (*Left panel from* De Bruyne et al. [79] and *right panel from* Marques et al. [80]; with permission from the American Heart Association)

Typically, Invasive pressure-derived FFR is measured at one point just beyond an angiographic stenosis. However, as shown in Figs. 6.8 and 6.11, no single value of CFR or FFR characterizes a coronary artery. Instead, a range of values along the branching vessel length, as illustrated by the "FFRpet" single view on Fig. 6.74, which shows a progressively more severe gradation of values along the vessel length, with proximal iso-contour values falling from 0.75 to 0.5 most distally, owing to the diffuse CAD underlying most if not all stenosis.

This proximal-to-distal gradation parallels the range of distal-to-proximal pull-back pressures along the vessel length [15], which are not currently acquired in clinically measured FFR. Because invasive pressure-derived FFR is a single measure just distal to the stenosis, it fails to account for more distal lower values seen by PET. FFRpet values are typically worse distally than the proximal pressure measurements, which are more comparable to the higher FFRpet iso-contour just distal to the stenosis than to the lower distal values. Moreover, for an occluded artery (as for the stent-caged diagonal branch in Fig. 6.74), pressure-derived FFR cannot be measured, but the relative distribution of stress perfusion in cc/min/g or FFRpet can be mapped. In this example, the minimum FFRpet reached 0.5. Blood pressure during dipyridamole stress was 94/44 mm Hg, for a mean blood pressure of 61 mm Hg. Multiplying this by the FFRpet of 0.5 suggests a stress subendocardial perfusion pressure of 31 mm Hg, as in Fig. 6.12 [24], at which ischemia occurs experimentally [20] and in humans [21]. Figure 6.75 shows automated quantitative subendocardial analysis for the same patient. This analysis identified a small, mild defect that was associated with low risk on long-term follow-up (as in Fig. 6.65) but that nevertheless caused definite angina and significant ST depression during dipyridamole stress.

The primary subendocardial perfusion metrics are automatically determined in the software, but the operator can examine every radius on any slice by scrolling through all the slices and sweeping the radius like a clock around each slice. In addition, for each tomographic slice of the stress images, the midpoint is determined between the stress epicardial boundary and the rest endocardial boundary projected onto the stress slice. For each radius, the area within the endocardial half/epicardial half of the stress activity profile determines the stress subendo/epicardial ratio for that radius. The stress subendo/epicardial ratio for size and severity are reported as the minimum stress subendo/epicardial ratio (0.62 in Fig. 6.75) and the % of LV with a stress subendo/epicardial ratio <0.8 (16% in this example). The final metrics account for stress-induced LV dilatation of 1.03 or 3%.

For severe, balanced three-vessel stenosis, as seen in Fig. 6.76, or severe diffuse narrowing, even small increases in coronary flow may cause a severe fall in pressure along the arterial length, thereby causing diffuse subendocardial ischemia, LV dilatation, decreased ejection fraction, and TID (transient ischemic dilatation). Figure 6.77 shows the automated quantitative

subendocardial analysis for the same patient, which indicates severe, diffuse subendocardial ischemia and ischemic LV dilatation.

Figure 6.78 illustrates a number of ways in which CFC by PET can offer solutions for common clinical perfusion abnormalites with or without symptoms without apparent angiographic stenosis [23].

Figure 6.79 illustrates interrelated physiology—CFC, FFRpet, and FFR by pressure wire—in complex CAD. Low coronary pressure during vasodilatory stress parallels the corresponding abnormal map of relative stress cc/min/g (FFRpet) and absolute values of CFC (*see* Figs. 6.12, 6.13, and 6.73). FFRpet maps the entire LV with the typical graded proximal-to-distal pressure and perfusion gradient along the arterial length. The usual clinical measurement of a single intracoronary FFR based on pressure fails to reveal this essential clinical insight provided by FFRpet and the CFC maps, or an invasive pressure pullback curve.

Figure 6.80 illustrates interrelated physiology of the FFR based on intracoronary pressure. FFR was validated by comparison to relative stress perfusion in cc/min/g, thereby documenting the interrelations of CFC, FFRpet, and FFR in Figs. 6.74, 6.75, 6.76, 6.77, 6.78, 6.79, and 6.80. For these correlations, a single value of relative stress cc/min/g were an average for the predefined distribution of a major coronary artery, compared with invasive artery-specific pressure-derived FFR. This single average relative stress cc/min/g for an arterial distribution cannot therefore show the per-pixel actual arterial distributions seen in Figs. 6.74, 6.79, 6.81, and 6.95.

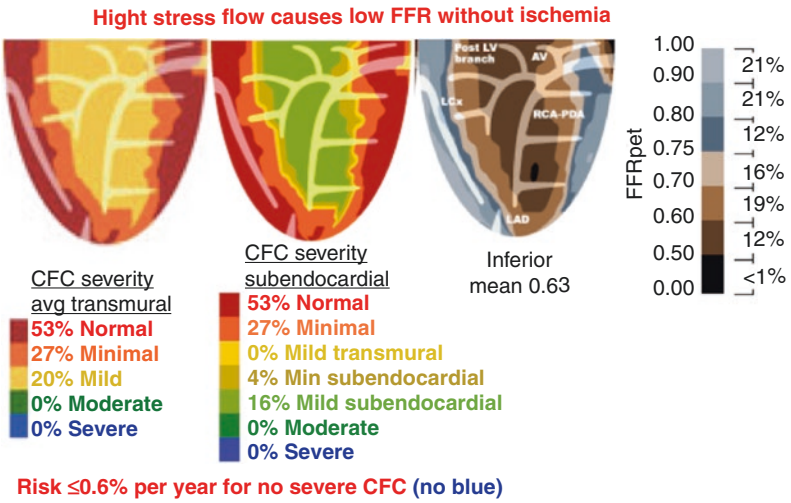

Fig. 6.81 Case example of the interrelated physiology of CFC, subendocardial ischemia, and FFRpet in an asymptomatic, active man who was able to do hard workouts without symptoms but had PET because of dense coronary calcium and hypercholesterolemia. PET showed excellent or adequate CFC (red and orange) for 80% OF LV with mildly reduced CFC (yellow) reflecting mildly reduced subendocardial to subepicardial ratio of myocardial perfusion. Relative stress flow expressed as a fraction of maximum stress ml/min/g or fractional flow reserve (FFRpet) by PET was ≤ 0.7 for 31% of LV. He had an ejection fraction of 66% by stress ECHO and no angina or STΔ during dipyridamole stress during dipyridamole stress PET. Since he is asymptomatic, should he have an invasive procedure for mild to moderately reduced subendocardial perfusion without angina? Figures 6.60, 6.64, and 6.65 indicate that the risk of MACE is very low, ≤ 0.6% per year for PET with no severely reduced CFC (no blue) suggesting that vigorous medical management is an appropriate option

Figure 6.81 shows a case example of the interrelated physiology of CFC, subendocardial ischemia, and FFRpet in an asymptomatic, active man who was able to do hard workouts without symptoms but who had PET because of dense coronary calcium. Since his CAD is asymptomatic, should he have an invasive procedure for mild to moderately reduced subendocardial perfusion without angina? Figures 6.60, 6.64, and 6.65 indicate that the risk of MACE is very low for this mild to moderately reduced CFC or FFRpet suggesting that vigorous medical management would be appropriate.

In Fig. 6.82, the relative subendocardial metrics for this same patient illustrates important new insights into the clinical coronary physiology. Low relative subendocardial perfusion does not mean ischemia or high risk if stress perfusion, CFR, and CFC are adequate and well above absolute thresholds for ischemia in cc/min/g. This patient's absolute transmural perfusion and CFC are well above the low absolute threshold for ischemia without angina or ST changes during PET stress imaging or hard exercise. Figure 6.65 shows that revascularization for mild to moderately reduced CFC is not associated with reduced MACE, as the risk of the procedure may be greater than the risk with medical treatment. When offered the objective data and the options for invasive and noninvasive management, this patient chose the noninvasive vigorous lifestyle and medical treatment.

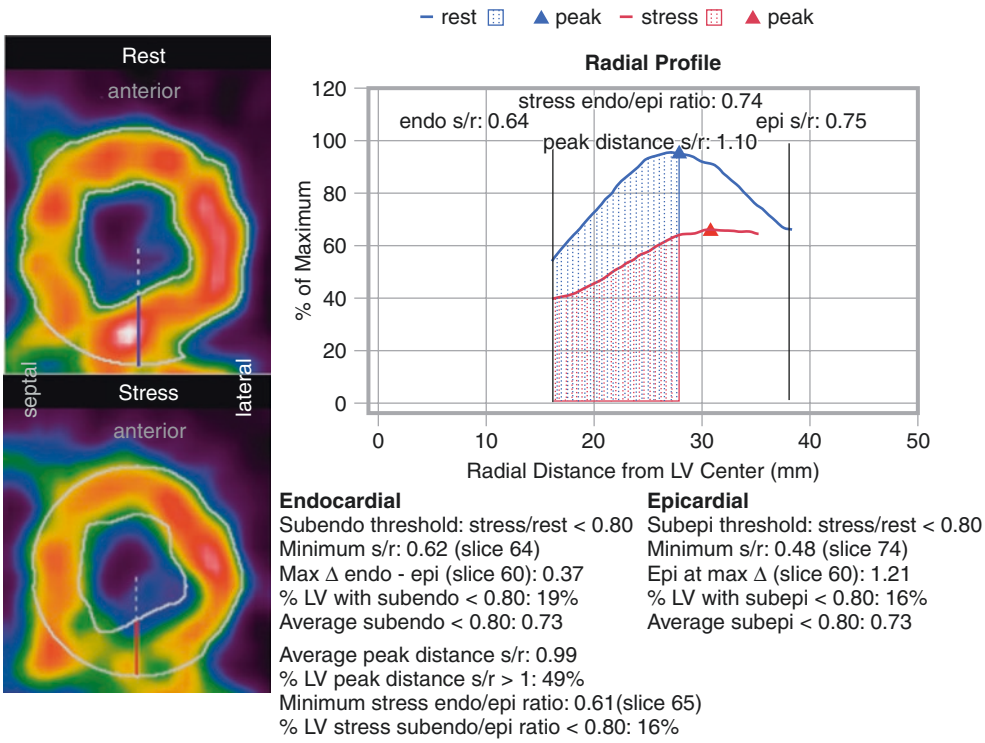

Fig. 6.82 Relative subendocardial metrics for the patient in Fig. 6.81. This case contrasts relative subendocardial metrics with absolute values of stress perfusion that are well above the threshold of low absolute perfusion for ischemia, here indicated by mildly reduced CFC (*yellow*) with no moderate (*no green*) or severely reduced pixels (*no blue*), associated with low risk. FFRpet is <0.7 (relative stress perfusion), and the diffuse and regional inferior subendocardial metrics are as follows: minimum subendocardial stress/rest ratio, 0.62; average subendocardial stress/rest ratio, 0.73; 19% of LV with subendocardial stress/rest ratio <0.8; minimum stress subendo/epicardial ratio, 0.61; 16% of LV with subendo/epicardial ratio <0.8; average radial peak distance stress/rest ratio, 0.99—all indicating CAD

Essentially all clinical outcome data in the literature and for this chapter are based on 2D PET scanners with the most widely used type of detectors, BGO (bismuth germinate oxide). 3D acquisition incurs such high activity that the standard 2D BGO system cannot make appropriate corrections for random coincidences, dead time loss, and scatter corrections. As shown in Fig. 6.83, current 3D scanners require a reduced dose of Rb-82 that limits the count density and statistical certainty required for detailed per-pixel perfusion or CFC maps to guide clinical management. Technology is being developed to make acquisition of full-dose Rb-82 and CFC pixel mapping possible using BGO as well as other non-BGO detectors, but their capacity has not yet been demonstrated clinically in the literature. The top 3D PET images on a BGO scanner show severe ring artifacts making unuseable images (upper left blue) or artifactual abnormalities (top center) compared to a normal 2D image of the same patient (right image). The graph below shows activity recovery by 3D is reduced to half of that by 2D for full dose Rb-82 using a BGO scanner.

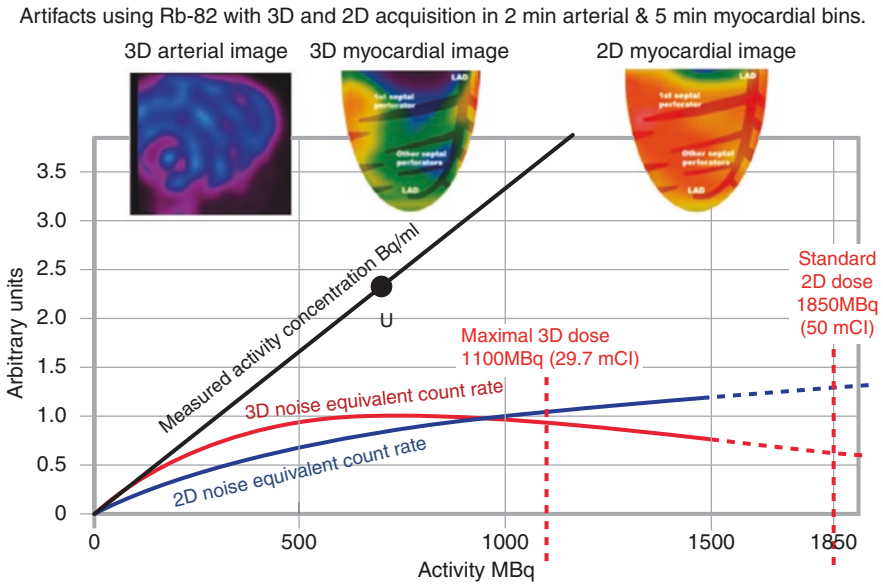

Fig. 6.83 Is all PET the same? A full 40- to 50-mCi dose of Rb-82 causes a fall in noise-free true counts for 3D acquisition (*dashed red line*) that is half of that for 2D acquisition (*dashed blue line*) [81]. Accordingly, current 3D scanners require a reduced dose of Rb-82 that limits regional and particularly per-pixel count density and statistical certainty required for detailed per-pixel perfusion or CFC maps to guide clinical management. (From Gould et al. [83]; with permissiom from Mosby)

Quantitative Myocardial Perfusion for Clinical Dilemmas

Severe CAD Missed on Angiograms

Both patients in Fig. 6.84 had known CAD with previous stents for angina. Both had ongoing angina, but coronary angiograms failed to show significant stenosis, so rest-stress PET was requested. In both cases, a severe CFC abnormality was identified and was corrected by retrograde wiring through a collateral channel.

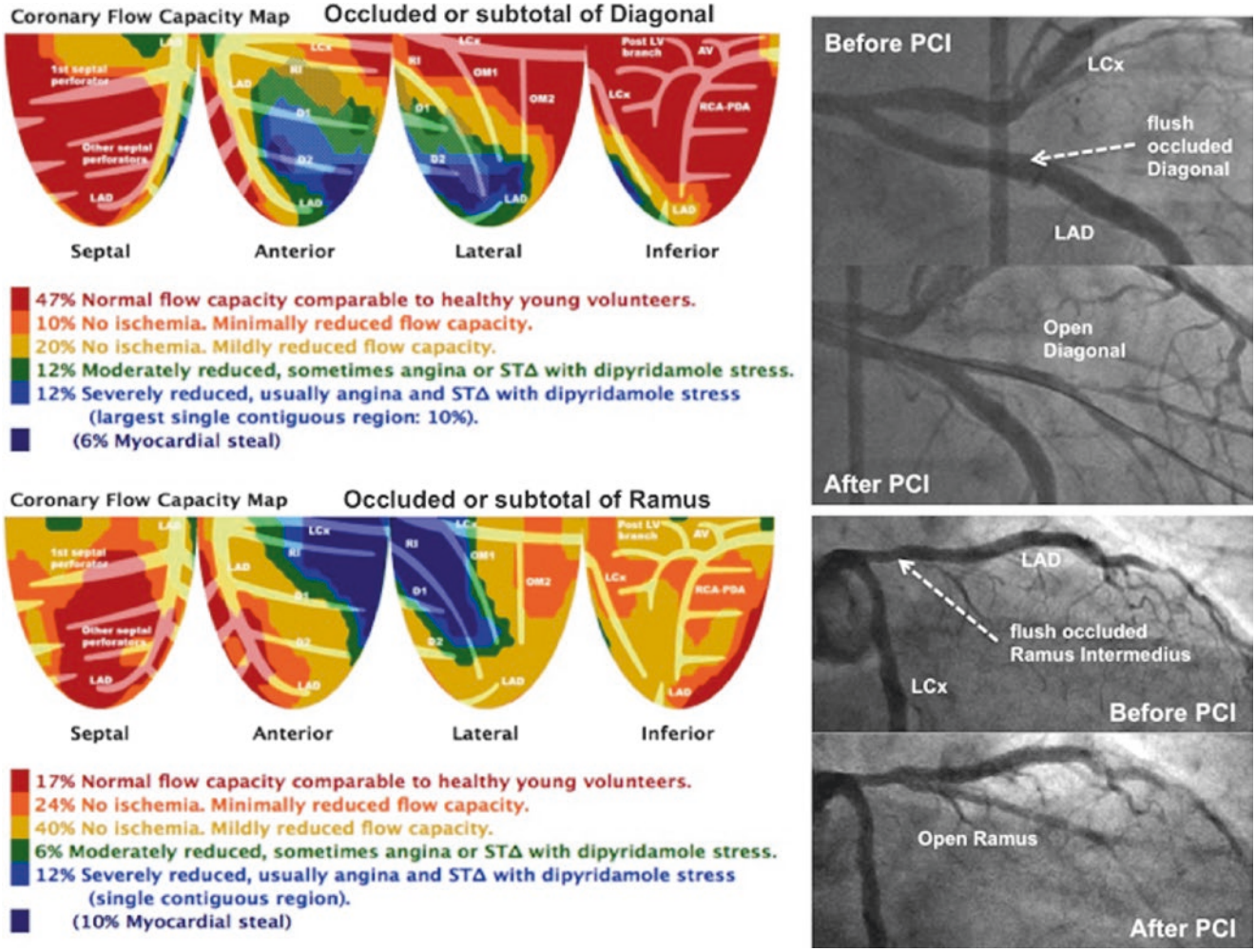

Fig. 6.84 Severe CAD missed by angiogram in two patients with previous stents for angina. Both had ongoing angina, but coronary angiograms failed to show significant stenosis, so rest-stress PET was requested. The upper case showed a large, severe CFC abnormality in the distribution of a large diagonal branch jailed by an LAD stent, with myocardial steal indicating collaterals. With this knowledge, flush occlusion was opened by retrograde wiring through a collateral channel to the origin of the diagonal, as seen on the cine inset. For the lower case, the CFC map showed a severe abnormality in the distribution of a ramus Intermedius due to flush occlusion at its origin. This insight also permitted stenting through a retrograde wire through a collateral channel

Figure 6.85 illustrates the case of a patient with angina who was told he had a normal angiogram. He requested a PET study, which showed severely abnormal CFC with 4 mm ST depression and hypotension; the ejection fraction fell from 66% to 45%, all characteristic of severe left main (LM) stenosis. Re-review and repeat of the angiogram in addition to CTA confirmed severe LM stenosis, leading to coronary bypass surgery.

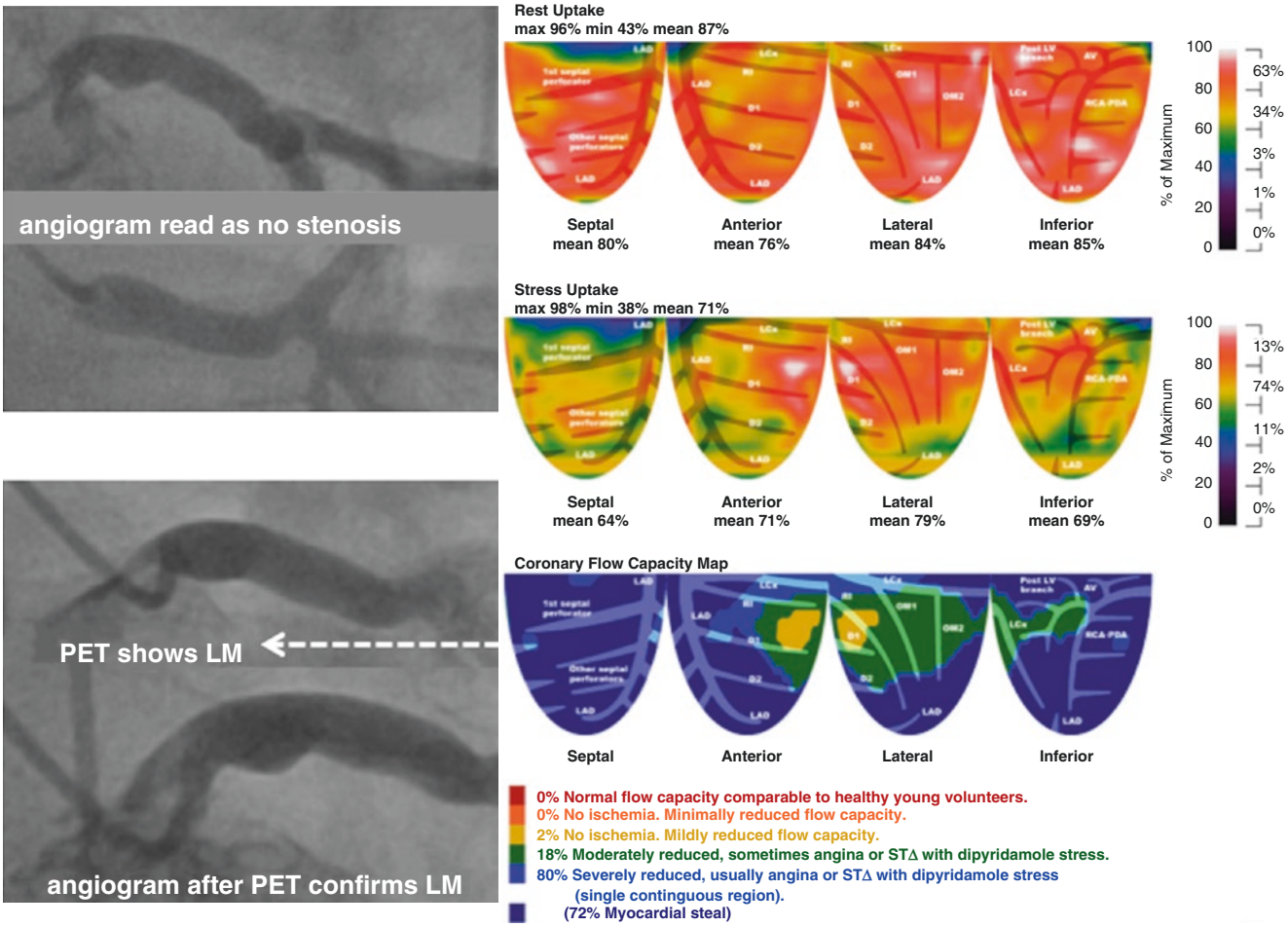

Fig. 6.85 Severe left main stenosis missed on angiogram

Recurrent Angina after Surgery

The patient in Fig. 6.86 had recurrent angina after coronary bypass surgery. Rest-stress PET showed defects indicating a patent left internal mammary artery (LIMA) to LAD graft but progressive disease proximal to the graft insertion, involving the first septal perforator and the first diagonal branch. Usually stent caged branches develop collaterals and angina resolves over weeks to months. However, if needed knowing the source, severity and size of the ischemic region, stenting through the mesh of the caging stent to open the stent blocked branch is usually an effective intervention. This pattern of stress defects in the first perforator and diagonal branches with adequate perfusion in the LAD distribution is typical of severe disease proximal to a patent bypass graft to LAD as also seen in Fig. 6.2.

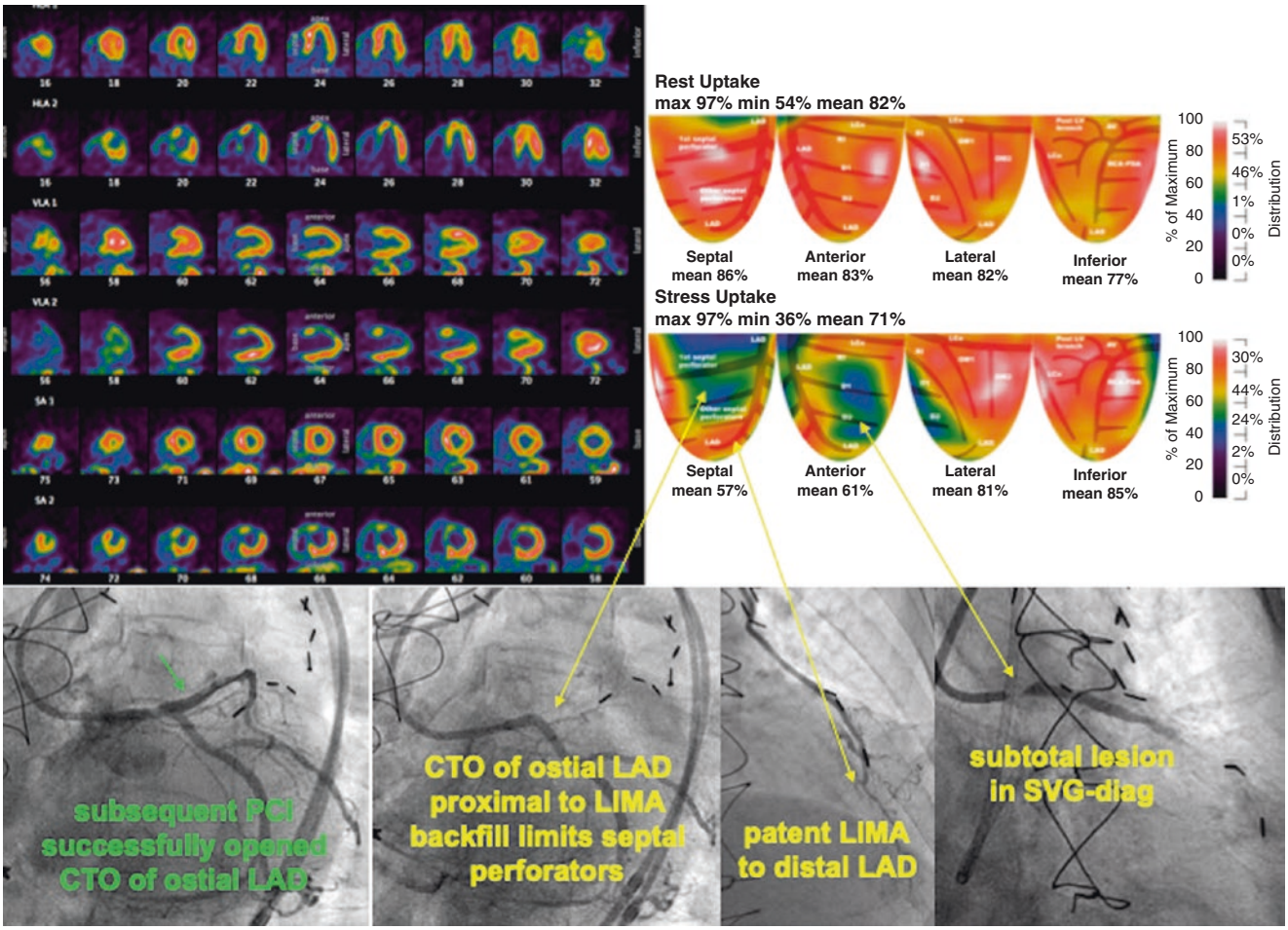

Fig. 6.86 In a patient with recurrent angina after CABG, rest-stress PET showed a large septal and moderate stress defect in a D1 distribution, indicating a patent left internal mammary artery (LIMA) to LAD graft but progressive disease proximal to the graft insertion. The proximal disease involved the first septal perforator and the first diagonal branch, producing this typical "butterfly defect" (the green areas of the septum and diagonal defects resemble wings and central yellow region in the LAD distribution with mildly reduced CFC resemble the body of a butterfly). The angiogram insets confirm the PET findings, with chronic total occlusion (CTO) of the ostial LAD and stenosis of the diagonal bypass graft. SVG saphenous vein graft

The patient in Fig. 6.87 underwent successful stenting of a severe LAD stenosis proximal to the first septal perforator, but the patient had ongoing angina for which PET was requested. The post-stent PET showed severely reduced CFC with myocardial steal; the LAD stent was occluding the first septal branch, thereby explaining continued angina, which usually resolves by progressive growth of collaterals.

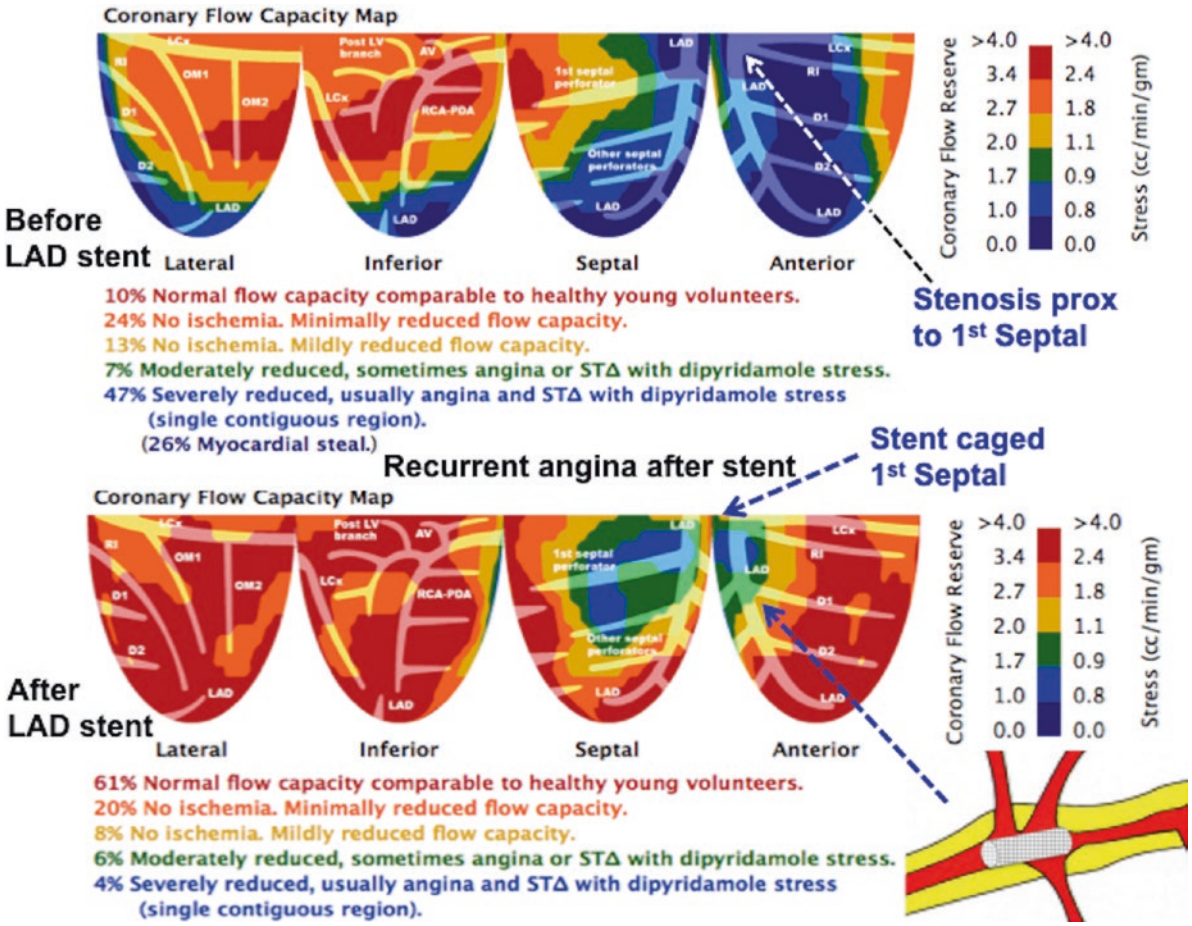

Fig. 6.87 This patient underwent successful stenting of a severe LAD stenosis proximal to the first septal perforator, which was correctly predicted by PET (*upper panel*). PET was requested because of continued angina after the LAD stent angina. The post-stent PET showed severely reduced CFC with myocardial steal indicating collaterals due to the LAD stent jailing and occluding the first septal branch, thereby explaining the continued angina. Typically, angina from septal occlusion resolves over months to a year with progressive collateral formation

Progression and Regression of CAD

Figure 6.88 shows single-quadrant views of four different patients with progression or regression on long-term follow-up of focal stenosis or diffuse CAD [82–85].

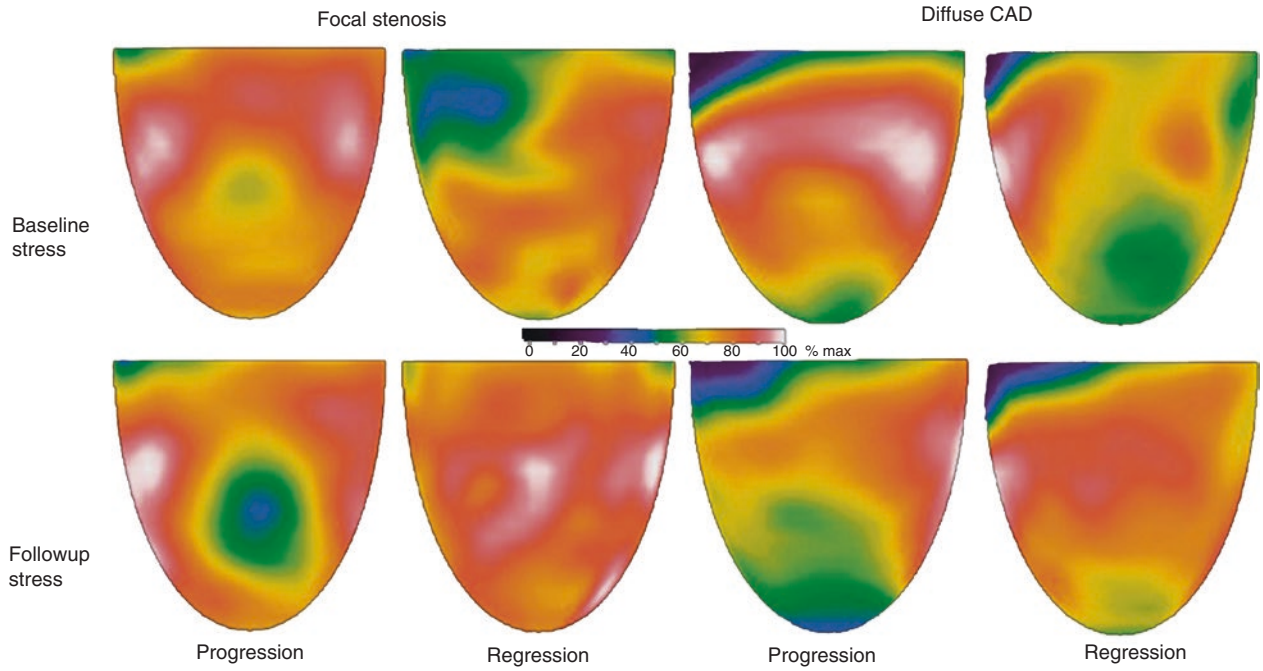

Fig. 6.88 Progression and regression of CAD four different patients, each shown at baseline (*top*) and long-term follow-up (*bottom*) with progression or regression of focal stenosis or the longitudinal base-to-apex perfusion gradient of diffuse CAD

The Unmeasured Elephants in Cardiology: Methods Thinking Versus Physiology Thinking; Subendocardial Perfusion; Low-Risk Versus High-Risk Angina

In the field of cardiac imaging, *Methods Thinking* explains many of the controversies and conflicting literature about methods and quantitative measurements, beyond differences in imaging scanners, radionuclides, and protocols. Methods Thinking means a thought silo on methodology, viewing different measurements competitively, such as CFR versus stress flow alone, or relative CFR or relative stress perfusion or relative activity images with no quantitative perfusion or longitudinal perfusion gradients, or all of these versus invasive pressure-based FFR. Methods silo thinking fails to see the essential continuum of integrated clinical physiologic quantification identifying high mortality risk that is reduced by revascularization or that incurs the lowest risk by intense lifestyle and medical treatment alone.

Figure 6.89 illustrates *Methods Thinking*. This graph shows the risk of MACE for pixel-based, size - severity abnormalities of CFC, CFR, and relative stress defect (defined as % of LV with relative activity ≤60% of maximum activity). All three PET quantitative metrics predict MACE for given size - severity. However, if CFC were not measured or plotted, narrow Methods Thinking focusing on CFR alone would conclude that CFR provides complete assessment of risk related to size-severity of abnormal quantitative perfusion. However, broader Physiologic Thinking integrating all perfusion data by also plotting size of severely reduced CFC abnormalities reveals that CFR and relative stress defects of comparable size do not provide adequate risk stratification compared to CFC.

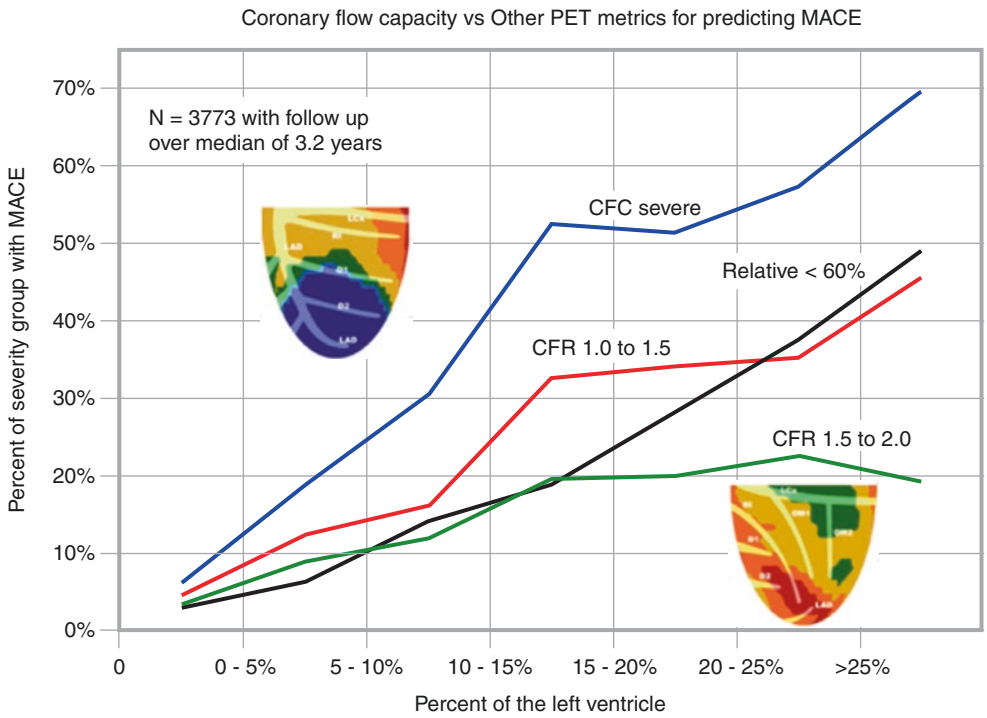

Fig. 6.89 Methods thinking

Physiology Thinking (Fig. 6.90). In addition to understanding CFC versus CFR, Physiologic Thinking explains angina and ST depression ≥1mm during dipyridamole stress with only moderately or mildly reduced CFC associated with low risk of MACE. For mildly or moderately reduced CFC, the relative tomograms show reduced subendocardial/subepicardial ratio and subendocardial ischemia. Mean transmural stress perfusion in ml/min/g is the average of high subepicardial and low subendocardial perfusion. This average may be only moderately or mildly reduced that does not reveal the transmural perfusion gradient. Physiologic thinking integrates known coronary pathophysiology with quantitative perfusion and subendocardial/subepicardial ratio on relative tomograms for clinically assessing low versus high risk angina.

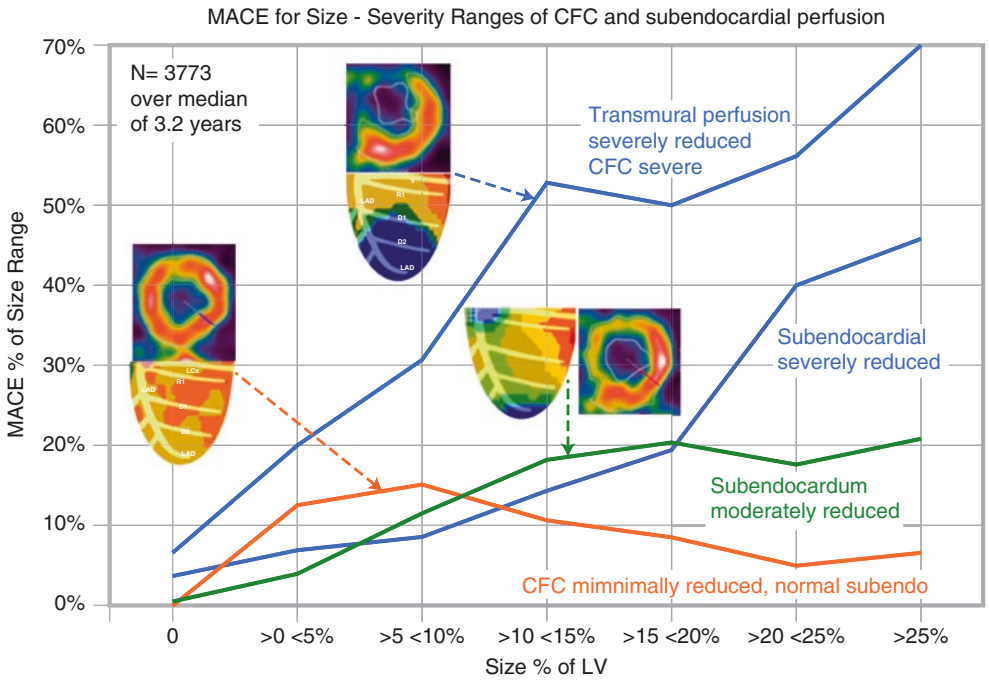

Fig. 6.90 Physiology thinking

For an asymptomatic man even during exercise, Fig. 6.91 presents an example of physiology thinking in complex CAD. All the stress perfusion abnormalities identified are in the distal distribution of the distal LAD and first obtuse marginal branch (OM1) as too small and distal for bypass surgery or stenting and well collateralized indicated by myocardial steal by PET. The large severe defect in the Left circumflex distribution (LCx) might be a revascularization target on angiogram. In view of the PET findings, repeat angiogram was recommended, to confirm the complex predominantly distal and diffuse disease and to assess the accessibility of the LCx for potential PCI. The angiogram (Fig. 6.92) confirmed the PET in each detail. Collaterals are not visible on the angiogram, but fine collaterals are commonly not visible despite physiologic evidence of their benefit by the absence of angina in daily activities, viable myocardium, and normal ejection fraction other than during dipyridamole stress with myocardial steal that does not occur during normal activities. Thus, the angiogram confirmed the PET findings of predominantly diffuse or distal disease. Because the patient had good resting LV function and no symptoms with daily activities, and the diffuse CAD was inappropriate for revascularization, the cardiologist and patient concluded that medical treatment remained the best option.

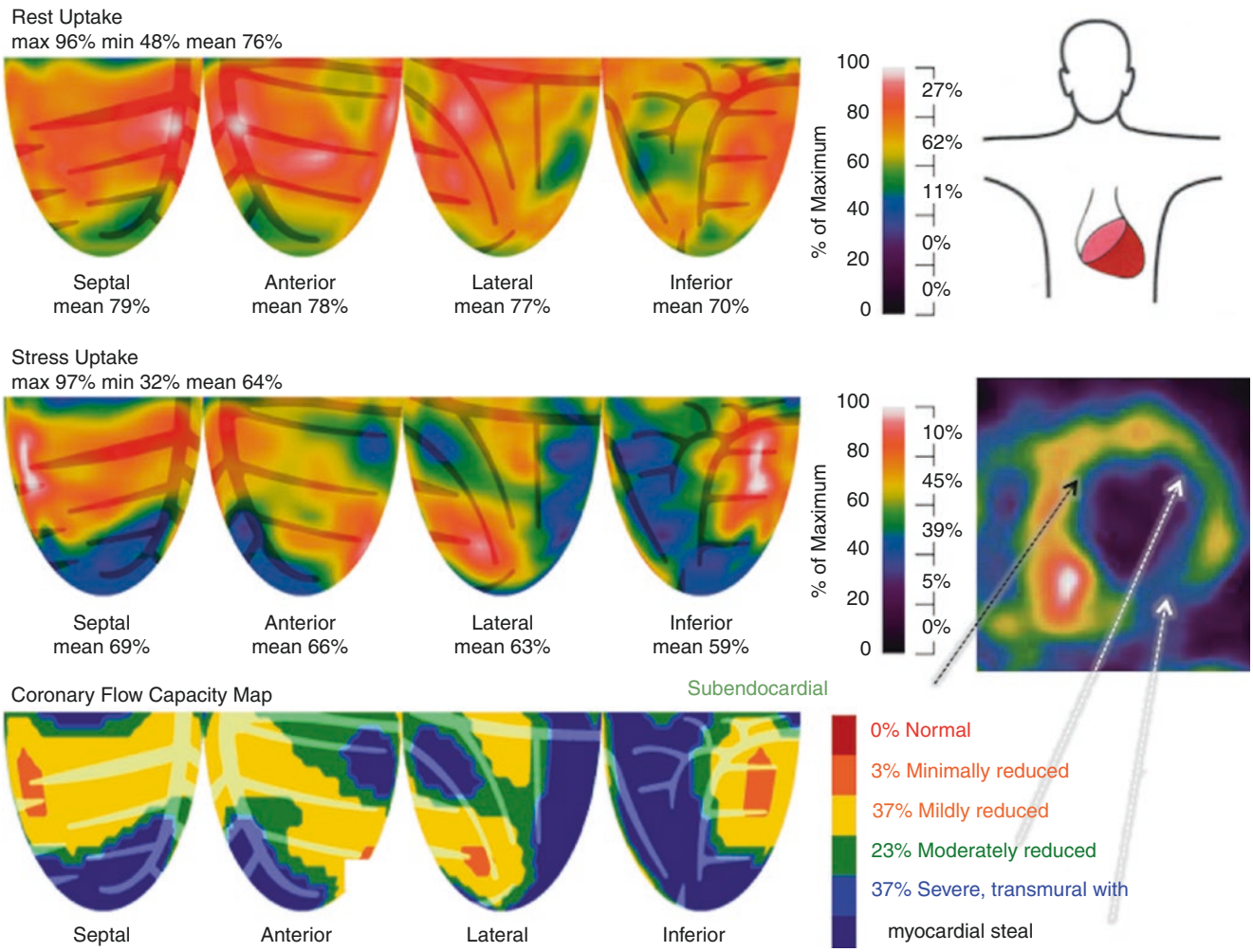

Fig. 6.91 An example of physiology thinking in complex CAD. This asymptomatic patient with stents to the LAD and RCA 2 years previously was referred for routine follow-up PET. The relative activity images show a small mid inferolateral non-transmural scar comprising 4% of LV in the typical distribution of the distal LCx (or OM3). In addition, there is a small, apical non-transmural scar comprising 3% of LV in the distal LAD distribution. With stress, the relative defects are large and severe, with CFC severely reduced to myocardial steal (*dark blue*), indicating viable myocardium with severe stenosis or occlusion and collateral perfusion in several areas: (1) the mid to distal LAD, wrapping around the apex with distal to large patent diagonals supplying the anterior wall; (2) the OM1 branch; (3) the mid LCx distal to a patent OM2; and (4) the mid RCA. CFC was mildly reduced diffusely in the remainder of the LV (*yellow*). With dipyridamole stress, the patient developed angina and 3 mm of ST depression. The ejection fraction fell from 60% to 52%, with abnormal TID of 1.28, all reflecting severe global subendocardial ischemia (as shown in the tomogram inset) in addition to regional transmural ischemia that was relieved by intravenous aminophylline, metoprolol, and sublingual nitroglycerin

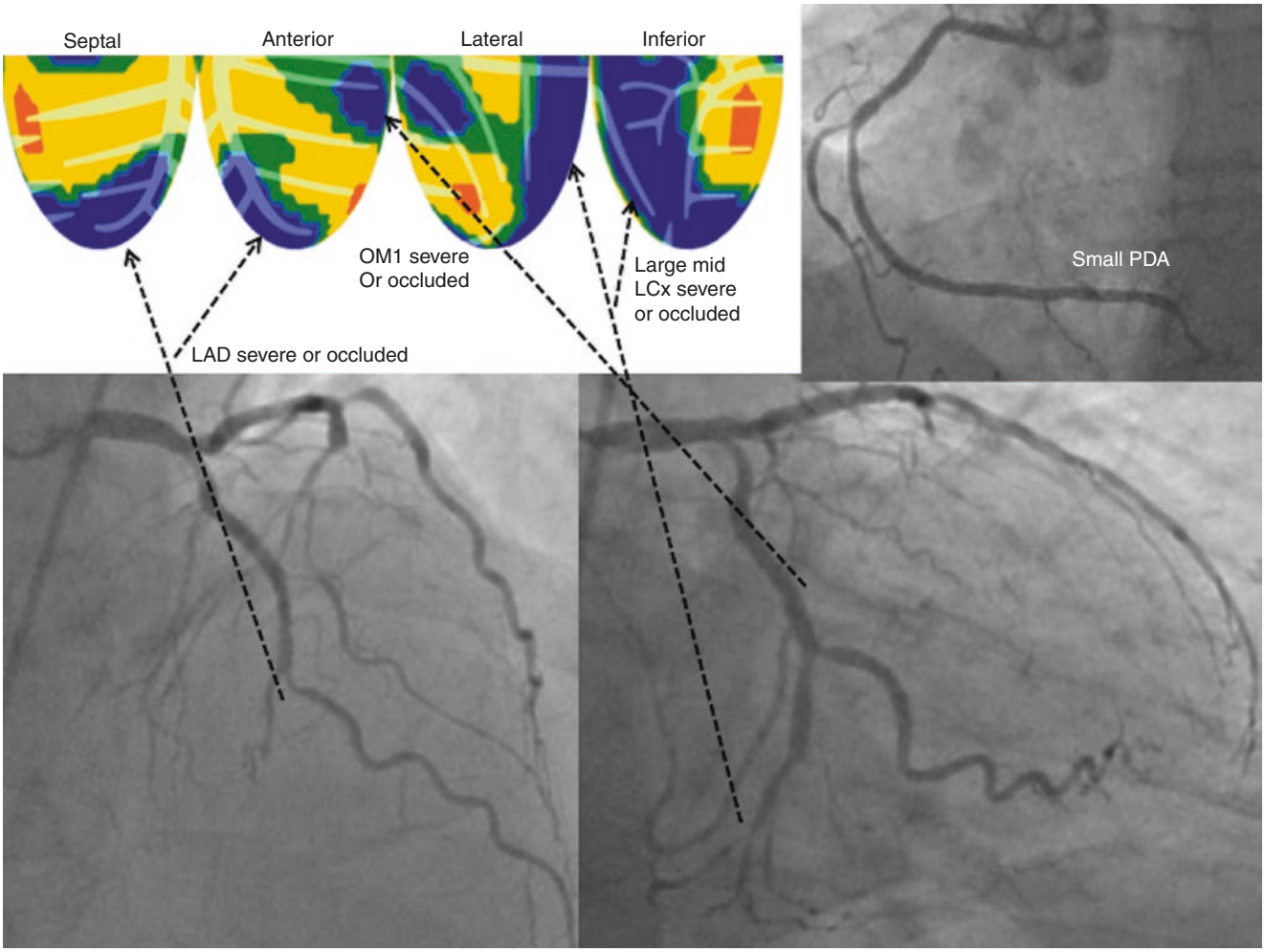

Fig. 6.92 Angiography confirming the PET findings for the patient in Fig. 6.91, showing severe diffuse distal disease of the LAD, LCx, and RCA [86]

Figure 6.93 presents an example of Methods thinking versus Physiology thinking for atypical chest pain without stenosis. The patient is a 61-year-old man with angina at rest and dyspnea on exertion without angina, poorly controlled hypertension and hyperlipidemia, dense coronary calcium, and prior stents to the LAD and LCx. Recent angiograms showed 20% diameter stenosis of LAD and RCA with patent stents. Dipyridamole stress caused definite angina and 1.2 mm ST depression, relieved by intravenous aminophylline and sublingual nitroglycerin despite very high uniform, homogeneous stress flow of 2.9 cc/min/g. These results indicate excellent small vessel function with no flow-limiting stenosis. An observer using Methods thinking would conclude that the quantitative measurements—stress perfusion, CFR, and CFC—are wrong or useless because they are not associated with definite angina and significant ST depression during stress. However, open-minded Physiology thinking about the data provides an important physiologic insight. With diffuse epicardial CAD and preserved small vessel function, the high coronary blood flow during dipyridamole stress generates falling coronary pressure owing to

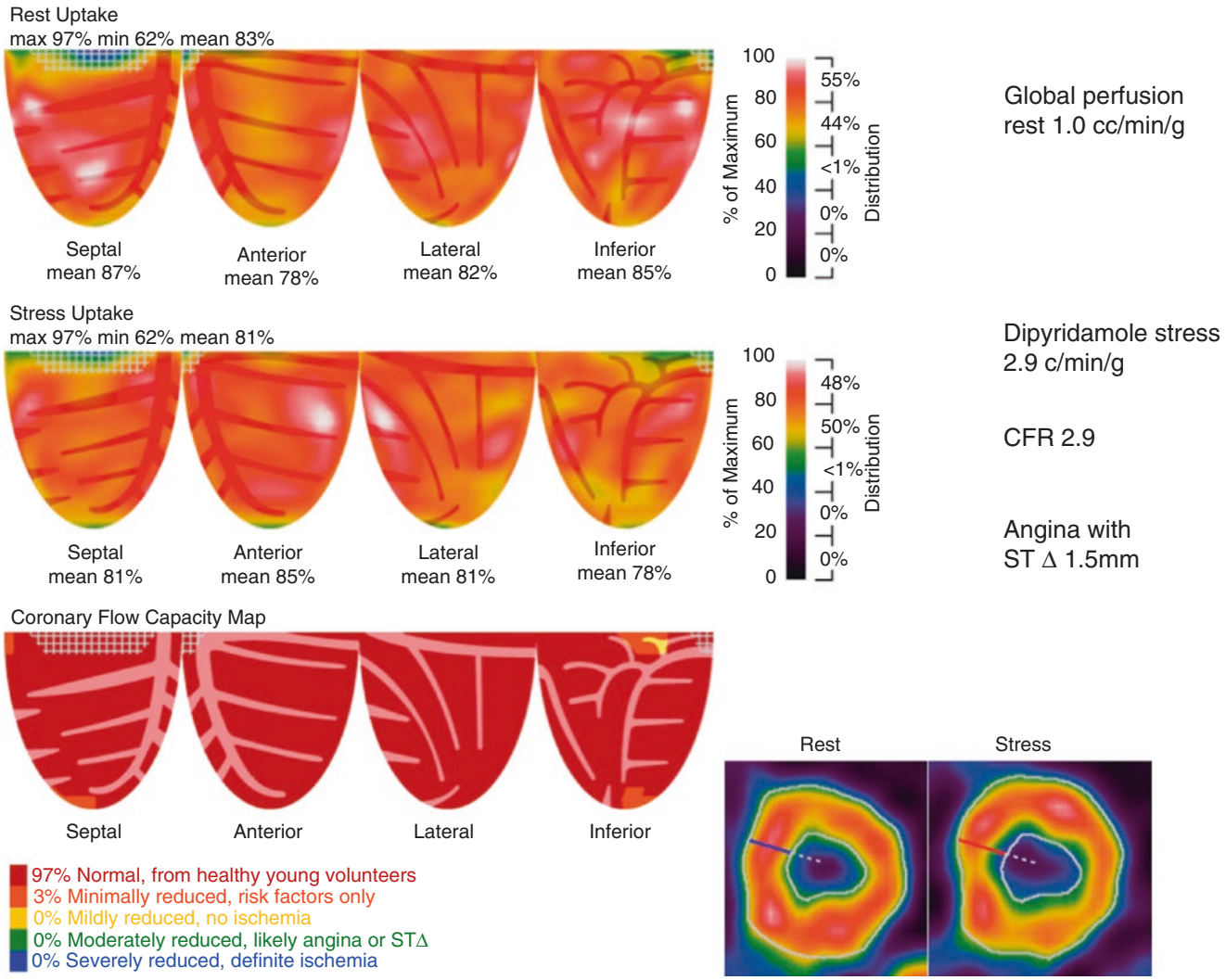

Fig. 6.93 Methods thinking versus physiology thinking for atypical chest pain without stenosis

viscous energy loss, with resulting subendocardial ischemia shown in the tomographic view. The *white dashed lines* outline the endocardial borders of the resting relative images projected onto the stress image, revealing global reduction of subendocardial perfusion, causing angina and ST depression, quantitatively analyzed in Fig. 6.94. All the results shown there are consistent with global subendocardial ischemia manifest as angina and significant ST depression during dipyridamole stress. In this case, the high stress perfusion at peak mid-wall activity is high enough to preclude a longitudinal base-to-apex gradient, as may be seen with more severe diffuse narrowing or combined stenosis plus diffuse CAD. The comprehensive physiologic data in this case explain ischemia during dipyridamole stress and, with the clinical history, suggest an element of coronary spasm associated with endothelial dysfunction of diffuse CAD needing intense management of angina and risk factors. In our database of 8000 cases with 10-year follow-up, a normal CFC is associated with a low risk of adverse events if medical treatment is adequate, as in the plots in Fig. 6.64.

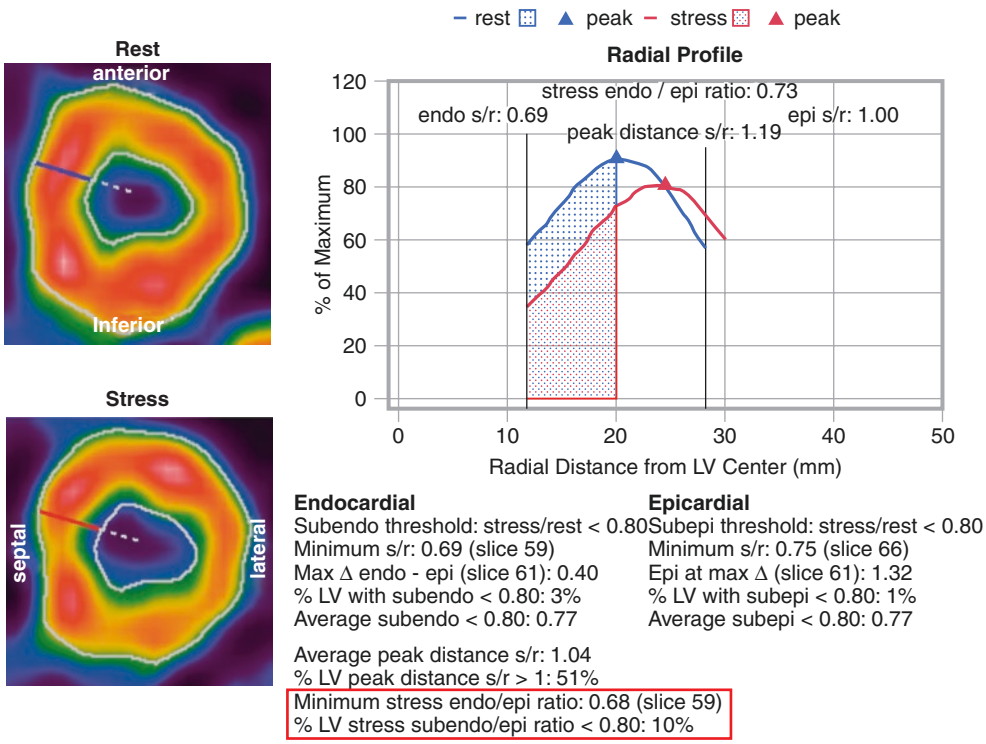

Fig. 6.94 Quantitative subendocardial analysis of the patient in Fig. 6.93. The *blue line* plots the radial relative activity profile of the rest tomogram slice, and the *red line* plots the stress radial relative activity profile of the stress tomogram slice. The distance from peak activity of the rest profile to the rest endocardial boundary defines the subendocardium. The subendocardial stress/rest ratio is the area under the red profile divided by the area under the blue profile for each of 64 radii of 20 tomographic slices for the whole LV. The stress subendo/epicardial ratio is the ratio of the subendocardial half of each radius divided by the subepicardial half of each radius across the LV wall. As outlined by the *red box*, the minimum stress subendo/epicardial ratio is 0.68, and 10% of the LV has a subendo/epicardial ratio <0.8

Figure 6.95 illustrates a case example of Physiology thinking for atypical chest pain without stenosis in a 77-year-old woman who had hypertension, hyperlipidemia, insulin-dependent diabetes, a strong family history of CAD, and dense coronary calcium by CT. More than 7 years after PCI and 4 years after a normal PET, she developed non-exertional chest pain radiating down her left arm, which she associated with spikes in blood sugar and systolic blood pressure. Because of her atypical symptoms, rest-stress PET was done. Both CFC and FFRpet at the apex were worse than on PET 4 years previously, indicating mild progression of diffuse CAD, primarily of the LAD wrapping around the apex. The short-axis relative tomo-

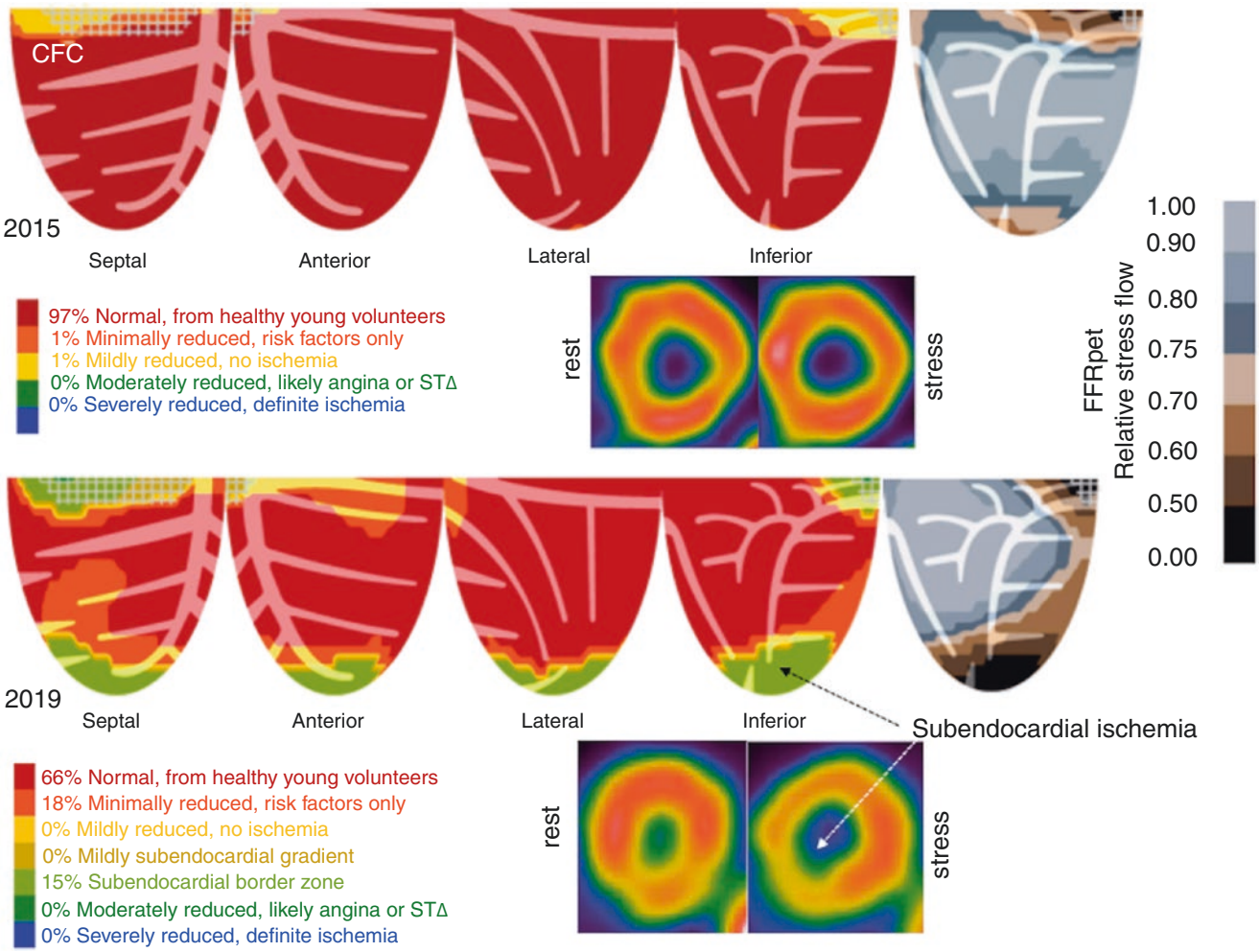

Fig. 6.95 Physiology thinking for atypical chest pain without stenosis in a 77-year-old woman who had hypertension, hyperlipidemia, insulin-dependent diabetes, a strong family history of CAD, and dense coronary calcium by CT. She underwent PCI of the RCA for angina 8 years previously. A PET 4 years previously (top) was normal, with no angina and no STΔ during dipyridamole stress. She was subsequently asymptomatic until the last 6 months, when she developed non-exertional chest pain radiating down her left arm. She definitely associated it with her blood sugar spiking to 300 mg/dL and systolic blood pressure spikes to over 180 mm Hg. Because of her atypical symptoms, rest-stress PET was done. Initial baseline blood pressure was 180/98, falling to 132/88 before stress imaging. With dipyridamole stress, she developed definite typical, moderately severe angina radiating down her left arm with 1.5 mm ST depression relieved by aminophylline (150 mg) and metoprolol (5 mg). Her PET showed high average global resting perfusion at 1.7 cc/min/g, consistent with hypertension, and high average global stress perfusion of 2.5 mL/min/g with no regional abnormalities. Ejection fraction was 77% at rest and 75% with stress, both excellent, within the range of method repeatability. Her CFC (bottom), shown in four quadrant views with the relative map of stress cc/min/g, and FFRpet (in a single inferior view) was excellent and well above ischemic levels for average transmural perfusion except at the apex. At the apex, the relative map of stress cc/min/g (FFRpet) was 0.5. Both CFC and FFRpet at the apex were worse than on PET 4 years previously, indicating mild progression of diffuse CAD, primarily of the LAD wrapping around the apex. The short-axis relative tomograms showed low subendocardial perfusion at the apex, objectively quantified in Fig. 6.96, thereby explaining her dipyridamole-induced angina and ST depression

grams showed low subendocardial perfusion at the apex, objectively quantified in Fig. 6.96, thereby explaining her dipyridamole-induced angina and ST depression. The occurrence of her angina with blood glucose spikes is consistent with its documented impairment of endothelial-mediated vasodilatation, thereby causing spiking blood pressure, increased coronary blood flow demands, diffuse coronary constriction, and thence subendocardial ischemia exacerbated by her left ventricular hypertrophy, which further compromises subendocardial perfusion. Again, "Physiology thinking" and comprehensive integrated quantification explained heratypical symptoms, which needed more intense risk factor management for low-risk angina.

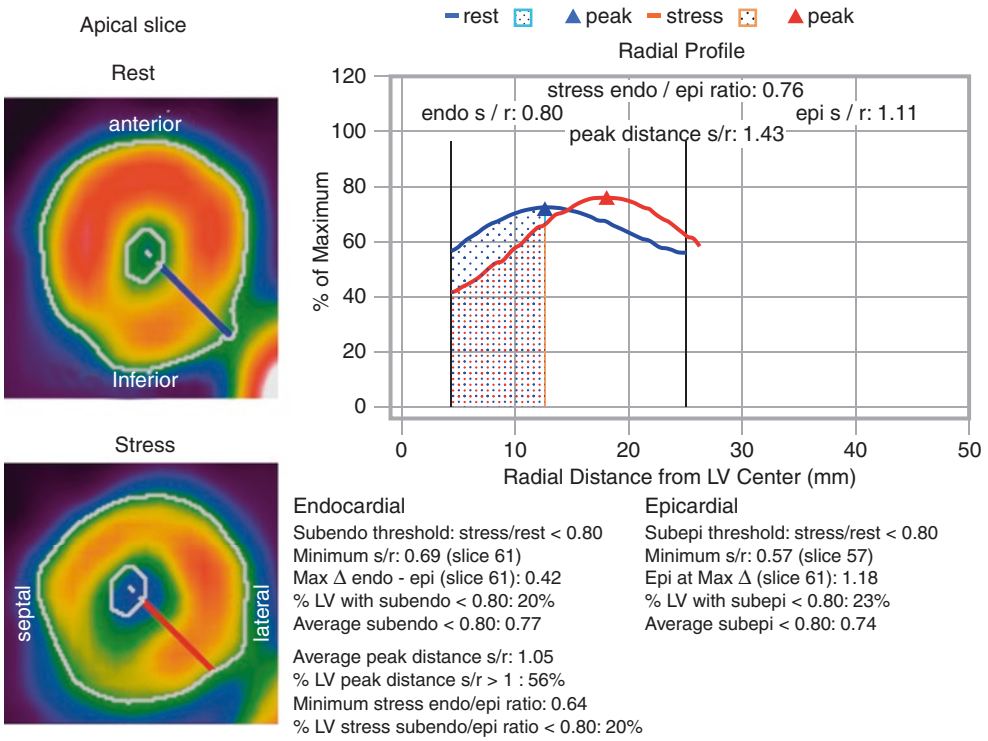

Fig. 6.96 Subendocardial analysis for the woman in Fig. 6.95, whose angina and ST change during dipyridamole PET stress are explained by mild apical subendocardial ischemia, as objectively quantified: minimum subendocardial stress/rest ratio, 0.69; average subendocardial stress/rest ratio, 0.77; 20% of LV with subendocardial stress/rest ratio <0.8; minimum stress subendo/epicardial ratio, 0.64; and 22% of LV with subendo/epicardial ratio <0.8—all results that indicate mild apical subendocardial ischemia manifest as angina and significant ST depression during dipyridamole stress. These objective findings indicate mild diffuse epicardial narrowing with excellent small vessel function sufficient to maximize coronary flow (2.5 cc/min/g) that generates a pressure gradient along the LAD, and therefore the low FFRpet and low subendocardial perfusion causing angina and ST changes

In randomized trials of revascularization guided by angiography or FFR, angina relief fails to reduce the rate of subsequent MI or death. The data and case examples in this chapter suggest a potential explanation for this apparent paradox. The case examples of severely reduced CFC (*blue*), indicating severely reduced transmural perfusion with angina (as in Figs. 6.2, 6.46, 6.54, 6.55, 6.62, 6.63, 6.74, 6.76, 6.79, 6.84, 6.85, 6.87, and 6.91) are associated with high risk of death, MI, or stroke—as shown in Fig. 6.64; the risk is reduced by revascularization in Fig. 6.65. However—as in Figs. 6.26 and 6.74 (after PCI), 6.78a, b, and e, 6.81, 6.87 (after PCI), 6.93, and 6.95—mild to moderately reduced CFC (*yellow* or *green*) is associated with low risk of death, MI, or stroke, as seen in the Kaplan Meier plots of Fig. 6.64; the risk in these cases may actually be increased by revascularization (as in Fig. 6.65) because the risk of the procedure is greater than the risk from medical treatment alone. In these cases of mild to moderately reduced CFC, angina is due to reduced subendocardial perfusion that does not reach transmural severity associated with high risk.

Moreover, abnormal subendocardial perfusion not reaching the high-risk transmural severity threshold for ischemia reveals the unpredictability of angina for mild to moderately reduced stress perfusion CFR or CFC. For example, stress perfusion CFC and subendocardial metrics for cases with dipyridamole-induced angina and significant STΔ in Figs. 6.93–6.94

and 6.95–6.96 are comparable or less severe than the case example in Figs. 6.81 and 6.82, which had no angina or ECG changes during dipyridamole or exercise stress.

The patient in Figs. 6.95 and 6.96 had initial blood pressure of 180 mm Hg with corresponding high resting perfusion of 1.7 cc/min/g, indicating high flow demands that may cause ischemia despite high stress perfusion of 2.8 cc/min/g. Her FFRpet dropped to <0.5 at the apex, suggesting a severe gradient along the LAD length, which, with LV hypertrophy and high flow demand of hypertension and dipyridamole tachycardia, explained her angina.

Finally, patients in Figs. 6.74, 6.75, 6.81, 6.82, 6.91, 6.92, 6.93, 6.94, 6.95, and 6.96 had angina and significant ECG ST depression during dipyridamole stress. However, the patients in Figs. 6.81 and 6.91 had no angina and the patient in Figs. 6.95 and 6.96 had angina only when blood sugar exceeded 300 mg/dL with no exertional angina. Of all cases with severely reduced CFC only 48% had angina or significant ST depression with dipyridamole stress. Of patients with no severely reduced CFC but reduced subendocardial perfusion, only 23% had angina or significant ST depression with dipyridamole stress.

Clinical "subendocardial ischemia" (angina with STΔ >1 mm) and FFR <0.8, are commonly invoked to justify revascularization. However, we observe reduced relative subendocardial perfusion or FFRpet <0.8 commonly with no angina or STΔ associated with exercise or dipyridamole stress. With no severely reduced CFC, such patients have a low risk of MACE that is not reduced (and may be increased) by revascularization. These examples illustrate that quantifying physiologic severity of CAD underlying angina and "Physiology Thinking" are essential for understanding each patient's symptoms and coronary physiology, for their fully informed consent, and for individualized optimal management of low-risk angina versus high-risk angina.

Figure 6.97 summarizes CFC, low-risk angina, high-risk angina, and subendocardial perfusion.

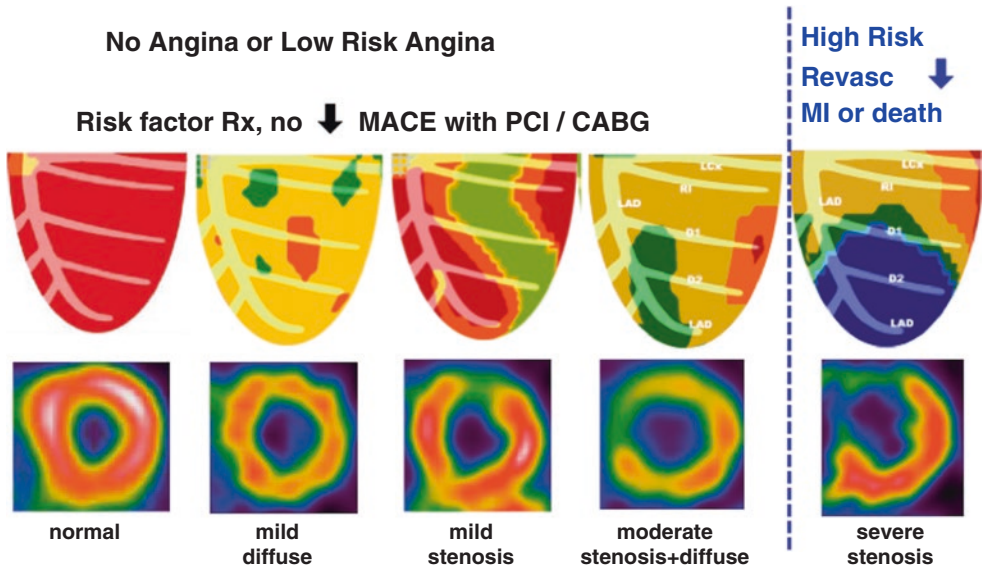

Fig. 6.97 Summary of CFC, low-risk angina, high-risk angina, and subendocardial perfusion

Subendocardial perfusion is the unmeasured elephant in cardiology, here related to mild or moderately reduced CFC (*yellow* or *green*), where the reduced relative subendocardial perfusion does not extend to severely reduced transmural perfusion. High-risk angina corresponds to severely reduced transmural CFC (*blue* CFR ≤1.3 and stress cc/min/g ≤0.8; see Figs. 6.51 and 6.52), for which revascularization reduces risk of death or MI (*see* Fig. 6.65).

Financial Support and Relationships with Industry Research supported by internal funds of the Weatherhead PET Center.

NPJ received institutional licensing and consulting agreement with Boston Scientific for the smart minimum FFR algorithm; received significant institutional research support from St. Jude Medical (CONTRAST, NCT02184117) and Philips Volcano Corporation (DEFINE-FLOW, NCT02328820) for studies using intracoronary pressure and flow sensors; and has a patent pending on diagnostic methods for quantifying aortic stenosis and TAVI physiology.

KLG receives internal funding from the Weatherhead PET Center for Preventing and Reversing Atherosclerosis and is the 510(k) applicant for FDA approved HeartSee K171303 PET software. To avoid any conflict of interest, KLG has assigned any royalties to the University of Texas for research or student scholarships; has no consulting, speakers, or board agreements; and receives no funding from PET-related or other corporate entities.

References

1. Gould KL, Lipscomb K, Hamilton GW. Physiologic basis for assessing critical coronary stenosis. Instantaneous flow response and regional distribution during coronary hyperemia as measures of coronary flow reserve. Am J Cardiol. 1974;33:87–94.
2. Gould KL, Gewirtz H, Narula J. Coronary blood flow and myocardial ischemia. In: Fuster V, Harrington RA, Narula J, Eapen ZJ, editors. Hurst's the heart. 14th ed. New York: McGraw Hill; 2017. p. 893–922.
3. Gould KL, Hamilton GW, Lipscomb K, Kennedy JW. A method for assessing stress induced regional malperfusion during coronary arteriography: experimental validation and clinical application. Am J Cardiol. 1974;34:557–64.
4. Gould KL. Noninvasive assessment of coronary stenoses by myocardial perfusion imaging during pharmacologic coronary vasodilatation. I. Physiologic basis and experimental validation. Am J Cardiol. 1978;41:267–78.
5. Gould KL, Westcott JR, Albro PC, Hamilton GW. Noninvasive assessment of coronary stenoses by myocardial imaging during coronary vasodilatation. II. Clinical methodology and feasibility. Am J Cardiol. 1978;41:279–87.
6. Albro PC, Gould KL, Westcott RJ, Hamilton GW, Ritchie JL, Williams DL. Noninvasive assessment of coronary stenoses by myocardial imaging during pharmacologic coronary vasodilatation. III. Clinical trial. Am J Cardiol. 1978;42:751–60.
7. Gould KL. Assessment of coronary stenoses by myocardial perfusion imaging during pharmacologic coronary vasodilatation. IV. Limits of stenosis detection by idealized, experimental, cross-sectional myocardial imaging. Am J Cardiol. 1978;42:761–8.
8. Gould KL, Schelbert HR, Phelps ME, Hoffman EJ. Noninvasive assessment of coronary stenoses with myocardial perfusion imaging during pharmacologic coronary vasodilatation. V. Detection of 47 percent diameter coronary stenosis with intravenous nitrogen-13 ammonia and emission-computed tomography in intact dogs. Am J Cardiol. 1979;43:200–8. *Awarded the George von Hevesy Prize for Research in Nuclear Medicine, at the World Federation of Nuclear Medicine, September 17, 1978, Washington, DC*.
9. Schelbert HR, Wisenberg G, Phelps ME, Gould KL, Eberhard H, Hoffman EJ, et al. Noninvasive assessment of coronary stenosis by myocardial imaging during pharmacologic coronary vasodilation. VI. Detection of coronary artery disease in man with intravenous N-13 ammonia and positron computed tomography. Am J Cardiol. 1982;49:1197–207.
10. Kirkeeide R, Gould KL, Parsel L. Assessment of coronary stenoses by myocardial imaging during coronary vasodilation. VII. Validation of coronary flow reserve as a single integrated measure of stenosis severity accounting for all its geometric dimensions. J Am Coll Cardiol. 1986;7:103–13.
11. Gould KL, Goldstein RA, Mullani N, Kirkeeide R, Wong G, Smalling R, et al. Noninvasive assessment of coronary stenoses by myocardial imaging during pharmacologic coronary vasodilation. VIII. Feasibility of 3D cardiac positron imaging without a cyclotron using generator produced Rb-82. J Am Coll Cardiol. 1986;7:775–92.
12. Gould KL, Kirkeeide R, Johnson NP. Coronary branch steal – experimental validation and clinical implications of interacting stenosis in branching coronary arteries. Circ Cardiovasc Imaging. 2010;3:701–9.
13. Gould KL, Nakagawa Y, Nakagawa N, Sdringola S, Hess MJ, Haynie M, et al. Frequency and clinical implications of fluid dynamically significant diffuse coronary artery disease manifest as graded, longitudinal, base to apex, myocardial perfusion abnormalities by non-invasive positron emission tomography. Circulation. 2000;101:1931–9.
14. Gould KL. Coronary artery stenosis and reversing atherosclerosis. 2nd ed. London: Arnold Publishers; 1999. *A textbook of coronary pathophysiology, quantitative coronary arteriography, and cardiac PET.*
15. De Bruyne B, Hersbach F, Pijls NH, Bartunek J, Bech JW, Heyndrickx GR, et al. Abnormal epicardial coronary resistance in patients with diffuse atherosclerosis but "Normal" coronary angiography. Circulation. 2001;104:2401–6.
16. Johnson NP, Kirkeeide RL, Gould KL. Is discordance of coronary flow reserve and fractional flow reserve due to methodology or clinically relevant coronary pathophysiology? Supplement JACC Cardiovasc Imaging. 2012;5:193–202.
17. Lipscomb K, Gould KL. Mechanism of the effect of coronary artery stenosis on coronary flow in the dog. Am Heart J. 1975;89:60–7.
18. Gould KL, Kirkeeide RL, Buchi M. Coronary flow reserve as a physiologic measure of stenosis severity. Part I. Relative and absolute coronary flow reserve during changing aortic pressure and cardiac workload. Part II. Determination from arteriographic stenosis dimensions under standardized conditions. J Am Coll Cardiol. 1990;15:459–74.
19. Pijls NHJ, van Son JAM, Kirkeeide RL, Bruyne BD, Gould KL. Experimental basis of determining maximal coronary myocardial and collateral blood flow by pressure measurements for assessing functional stenosis severity before and after PTCA. Circulation. 1993;86:1354–67.
20. Smalling RW, Kelley K, Kirkeeide RL, Fisher DJ. Regional myocardial function is not affected by severe coronary depressurization provided coronary blood flow is maintained. J Am Coll Cardiol. 1985;5:948–55.
21. Seiler C. Collateral circulation of the heart. Dordrecht: Springer; 2009.
22. Gould KL, Kelley KO, Bolson EL. Experimental validation of quantitative coronary arteriography for determining pressure-flow characteristics of coronary stenoses. Circulation. 1982;66:930–7.
23. Gould KL, Kelley KO. Physiological significance of coronary flow velocity and changing stenosis geometry during coronary vasodilation in awake dogs. Circ Res. 1982;50:695–704.
24. Hoffman JIE, Buckberg GD. The myocardial oxygen supply:demand index revisited. J Am Heart Assoc. 2014;3:e000285. https://doi.org/10.1161/JAHA.113.000285.
25. Gould KL, Johnson NP. Coronary physiology: beyond CFR in microvascular angina. J Am Coll Cardiol. 2018;72:2642–62.
26. Danad I, Raijmakers PG, Harms HJ, Heymans MW, van Royen N, Lubberink M, et al. Impact of anatomical and functional severity of coronary atherosclerotic plaques on the transmural perfusion gradient: a [^{15}O]H_2O PET study. Eur Heart J. 2014;35:2094–105.
27. Gould KL, Johnson NP, Bateman TM, Beanlands RS, Bengel FM, Bober R, et al. Anatomic versus physiologic assessment of coronary artery disease: role of CFR, FFR, and PET imaging in revascularization decision-making. J Am Coll Cardiol. 2013;62:1639–53.
28. Gupta A, Taqueti VR, van de Hoef TP, Bajaj NS, Bravo PE, Murthy VL, et al. Integrated noninvasive physiological assessment of coronary circulatory function and impact on cardiovascular mortality in patients with stable coronary artery disease. Circulation. 2017;136:2325–36.
29. Danad I, Raijmakers PG, Appelman YE, Harms HJ, de Haan S, van den Oever ML, et al. Hybrid imaging using quantitative $H_2{}^{15}O$ PET and CT-based coronary angiography for the detection of coronary artery disease. J Nucl Med. 2013;54:55–63.
30. Gewirtz H, Dilsizian V. Integration of quantitative positron emission tomography absolute myocardial blood flow measurements in the clinical management of coronary artery disease. Circulation. 2016;133:2180–96.
31. Driessen RS, Danad I, Stuijfzand WJ, Raijmakers PG, Schumacher SP, van Diemen PA, et al. Comparison of coronary computed tomog-

raphy angiography, fractional flow reserve, and perfusion imaging for ischemia diagnosis. J Am Coll Cardiol. 2019;73:161–73.
32. Danad I, Raijmakers PG, Driessen RS, Leipsic J, Raju R, Naoum C, et al. Comparison of coronary CT angiography, SPECT, PET, and hybrid imaging for diagnosis of ischemic heart disease determined by fractional flow reserve. JAMA Cardiol. 2017;2:1100–7.
33. Maaniitty T, Stenström I, Bax JJ, Uusitalo V, Ukkonen H, Kajander S, et al. Prognostic value of coronary CT angiography with selective PET perfusion imaging in coronary artery disease. JACC Cardiovasc Imaging. 2017;10:1361–70.
34. Knuuti J, Ballo H, Juarez-Orozco LE, Saraste A, Kolh P, Rutjes AW, et al. The performance of non-invasive tests to rule-in and rule-out significant coronary artery stenosis in patients with stable angina: a meta-analysis focused on post-test disease probability. Eur Heart J. 2018;39:3322–30.
35. Koo BK, Erglis A, Doh JH, Daniels DV, Jegere S, Kim HS, et al. Diagnosis of ischemia-causing coronary stenoses by noninvasive fractional flow reserve computed from coronary computed tomographic angiograms. Results from the prospective multicenter DISCOVER-FLOW (Diagnosis of Ischemia-Causing Stenoses Obtained Via Noninvasive Fractional Flow Reserve) study. J Am Coll Cardiol. 2011;58:1989–97.
36. Tu S, Barbato E, Koszegi Z, Yang J, Sun Z, Holm N, et al. Fractional flow reserve calculation from 3-dimensional quantitative coronary angiography and TIMI frame count. JACC Cardiovasc Interv. 2014;7:768–77.
37. Murthy VL, Naya M, Taqueti VR, Foster CR, Gaber M, Hainer J, et al. Effects of sex on coronary microvascular dysfunction and cardiac outcomes. Circulation. 2014;129:2518–27.
38. Stenström I, Maaniitty T, Uusitalo V, Pietilä M, Ukkonen H, Kajander S, et al. Frequency and angiographic characteristics of coronary microvascular dysfunction in stable angina: a hybrid imaging study. Eur Heart J Cardiovasc Imaging. 2017;18:1206–13.
39. Gould KL, Johnson NP, Roby AE, Nguyen T, Kirkeeide R, Haynie M, et al. Regional artery specific thresholds of quantitative myocardial perfusion by PET associated with reduced MI and death after revascularization in stable coronary artery disease. J Nucl Med. 2019;60:410–7.
40. Gould KL. Does coronary flow trump coronary anatomy? JACC Cardiovasc Imaging. 2009;2:1009–23.
41. Sdringola S, Johnson NP, Kirkeeide RL, Cid E, Gould KL. Impact of unexpected factors on quantitative myocardial perfusion and coronary flow reserve in young, asymptomatic volunteers. JACC Cardiovasc Imaging. 2011;4:402–12.
42. Johnson NP, Gould KL. Physiologic basis for angina and ST change: PET-verified thresholds of quantitative stress myocardial perfusion and coronary flow reserve. JACC Cardiovasc Imaging. 2011;4:990–8. *Awarded the 2011 Young Author Achievement Award by the Journal of the American College of Cardiology Cardiovascular Imaging.*
43. Johnson NP, Gould KL. Integrating noninvasive absolute flow, coronary flow reserve, and ischemic thresholds into a comprehensive map of physiologic severity. JACC Cardiovasc Imaging. 2012;5:430–40.
44. Johnson NP, Pijls NH, De Bruyne B, Bech GJ, Kirkeeide RL, Gould KL. A black and white response to the "gray zone" for fractional flow reserve measurements. JACC Cardiovasc Interv. 2014;7:227–8.
45. Johnson NP, Gould KL. Regadenoson versus dipyridamole hyperemia for cardiac PET imaging. JACC Cardiovasc Imaging. 2015;8:438–47.
46. Johnson NP, Gould KL, Di Carli MF, Taqueti VR. Invasive FFR and noninvasive CFR in the evaluation of ischemia: what is the future? J Am Coll Cardiol. 2016;67:2772–88.
47. Kitkungvan D, Johnson NP, Roby AE, Patel MB, Kirkeeide R, Gould KL. Routine clinical quantitative rest stress myocardial perfusion for managing coronary artery disease: clinical relevance of test-retest variability. JACC Cardiovasc Imaging. 2017;10:565–77.
48. Kitkungvan D, Lai D, Zhu H, Roby AE, Johnson NP, Steptoe DD, et al. Optimal adenosine stress for maximum stress perfusion, coronary flow reserve, and pixel distribution of coronary flow capacity by Kolmogorov-Smirnov analysis. Circ Cardiovasc Imaging. 2017;10. pii:e005650. https://doi.org/10.1161/CIRCIMAGING.116.005650.
49. Gould KL, Schelbert H, Narula J. Positron emission tomography in heart disease. In: Fuster V, Harrington RA, Narula J, Eapen ZJ, editors. Hurst's the heart. 14th ed. New York: McGraw Hill; 2017. p. 553–605.
50. Javadi MS, Lautamäki R, Merrill J, Voicu C, Epley W, McBride G, Bengel FM. Definition of vascular territories on myocardial perfusion images by integration with true coronary anatomy: a hybrid PET/CT analysis. J Nucl Med. 2010;51:198–203.
51. Bom MJ, Schumacher SP, Driessen RS, Raijmakers PG, Everaars H, van Diemen PA, et al. Impact of individualized segmentation on diagnostic performance of quantitative positron emission tomography for haemodynamically significant coronary artery disease. Eur Heart J Cardiovasc Imaging. 2019;20:525–32. https://doi.org/10.1093/ehjci/jey201.
52. Ortiz-Perez JT, Rodriguez J, Meyers SN, Lee DC, Davidson C, Wu E. Correspondence between the 17-segment model and coronary arterial anatomy using contrast-enhanced cardiac magnetic resonance imaging. JACC Cardiovasc Imaging. 2008;1:282–93.
53. Pereztol-Valdés O, Candell-Riera J, Santana-Boado C, Angel J, Aguadé-Bruix S, Castell-Conesa J, et al. Correspondence between left ventricular 17 myocardial segments and coronary arteries. Eur Heart J. 2005;26:2637–43.
54. Thomassen A, Petersen H, Johansen A, Braad PE, Diederichsen AC, Mickley H, et al. Quantitative myocardial perfusion by O-15-water PET: individualized vs. standardized vascular territories. Eur Heart J Cardiovasc Imaging. 2015;16:970–6.
55. Donato P, Coelho P, Santos C, Bernardes A, Caseiro-Alves F. Correspondence between left ventricular 17 myocardial segments and coronary anatomy obtained by multi-detector computed tomography: an ex vivo contribution. Surg Radiol Anat. 2012;34:805–10.
56. Cerci RJ, Arbab-Zadeh A, George RT, Miller JM, Vavere AL, Mehra V, et al. Aligning coronary anatomy and myocardial perfusion territories: an algorithm for the CORE320 multicenter study. Circ Cardiovasc Imaging. 2012;5:587–95.
57. Yoshida K, Mullani N, Gould KL. Coronary flow and flow reserve by positron emission tomography simplified for clinical application using Rb-82 or N-13 ammonia. J Nucl Med. 1996;37:1701–12.
58. Vasquez AF, Johnson NP, Gould KL. Variation in quantitative myocardial perfusion due to arterial input selection. JACC Cardiovasc Imaging. 2013;6:559–68.
59. Bachrach SL, Carson RE. In hot blood—quantifying the arterial input. JACC Cardiovasc Imaging. 2013;6:569–73.
60. Renaud JM, DaSilva JN, Beanlands RS, DeKemp RA. Characterizing the normal range of myocardial blood flow with ^{82}rubidium and ^{13}N-ammonia PET imaging. J Nucl Cardiol. 2013;20:578–91.
61. Araujo L, Lammertsma AA, Rhodes CG, McFalls EO, Iida H, Rechavia E, et al. Noninvasive quantification of regional myocardial blood flow in coronary artery disease with oxygen-15-labeled carbon dioxide inhalation and positron emission tomography. Circulation. 1991;83:875–85.
62. Bol A, Melin JA, Vanoverschelde JL, Baudhuin T, Vogelaers D, De Pauw M, et al. Direct comparison of [13N]ammonia and [15O]water estimates of perfusion with quantification of

regional myocardial blood flow by microspheres. Circulation. 1993;87:512–25.
63. Johnson NP, Gould KL. Partial volume correction incorporating Rb-82 positron range for quantitative myocardial perfusion PET based on systolic-diastolic activity ratios and phantom measurements. J Nucl Cardiol. 2011;18:247–58.
64. Gould KL, Pan T, Loghin C, Johnson N, Guha A, Sdringola S. Frequent diagnostic errors in cardiac PET-CT due to misregistration of CT attenuation and emission PET images: a definitive analysis of causes, consequences and corrections. J Nucl Med. 2007;48:1112–21.
65. Loghin C, Sdringola S, Gould KL. Common artifacts in PET myocardial perfusion images due to attenuation-emission misregistration. J Nucl Med. 2004;45:1029–39.
66. Johnson NP, Pan T, Gould KL. Shifted helical computed tomography to optimize cardiac positron emission tomography–computed tomography coregistration: quantitative improvement and limitations. Mol Imaging. 2010;9:256–67.
67. Murthy VL, Naya M, Foster CR, Hainer J, Gaber M, Di Carli G, et al. Improved cardiac risk assessment with noninvasive measures of coronary flow reserve. Circulation. 2011;124:2215–24.
68. Herzog BA, Husmann L, Valenta I, Gaemperli O, Siegrist PT, Tay FM, et al. Long-term prognostic value of 13N-ammonia myocardial perfusion positron emission tomography added value of coronary flow reserve. J Am Coll Cardiol. 2009;54:150–6.
69. Taqueti VR, Hachamovitch R, Murthy VL, Naya M, Foster CR, Hainer J, et al. Global coronary flow reserve is associated with adverse cardiovascular events independently of luminal angiographic severity and modifies the effect of early revascularization. Circulation. 2015;131:19–27.
70. van de Hoef TP, Echavarría-Pinto M, van Lavieren MA, Meuwissen M, Serruys PW, Tijssen JG, et al. Diagnostic and prognostic implications of coronary flow capacity: a comprehensive cross-modality physiological concept in ischemic heart disease. JACC Cardiovasc Interv. 2015;8:1670–80.
71. van de Hoef TP, van Lavieren MA, Damman P, Delewi R, Piek MA, Chamuleau SA, et al. Physiological basis and long-term clinical outcome of discordance between fractional flow reserve and coronary flow velocity reserve in coronary stenoses of intermediate severity. Circ Cardiovasc Interv. 2014;7:301–11.
72. Hamaya R, Yonetsu T, Kanaji Y, Usui E, Hoshino M, Yamaguchi M, et al. Diagnostic and prognostic efficacy of coronary flow capacity obtained using pressure-temperature sensor-tipped wire–derived physiological indices. JACC Cardiovasc Interv. 2018;11:728–37.
73. Hoshino M, Kanaji Y, Hamaya R, Kanno Y, Hada M, Yamaguchi M, et al. Prognostic value of thermodilution-derived coronary flow capacity in patients with deferred revascularization. EuroIntervention. 2019. pii: EIJ-D-19-00029. https://doi.org/10.4244/EIJ-D-19-00029. [Epub ahead of print].
74. Stuijfzand WJ, Uusitalo V, Kero T, Danad I, Rijnierse MT, Saraste A, et al. Relative flow reserve derived from quantitative perfusion imaging may not outperform stress myocardial blood flow for identification of hemodynamically significant coronary artery disease. Circ Cardiovasc Imaging. 2015;8. pii: e002400. https://doi.org/10.1161/CIRCIMAGING.114.002400.
75. Virmani R. Are our tools for the identification of TCFA ready and do we know them? JACC Cardiovasc Imaging. 2011;4:656–8.
76. Tian J, Ren X, Vergallo R, Xing L, Yu H, Jia H, et al. Distinct morphological features of ruptured culprit plaque for acute coronary events compared to those with silent rupture and thin-cap fibroatheroma: a combined optical coherence tomography and intravascular ultrasound study. J Am Coll Cardiol. 2014;63:2209–16.
77. Arbab-Zadeh A, Fuster V. The myth of the "vulnerable plaque": transitioning from a focus on individual lesions to atherosclerotic disease burden for coronary artery disease risk assessment. J Am Coll Cardiol. 2015;65:846–55.
78. Bom MJ, Schumacher SP, Driessen RS, Raijmakers PG, Everaars H, van Diemen PA, et al. Impact of individualized segmentation on diagnostic performance of quantitative positron emission tomography for haemodynamically significant coronary artery disease. Eur Heart J Cardiovasc Imaging. 2019;20:21–30.
79. De Bruyne B, Baudhuin T, Melin JA, Pijls NH, Sys SU, Bol A, et al. Coronary flow reserve calculated from pressure measurements in humans. Validation with positron emission tomography. Circulation. 1994;89:1013–22.
80. Marques KM, Knaapen P, Boellaard R, Lammertsma AA, Westerhof N, Visser FC. Microvascular function in viable myocardium after chronic infarction does not influence fractional flow reserve measurements. J Nucl Med. 2007;48:1987–92.
81. deKemp RA, Yoshinaga K, Beanlands RSB. Will 3-dimensional PET-CT enable the routine quantification of myocardial blood flow? J Nucl Cardiol. 2007;14:380–97.
82. Gould KL, Martucci JP, Goldberg DI, Hess MJ, Edens RP, Latifi R, Dudrick SJ. Short-term cholesterol lowering decreases size and severity of perfusion abnormalities by positron emission tomography after dipyridamole in patients with coronary artery disease. Circulation. 1994;89:1530–8.
83. Gould KL, Ornish D, Scherwitz L, Brown S, Edens RP, Hess MJ, et al. Changes in myocardial perfusion abnormalities by positron emission tomography after long-term, intense risk factor modification. JAMA. 1995;274:894–901.
84. Sdringola S, Nakagawa K, Nakagawa Y, Yusuf W, Mullani N, Haynie M, et al. Combined intense lifestyle and pharmacologic lipid treatment further reduce coronary events and myocardial perfusion abnormalities compared to usual care cholesterol lowering drugs in coronary artery disease. J Am Coll Cardiol. 2003;41:262–72. *Chosen for Highlights of the Year in J Am Coll Cardiol. 2003 (JACC 2003;42:2164).*
85. Sdringola S, Boccalandro F, Loghin C, Gould KL. Mechanisms of progression and regression of coronary artery disease by PET related to treatment intensity and clinical events at long-term follow-up. J Nucl Med. 2006;47:59–67.
86. Gould KL. From experimental to clinical coronary physiology. Circ Res. 2018;123:1124–6.